APPLICATION OF FRACTALS IN THE DESIGN OF MULTIBAND WAVEGUIDE FILTER, POWER DIVIDER AND METAMATERIAL

A DISSERTATION

Submitted in partial fulfillment of the requirements for the award of the degree of

MASTER OF TECHNOLOGY

in

ELECTRONICS AND COMMUNICATION ENGINEERING

(With Specialization in RF and Microwave Engineering)

By

VIBHORE KUMAR

DEPARTMENT OF ELECTRONICS AND COMPUTER ENGINEERING

INDIAN INSTITUTE OF TECHNOLOGY ROORKEE

ROORKEE -247 667 (INDIA)

SEPTEMBER, 2010

CANDIDATE'S DECLARATION

I hereby declare that the work, which is presented in this dissertation report entitled, **"APPLICATION OF FRACTALS IN THE DESIGN OF MULTIBAND WAVEGUIDE FILTER, POWER DIVIDER AND METAMATERIAL"** towards the partial fulfillment of the requirements for the award of the degree of **Master of Technology** with specialization in **RF and Microwave Engineering**, submitted in the Department of Electronics and Computer Engineering, Indian Institute of Technology Roorkee, Roorkee (India) is an authentic record of my own work carried out during July 2009 to September 2010, under the guidance of **Dr. S.N. SINHA, Professor, Department of Electronics and Computer Engineering, Indian Institute of Technology Roorkee.**

I have not submitted the matter embodied in this dissertation for the award of any other Degree or Diploma.

Dated: 16/09/10
Place: Roorkee

Vibhore K.
VIBHORE KUMAR

CERTIFICATE

This is to certify that the above statement made by the candidate is correct to the best of my knowledge and belief.

Dated: 16.9.10
Place: Roorkee

S N Sinha
Dr. S.N. SINHA,
Professor, E&C Department,
IIT Roorkee,
Roorkee–247 667 (India).

ACKNOWLEDGMENT

It is my privilege and pleasure to express my profound sense of respect, gratitude and indebtedness to my supervisor, **Dr. S.N. SINHA**, Professor, Department of Electronics and Computer Engineering , Indian Institute of Technology, Roorkee, for his invaluable support throughout the dissertation work. His inspiration, guidance, constructive criticisms, encouragement and personal guidance provided a good basis for the present dissertation work.

I wish to express my warm and sincere thanks to **Dr. Dharmendra Singh**, Associate Professor, **Dr. N. K. Agarwal**, Emeritus Fellow, **Dr. B. Sinha**, Emeritus Fellow, **Dr. M. V Kartikeyan,** Professor, **Dr. N. P. Pathak**, Assistant Professor and **Dr. A. Patnaik,** Assistant Professor, for their kind help, moral support and for all I have learned from them directly or indirectly in class room contact hours or at other times.

During this work I have collaborated with many colleagues, for whom I have great regard, and I wish to extend my warmest thanks to all who have helped me with my work in Advanced Microwave Laboratory of Department of Electronic and Computer Engineering, Indian Institute of Technology Roorkee. Thanks are due to the Lab staff Wireless Communications Laboratory and Advanced Microwave Lab, Department of electronics and Computer Engineering, IIT Roorkee for providing necessary facilities.

My special sincere heartfelt gratitude to my family, whose sincere prayer, best wishes and unflinching encouragement has been a constant source of strength to me during the entire work. Without their loving support and understanding it would have been impossible for me to finish this work.

(Vibhore Kumar)

ABSTRACT

This work is intended to the applications of fractals in the design of various microwave passive components like waveguide filter, waveguide power divider and metamaterial. The idea of using fractals in the design is to achieve multiband behavior in the respective components.

In the first part of the dissertation basic theory of fractals, their properties, method of generation have been discussed along with the discussion on the waveguide filter, power divider and metamaterial. Also a designing scenario using fractals in these structures is overlooked with the aim to define established knowledge and possible future development of the research.

In the second part of the dissertation numerical simulations of the designed structures of waveguide filter, power divider and metamaterial using Microwave CST Studio, Ansoft HFSS is presented followed by experimental results. The graphical results are generated using MATLAB. And later a conclusion is drawn on the basis of these observations. Experimental results are in good agreement with the simulation results except some marginal errors.

CONTENTS

List of figures

List of Tables

CHAPTER – 1

INTRODUCTION

1.1 Brief Review

Communication both on earth and space is always needed. Microwave communication provides a very successful solution for these needs. Communication is considered to be one of the major drivers in the development and advancements of microwave technology. Waveguide passive components are an integral part of the modern communication systems, particularly for space applications which require low loss and high power handling capability. Typical examples of waveguide passive components include filters, power dividers etc. Microwave filters are used in all these systems to separate undesired signal frequencies from desired ones whereas microwave power dividers are used to drive more than one system with the same source. These passive components can be realized either by planer structures or by waveguide structures [1, 2]. Planer structure provides small size but relatively higher loss compared to waveguide structure that has higher quality factor and higher power handling capability than planer structure. The major drawback of waveguide structure is their bulky size which becomes a critical factor for several applications like satellite applications where minimization of weight is an important factor [3]. Therefore nowadays researchers are developing techniques to miniaturize the design of microwave passive components. Fractals are playing an important role in this regard [4].

Other hottest area of research in microwave engineering domain is metamaterials. For the past several years, metamaterials have been studied and a large number of papers have been published in the RF, terahertz and optical research areas. Metamaterials were briefly examined by Sivukhin in 1957 [5], and theoretically studied by Veselago in 1967 [6], and the topic was revisited by Pendry [7, 8]. Metamaterials are artificial electromagnetic structures which show both negative permittivity and negative permeability in a specific frequency range, and therefore are called negative refractive index (NRI) materials or double-negative (DNG) materials. These structures are artificially engineered using specific repetitive pattern of thin metal structure printed on a dielectric substrate. These structures can be one, two or

three dimensional and have their own advantages over naturally occurring materials [9]. Since we are using repetitive pattern of metal for designing these artificial structures therefore we may think of fractals as an alternative with their own advantages of having multiband, broadband and miniaturized nature. Because of the growing needs of the microwave passive components with miniaturization as the prime requisite this whole work is devoted to the applications of fractals in designing waveguide passive components filters, power divider and metamaterial.

1.2 Motivation and Scope

Microwave systems often need to distribute or to filter out RF power to various paths used for multiple applications [10, 11]. To filter out RF power we need filters and to divide power to various paths we need power dividers. Keeping in view the space applications [3] in microwave engineering we need microwave components which possess high power handling capability with low losses. Therefore, we prefer waveguide structures rather than planner structures. However size and weight of these components is of prime concern in this modern era in which every communication equipment is becoming more and more miniaturized. Therefore, we need designs which are lighter, simpler and of course from bandwidth point of view, are multiband or wideband depending on the requirement. Thus, we need waveguide structures which are multiband or wideband.

The H plane rectangular waveguide Tee junction is commonly used as power divider in the microwave and antenna feeding systems. However, its performance is limited because it provides a constant coupling over a wide range of frequencies. Therefore, we need a design in which the coupling of this junction can be varied by a suitably controlled coupling mechanism. Since fractal is one of the hottest research areas, it motivated us to consider its application to the design of H plane waveguide Tee junction (to work as power divider) and waveguide filters.

Metamaterial is another hot area of research in the microwave engineering since these materials offer several advantages over naturally occurring materials [9]. These structures can be artificially engineered using specific repetitive pattern of thin metal structure on a dielectric substrate. Repetitive pattern of metals in these artificial structures is difficult to design and therefore, research is required in this direction to find an alternative for these structures and also, because these repetitive metal structures are quite complex to understand

in terms of behaviour of propagating electromagnetic fields through them. Therefore, we need simpler structures, like structures having fractals, which can be modelled easily [8, 12]. Also fractal structures possess their own advantages in microwave engineering in that they offer a multiband behaviour which can result in a reduced size of the component [13]. This motivated us to take up the task of designing metamaterials using fractals.

Scope of this research work is very vast, because of growing demands of waveguide passive components which are multiband or wideband. Application of fractals in designing waveguide filter fulfils the need of multiband or wideband characteristics which is a prime requisite in this modern era. Also if we can design a power divider using conventional H plane Tee junction with multiband characteristics, where the bands can be controlled by suitable design of fractal diaphragms, it will result in considerable saving in terms of size and weight of the system. In addition, the position of these fractal diaphragms in the H-arm of H plane Tee junction can provide a changeable coupling. Further, fractal structures can provide a different class of metamaterials just by changing the fractal level or sample size, which may be useful in several applications.

1.3 Objective

The main objective of this dissertation is to use fractals for the design of various microwave passive waveguide structures like filters, power dividers and metamaterials keeping in mind the need of multiband behaviour. The tasks taken up in this dissertation are as follows

- To study different classes of waveguide filters and to draw an inference on this basis for designing the same.
- To study different waveguide power dividing/combining techniques and on this basis propose or design a waveguide power divider.
- To study and design a metamaterial structure which uses fractals, thereby making the resulting structure multiband as well as to propose an alternate way of designing these structures.

1.4 Problem Statement

"Application of Fractals in the Design of Multiband Waveguide Filter, Power Divider and Metamaterial"

The goal is to design

- A waveguide band pass filter using fractal diaphragms having two passband in 7 to 16 GHz frequency range with minimum attenuation -10dB.
- An H-plane rectangular waveguide Tee junction using fractal irises with improved performance over conventional H plane rectangular waveguide Tee junction power divider.
- A metamaterial structure based on fractals.

1.5 Organization of the Dissertation

The dissertation consists of six chapters. In *chapter 2,* a brief theory of fractals is presented along with a survey of work done on their applications in the design of Waveguide Filter, Power Divider and Metamaterials.

Chapter 3, presents the design methodology of waveguide bandpass filter along with simulation and experimental results. The waveguide filter structure is simulated using a theoretical approach and direct simulation on a commercial software and the results of these two simulations are compared to validate the theoretical approach.

In *chapter 4,* a design using fractal diaphragms is proposed for conventional (X-band) H-plane waveguide tee junction. Design is validated by simulation results and experimental measurements.

In *chapter 5,* a novel design for metamaterial consisting of fractals in a shielded waveguide environment is proposed and double negative (DNG) behaviour is verified by the simulation results and experimental measurements.

In *chapter 6* a summary on the basis of results of all the designed structures and future scope of work in this area is provided.

CHAPTER 2

Literature Survey

This chapter includes theory of fractals and their application in the design of Waveguide Filter, Power Divider and Metamaterial.

2.1 Fractals

In recent years, the science of fractal geometry has grown into a vast area of knowledge, with almost all branches of science and engineering gaining from the new insights it has provided. Fractal geometry is concerned with the properties of fractal objects, usually known as **fractals.** Fractals may be found in nature or generated using a mathematical recipe. The word fractal was originally coined by Benoit Mandelbrot in the early 1970's [14]. It is derived from the Latin word 'fractus' which means 'broken', i.e., fragmented, fractional or irregular. A fractal is a rough or fragmented geometric shape that can be subdivided in parts, each of which is (at least approximately) a reduced-size copy of the whole. Mandelbrot realized that it is very often impossible to describe nature using only Euclidean geometry, that is in terms of straight lines, circles, cubes, and such like. There are many definitions of a fractal. Possibly the simplest way to define a fractal is as an object *which appears self-similar under varying degrees of magnification.*

In effect, possessing symmetry across scale, with each small part of the object replicating the structure of the whole is the basic characteristic of fractals.

A few things that fractals can model are: plants, weather, fluid flow, geological activity, planetary orbits, human body, rhythms, socioeconomic patterns, music, clouds, mountains, coastlines etc. that do not correspond to simple geometric shapes. There are many mathematical structures like Sierpinski gasket, Cantor's comb, von Koch's Snowflake, the Mandelbrot set, the Lorenz attractor etc. Which have fractal shapes. Fig. 2.1 shows different types of fractals.

Due to properties such as space-filling ability, self-similarity and lacunarity, fractals have found applications in many fields like geography, biology and engineering. Fractals in electromagnetics have been used in the design of antennas, Frequency selective surfaces, Electromagnetic Band gap structures and Metamaterials.

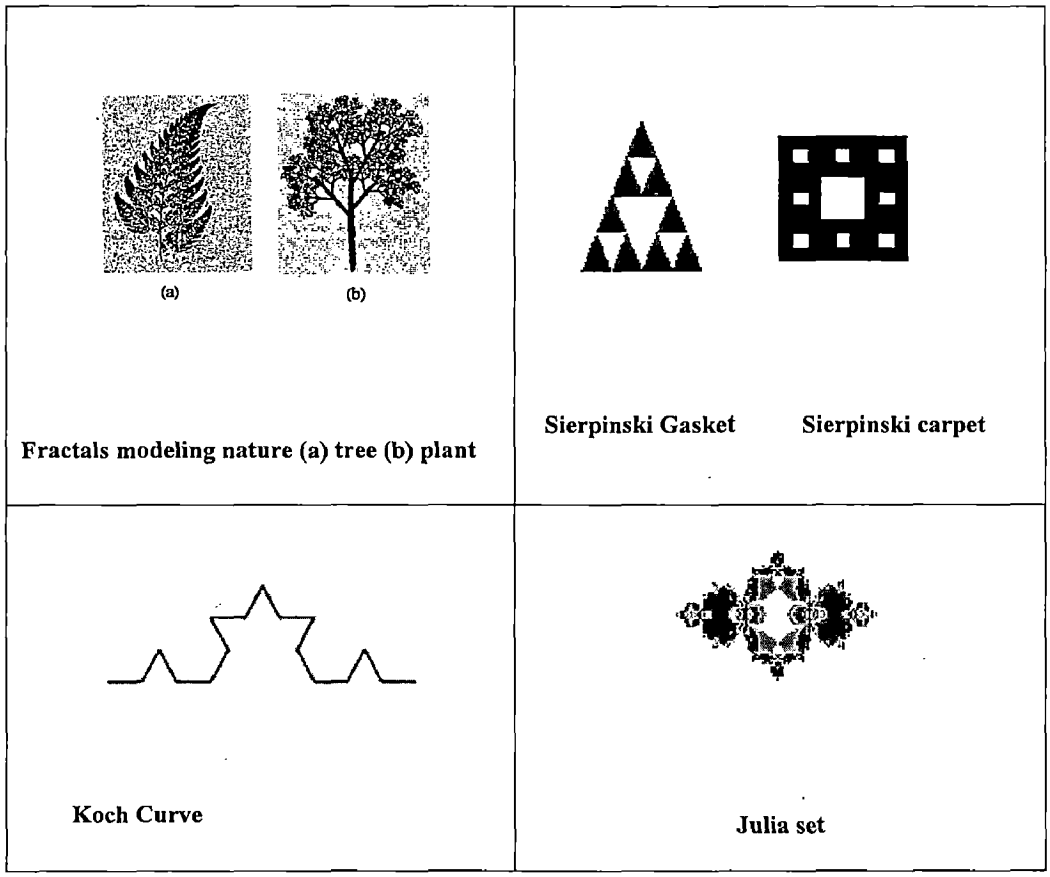

Fig. 2.1 Some Examples of fractals

Mandelbrot defined fractals in several ways. This depends on the definition of their dimension. *A fractal is a set for which the Haussdorff Besicovich dimension strictly exceeds its topological dimension* [15]. Every set having a non integer dimension is a fractal but it can also have integer dimension. Fractal is defined by a set such that [15]

- It has a fine structure with details on arbitrarily small scales.
- It is too irregular to be described by traditional geometry.
- It has some form of self similarity.
- It can be described in a simple way, recursively.
- It's dimension is greater than its topological dimension.

The dimension of a geometry can be defined in several ways, some examples are topological dimension, Euclidean dimension, self similarity dimension and Haussdorff dimension. The easiest to understand is self similarity dimension. An object is said to be self

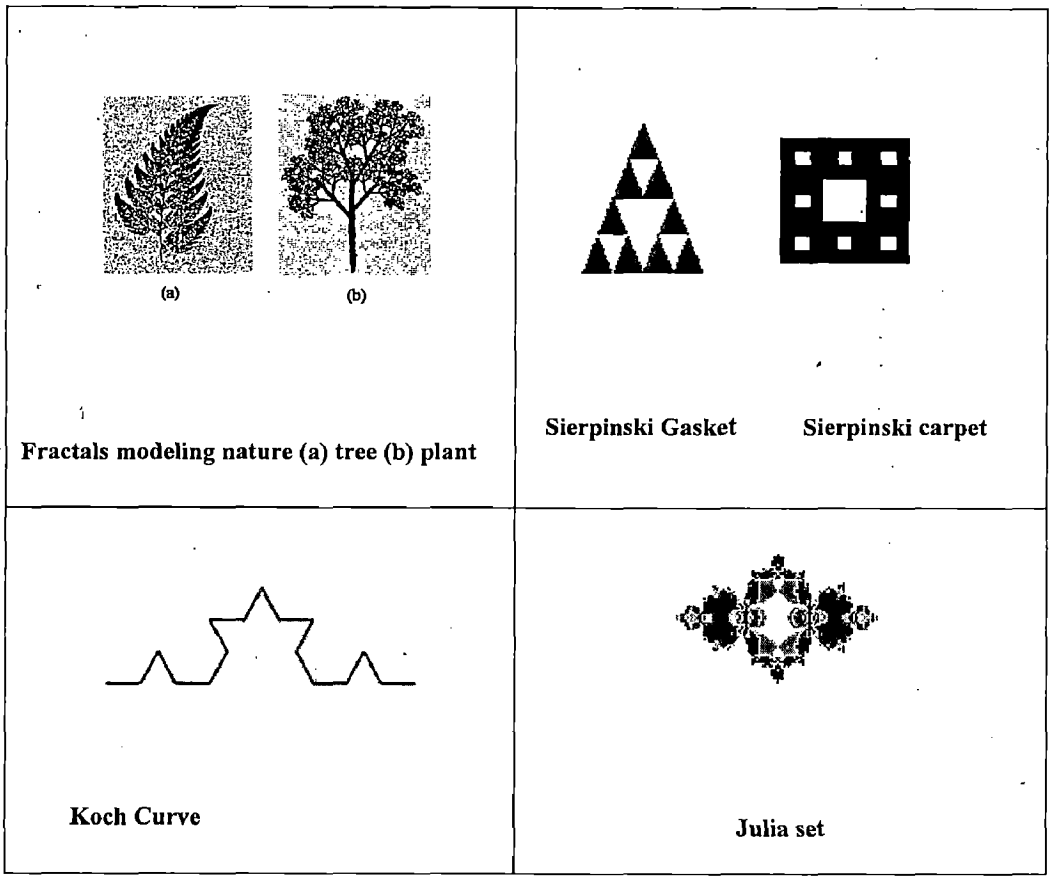

Fig. 2.1 Some Examples of fractals

Mandelbrot defined fractals in several ways. This depends on the definition of their dimension. *A fractal is a set for which the Haussdorff Besicovich dimension strictly exceeds its topological dimension* [15]. Every set having a non integer dimension is a fractal but it can also have integer dimension. Fractal is defined by a set such that [15]

- It has a fine structure with details on arbitrarily small scales.
- It is too irregular to be described by traditional geometry.
- It has some form of self similarity.
- It can be described in a simple way, recursively.
- It's dimension is greater than its topological dimension.

The dimension of a geometry can be defined in several ways, some examples are topological dimension, Euclidean dimension, self similarity dimension and Haussdorff dimension. The easiest to understand is self similarity dimension. An object is said to be self

similar if it looks roughly the same on any scale. If there are N copies of original geometry scaled down by a factor r, the self similarity dimension is defined as:

$$D = \frac{\log N}{\log \frac{1}{r}}$$

D does not need to be an integer as in Euclidean geometry but can be fraction as in Haussdorff dimension.

2.1.1 Properties of fractals

2.1.1.1 Self Similarity

Geometric figures are said to be *similar* if they have the same shape. Self-similarity can be related to as copies of figures within one large figure where each of small figures is copy of the larger figure. Fractals also have self- similarity e.g. is shown in Fig. 2.2 of the Sierpinski Triangle, outline of the figure is an equilateral triangle with infinitely many smaller and smaller triangles inside. All of these are similar to each other and to the original triangle hence shows self-similarity. However it should be noted that not all self-similar objects are fractals.

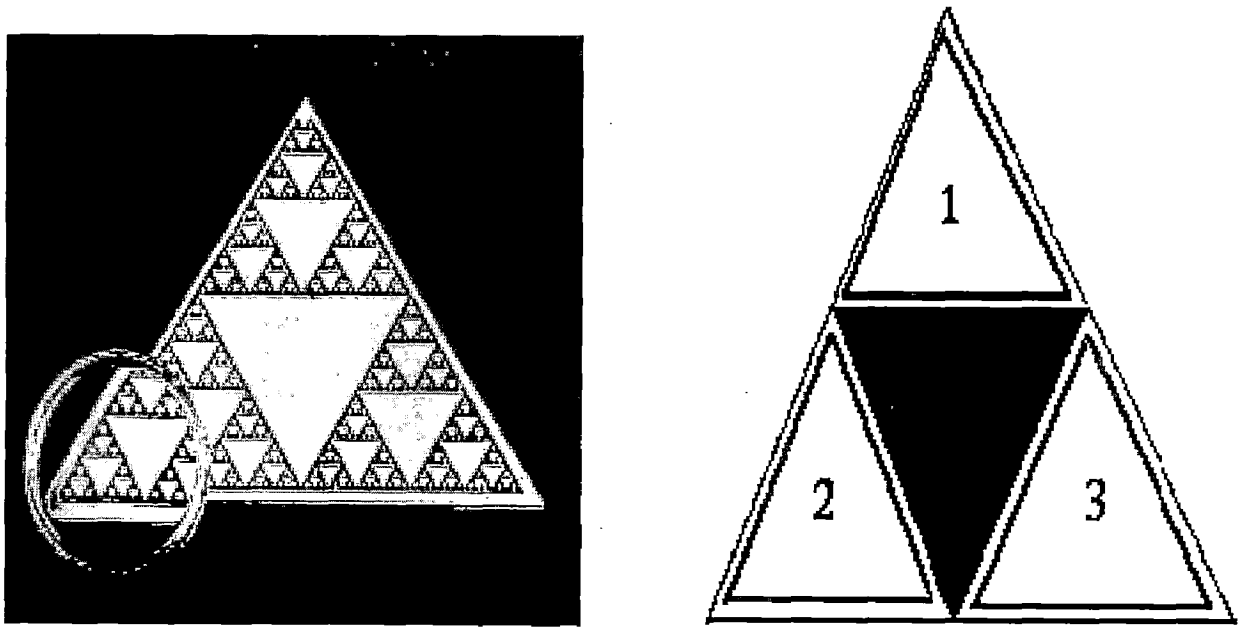

(a) **(b)**

Fig. 2.2. Sierpinski Triangle

2.1.1.2 Fractional Dimension

Dimensions form the main mathematical tool for the study of fractal sets. Fractional dimension is measure in one direction so as to find a position in space which is a fraction. Fractal dimension is a measure of the complexity in a given fractal pattern. Fractional dimension basically quantifies the static geometry of an object, an objective means to compare fractal sets and quantify the perception of how densely a fractal set occupies the space in which it exists.

2.1.1.3 Formation by Iteration

In many cases a fractal can be generated by a repeating pattern, which is typically a recursive or iterative process. In order to make a fractal of a familiar geometry the figure is operated on itself so that the new figure is more "complicated" following a recusive or iterative manner.

2.1.2 Fractals generation

Fractals are geometric shapes that are very complex and infinitely detailed. If we process a *zoom in* on a fractal surface a more clear picture can be viewed because of their recursive nature and due the fact that smaller sections have the same patteren as larger ones. Fractals are grouped into three major categories.

- ***Iterated function systems***
- ***Recurrence Systems***
- ***Random fractals***

2.1.2.1 Iterated Function System (IFS) [16]

These have a fixed geometric replacement rule (Cantor set, Sierpinski carpet, Sierpinski gasket, Peano curve, Koch snowflake, Harter-Heighway dragon curve).

Iterated function Scheme is a mathematical scheme for generating complex functions. This process can be described by an Iterative Function System (IFS). For this we define a set of functions $F = \{f_1, f_2, f_3, ...f_n\}$ with $f_i : X \to X \quad \forall i = 1,2,.....,n$ and a starting point $x_0 = X$. For f_R representing a function chosen at random from the set F, the sequence is

$x_0, f_R(x_0), f_R(f_R(x_0))$,....and so on. This sequence of points can then be plotted to make an a approximate fractal set. Most pre-fractal structures can be built by using the concept of iterated function system (IFS). Every IFS iteration is defined by a set of Q affine transformations in the plane $\{w_q\}_{q=1}^{Q} R^2 \to R^2$ which can be written as:

$$w_q(x) = A_q x + t_q = \begin{pmatrix} r_{q1}\cos\theta_{q1} & -r_{q2}\sin\theta_{q2} \\ r_{q1}\sin\theta_{q1} & r_{q2}\cos\theta_{q2} \end{pmatrix} \begin{pmatrix} x_1 \\ x_2 \end{pmatrix} + \begin{pmatrix} t_{q1} \\ t_{q2} \end{pmatrix}$$

Where x_1 and x_2 are the coordinates of point x. If $r_{q1} = r_{q2} = r_q$ with $0 < r_q < 1$, and $\theta_{q1} = \theta_{q2} = \theta_q$, the IFS transformation is a contractive similarity (angles are preserved) where r_q is the scale factor and θ_q is the rotation angle. The column matrix t_q is just a translation on the plane. Fig. 2.3 shows a Koch Curve and Fig. 2.4 shows the Sierpinski fractal obtained from a single triangle after applying set of transformations recursively. Fractal structures can be analyzed using the integral equation methods (IE), and methods of moments (MOM. Iterated function systems have proven to be a very powerful design tool because they provide a general framework for the description, classification, and manipulation of fractals.

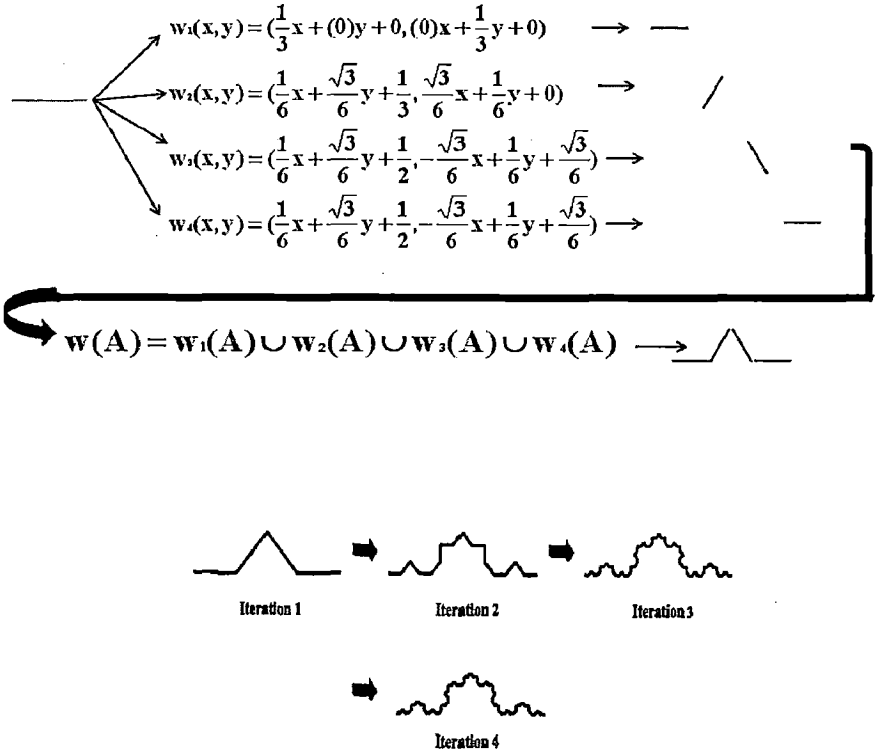

Fig. 2.3 Koch curve formed by iteration [16]

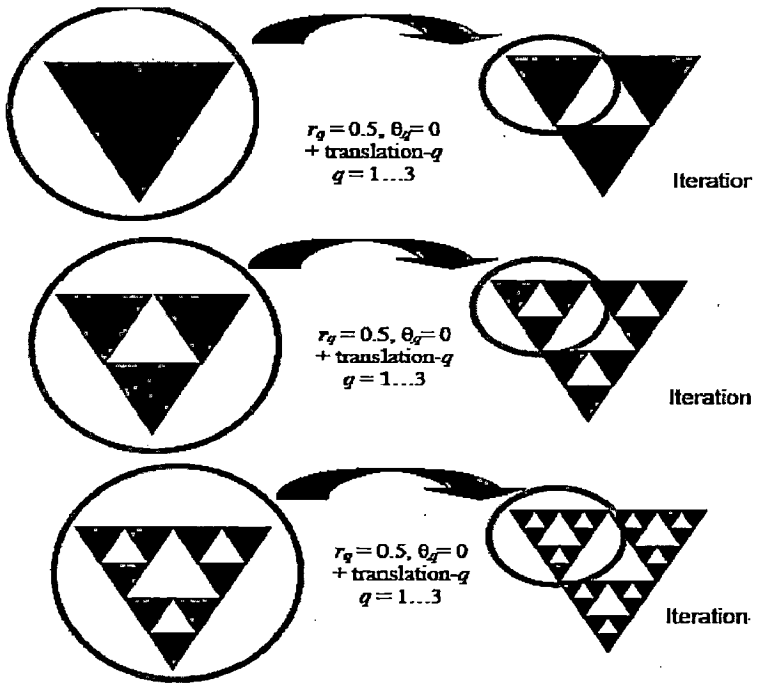

Fig.2.4 Sierpinski Triangle formed by iteration

2.1.2.2 Recurrence System [17]

Fractals defined by a recurrence relation at each point in a space (such as the complex plane). Examples of this type are the Mandelbrot set and the Lyapunov fractal. These are also called *escape-time fractals.*

2.1.2.3 Random Fractal [17]

These are generated by stochastic rather than deterministic processes, for example, fractal landscapes.

2.1.3 Generation of Devil's Staircase Fractal [18]

Devil's staircase is a type of borderline fractal. It is a fractal curve of dimension 1.0. For the construction of devil's staircase we take a square with sides of length 1. Then we start to construct the Cantor set on the base side (i.e., we take away successively middle thirds in the usual way). For each middle third of length $(1/3)^k$ which we take away, we paste in a rectangular column with width $(1/3)^k$ and a certain height. This process is shown in figure 2.5.

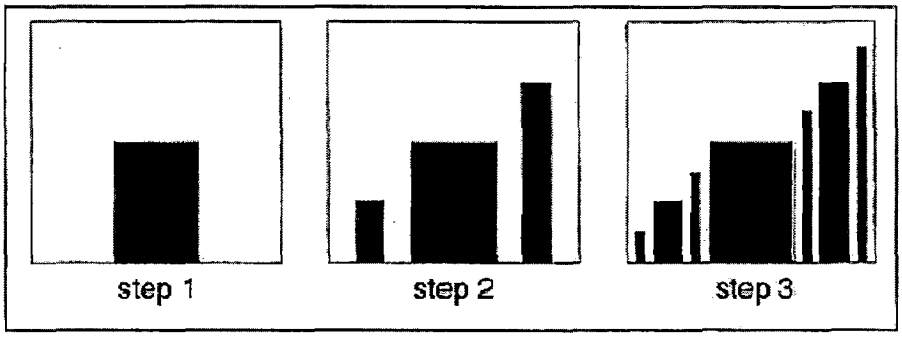

(a)

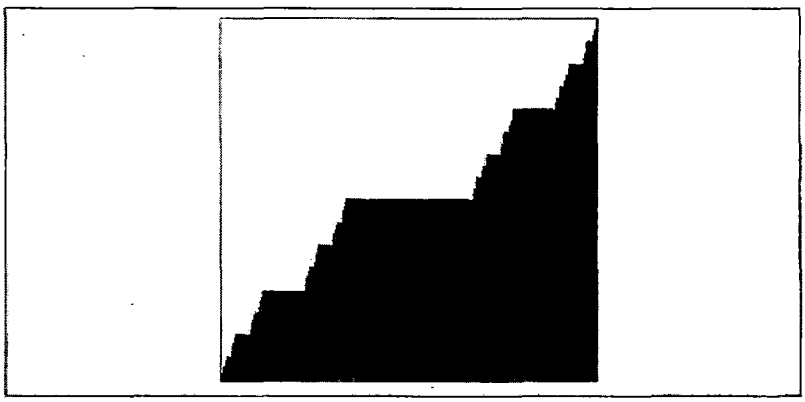

(b)

Fig. 2.5 Generation Steps of Devil's Staircase Fractal [18]

In the first step, a column is erected over the middle third of the base side— the interval [1/3, 2/3] — of the square with height 1/2. In the second step, we erect two columns, one of height 1/4 over the interval [1/9, 2/9] and the other of height 3/4 over the interval [7/9, 8/9]. In the third step, we erect four columns of heights 1/8, 3/8, 5/8, 7/8, and in the k^{th} step, we erect 2^{k-1} columns of heights $1/2^k$, $3/2^k$,……,$(2^k-1)/ 2^k$. In the limit, we obtain an area, the upper border of which is called the *devil's staircase.*

2.1.4 Application of Fractals

In microwave engineering fractals find a lot of applications. In modern times researchers are working on the size and weight reduction of microwave components as well as making it multiband or wideband. Use of fractals is single and ultimate solution of all these new modern requirements. In microwave engineering, we generally use fractals for making our

design multiband or wideband like in the design of wideband antennas [19] and multiband antennas [20].

Nowadays fractals have attracted the attention of researchers towards the design of other microwave components like waveguide filter [4], Power divider [21] and Metamaterial [22, 23].

2.2 Waveguide Filter

In the past years, many researchers have developed waveguide filters using periodic structures, which have been classically displaced into the waveguide longitudinally, to achieve a certain band-pass or band-stop behaviour. Fractals have also been used for their ability to behave as metallic walls near their resonance, and thereby allowing the realization of dual-frequency waveguides.

2.2.1 Types of Filters

- Finline and metal insert filters
- Waveguides Filters With Resonant Array Inserts along the length of the guide
- Waveguides Filters With Resonant Aperture Inserts

Finline and metal insert filters are traditional microwave filters [24]. Nowadays these type of filters are not used due to their higher cost of fabrication and a bulkier design. Also waveguide filters with resonant array inserted along the length of the guide have higher fabrication cost are less flexible in terms of parameters variations and have a high insertion loss as waveguide section tend to be very large [25].

In contrast by using a resonant structure like FSS or resonant aperture as transverse insert one can achieve a good filtering performance but with a much more lightweight design. Using this approach M. Ohira et al. have proposed a structure [26] as shown in Fig. 2.6.

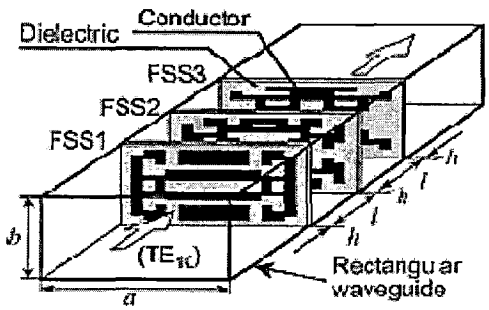

Fig. 2.6 Waveguide filter consisting of three FSSs [24]

This structure uses three FSSs. Each FSS has a pass band provided by resonance at common frequency as shown in following Fig. 2.7.

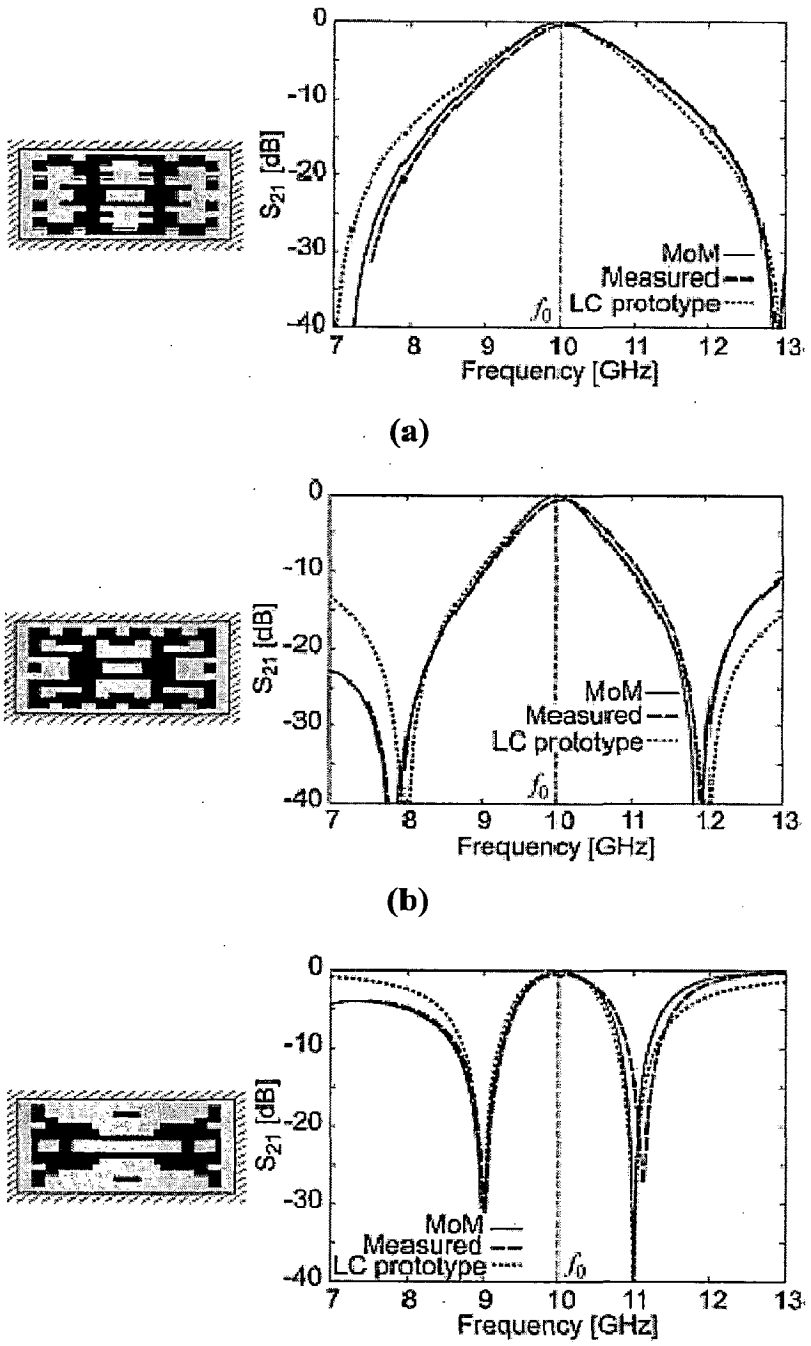

Fig. 2.7 Transmission response of FSSs. (a) FSS1. (b) FSS2. (c) FSS3 [26].

When these three FSSs are placed transversely inside a quarter wavelength waveguide following response is observed shown in Fig. 2.8.

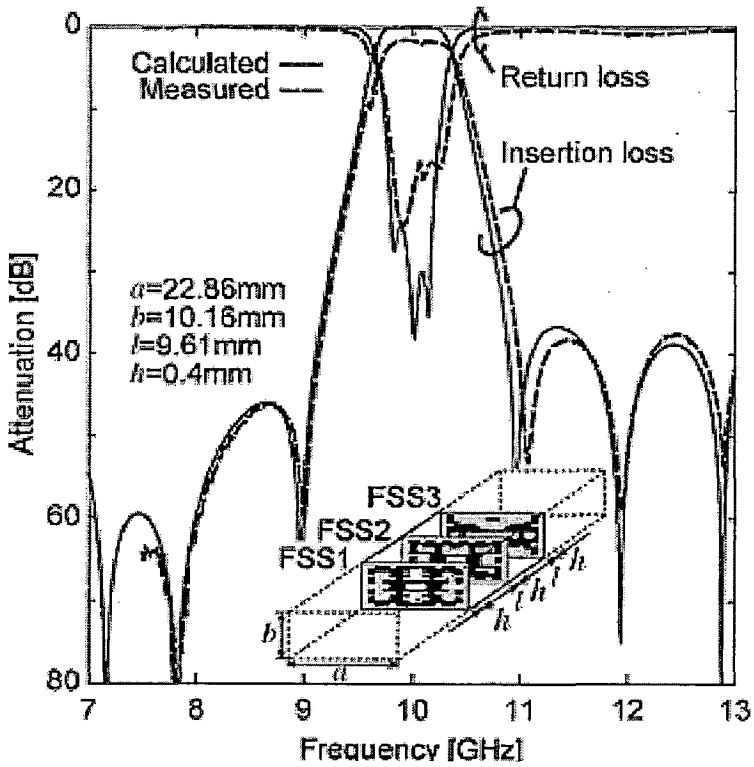

Fig. 2.8 Insertion loss and return loss of the waveguide filter [26].

Thus, insertion of these closely coupled irises produces a band pass filter behaviour.

2.3 Application of Fractals in the Design of Waveguide Filter:

D. Oloumi et al. [4] have used Koch first iteration fractal shaped irises and obtained a waveguide filter with increased bandwidth and reduced overall size.

Iris used is shown in Fig..2.9 and its dimensions are in table 2.1

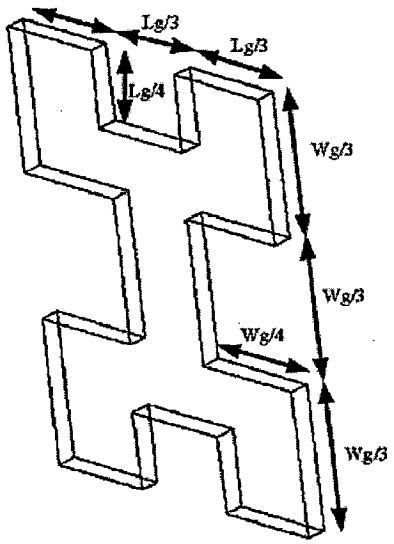

Fig. 2.9 A Koch first iteration fractal shaped iris[4].

TABLE 2.1[4]

DESIGN VALUES FOR FRACTAL IRISE IN INCHES

Dimension	1st IRIS	2nd IRIS	3rd IRIS
Lg	0.282	0.354	0.363
Lg/3	0.094	0.118	0.121
Lg/4	0.070	0.089	0.091
Wg	0.400	0.400	0.400
Wg/3	0.133	0.133	0.133
Wg/4	0.100	0.100	0.100

The number of iterations determines the iteration of the fractal, and as this iteration increases, the overall length increases by a factor of (4/3) per each iteration. Geometry of the waveguide filter using this iris is as shown below in Fig. 2.10.

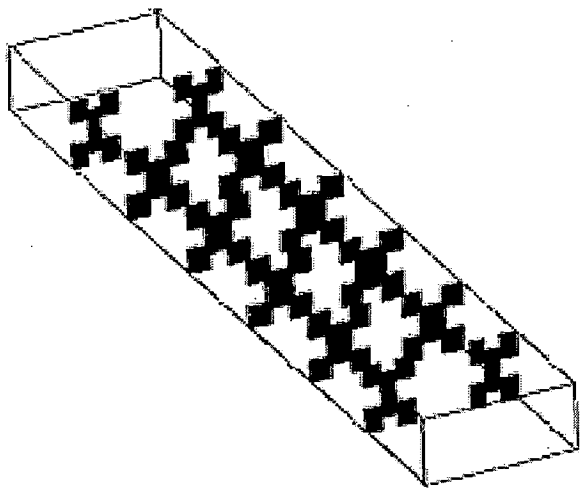

Fig. 2.10 Geometry of waveguide filter using Fractal [4]

Simulation and measured results of frequency of this Koch Fractal Filter are shown below in Fig.2.11

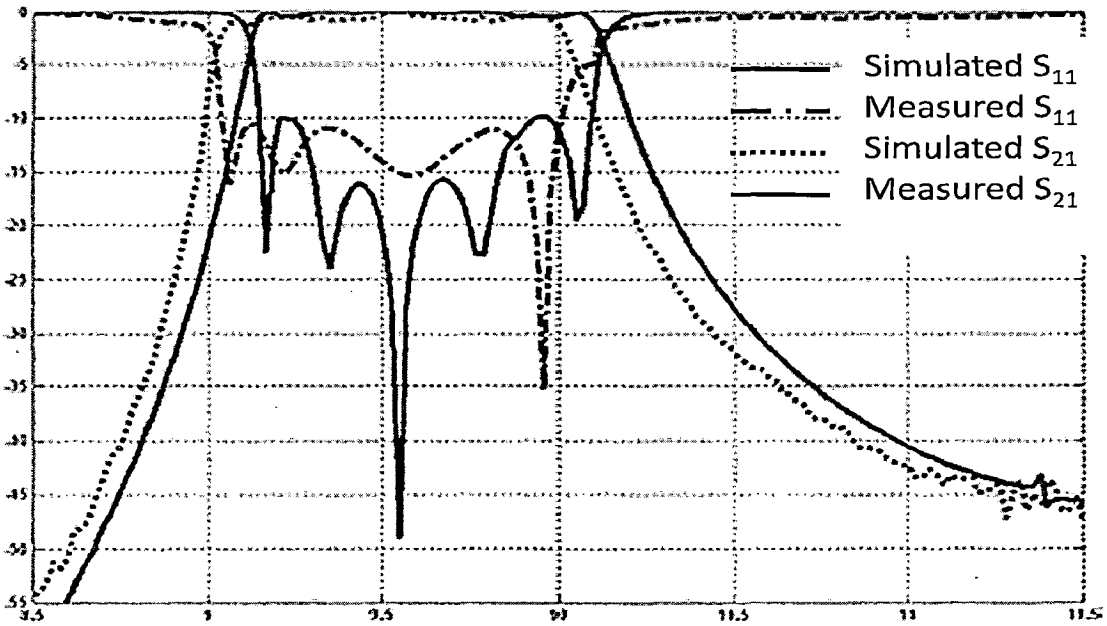

Fig. 2.11 Frequency response of Koch Fractal Filter [4]

Thus, by the application of fractal a wider bandwidth and size reduction in the overall filter structure is obtained.

2.3 POWER DIVIDER:

Power dividing/combining circuits are used in military and commercial communications systems at microwave and millimeter-wave frequencies extensively [10, 11]. When these circuits with low loss and wide bandwidth are needed, some circuit types, such as rectangular waveguide divider/combiner and coaxial waveguide divider/combiner are used. Typical power dividing/combining techniques consist of three stages. Dividing/combining of a signal to be amplified, amplification of each divided/combined signal and combining/dividing of the amplified signals. The H-plane rectangular waveguide T-junction is commonly used as power divider in the microwave frequency region. The waveguide T-junction can be regarded as a coupler with a big slot so from the point of view of coupling there is a necessity of improving the coupling performance of this T junction. To obtain higher output power and wideband characteristics, it is required to develop multiple-port power divider /combiner's of low insertion loss, high handling power and wideband characteristics. Power dividers/combiners can be classified into two categories.

- The non-resonant type such as 3-dB hybrids and radial-line dividers,
- The resonant type which uses a cylindrical cavity or a waveguide cavity.

Resonant type power divider can be realized by using frequency selective surfaces (FSS's) that can be multiband depending on the choice of fractal or any other geometry that we are interested in to use. But our focus will be on the FSS's that are generated by the fractals due to the fact that the application of fractals geometry brings a certain decrease on the total area of the metal irises and can produce a wideband or multiband characteristic to the design.

The H plane waveguide T junction is widely used and works very well in many cases. However, in some cases it also carries some associated disadvantages with it like insufficient bandwidth, very high input reflection, imperfect port matching etc. To improve the performance of this junction many measures are taken in practice.
Of these most common are.

- Adding tuning screws in the junction in order to improve its frequency characteristics
- Inserting inductive window or metal band-pass filter.
- Using a stepped H-plane waveguide T junction is helpful in improving the performance of matching and power dividing.

Ben-Qing Gao et al. [21] have proposed the insertion of metal irises with fractal geometry into the Cross face of the H-plane T-junction. They proposed two novel structures aiming at improving the performance of H-plane waveguide T-junction, namely

- Branch Crossing Coupler
- Low Reflection Power Divider

Geometry of H plane rectangular waveguide T- junction is shown in Fig. 2.12

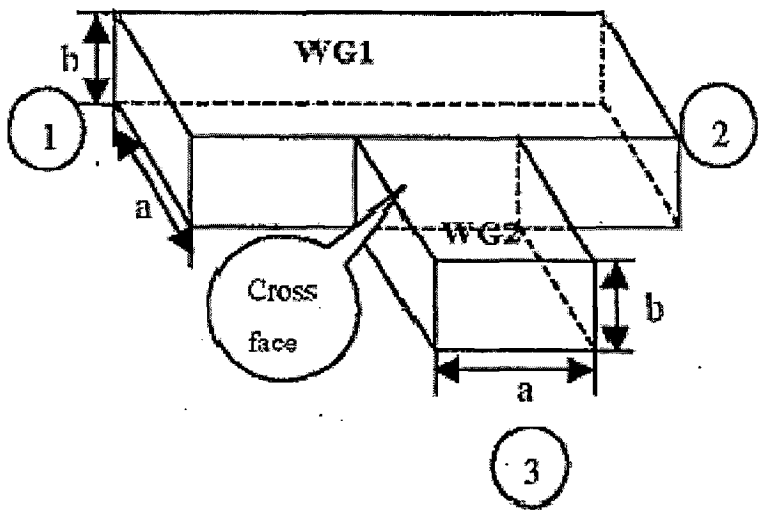

Fig. 2.12 Geometry of H- plane T junction [21]

It is composed of a through waveguide WG1 and a side waveguide WG2. Its Scattering Parameters are shown in Fig. 2.13.

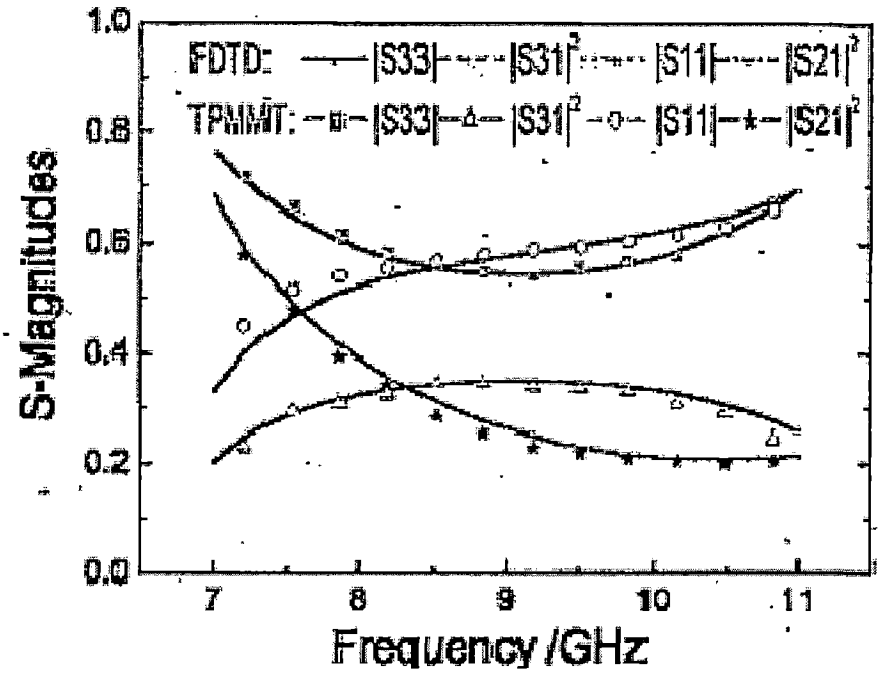

Fig. 2.13 Scattering coefficients of conventional H plane T-Junction [21]

Here, branch crossing coupler refers to a structure which couples more power to through arm (port-2 in present case) than H-arm (port-3 in present case). In addition low reflection power divider refers to a structure which has port-1 and port-2 matched and port-3 has low self reflection coefficient.

From the coupling Point of view, the power is inputted from port-1 and coupled to port-3. From Fig.2.13 it is evident that S_{31} lies between 0.2 to 0.3 (in magnitude), which is around -5dB. Therefore, it was concluded that H-plane T-junction works as a tight coupler i.e. microwave power which goes to port-3 (from port-1) is roughly 5dB less than that of the power that is inputted at port-1. However, feeding systems for antenna arrays require small power. Therefore, in need of couplers or an H-plane tee junction in the present case, which is able to couple less power to the H-arm they proposed a design which was having inductive irises, with fractal geometry, inserted into the cross face of H-plane tee junction. In this way the resulting structure turned into a *branch crossing coupler.*

The need of *low reflection power divider* is due to the fact that the three-port network cannot be matched at the same time for all the three ports and also, the discontinuity in the junction also causes unavoidable reflection. From figure 2.13 it can be observed that S_{33} (the

reflection coefficient of port 3), lies between 0.6 to 0.8, which is fairly high range of self reflection coefficient. Therefore, it is essential to reduce this self reflection of por-3 in H-plane T-junction. For this purpose, they proposed a design which was having capacitive irises, with fractal geometry, inserted into the cross face of H-plane tee junction. In this way the resulting structure turned into a *low reflection power divider.*

2.3.1 Branch Crossing Coupler

Ben-Qing Gao et al. proposed two kinds of branch crossing couplers by inserting two kinds of fractal inductive irises in the cross face of H plane T-junction. These two kinds of fractal irises are of the type of Cantor order-1 fractal and cantor order-2 fractal respectively, as shown in figure 2.14. By adjusting the dimensions of these two irises they obtained two kinds of couplers which were having -15.4dB and -20dB coupling (i.e. the value of $|S_{31}|$) respectively. The dimensions of these irises is listed in Table 2.2

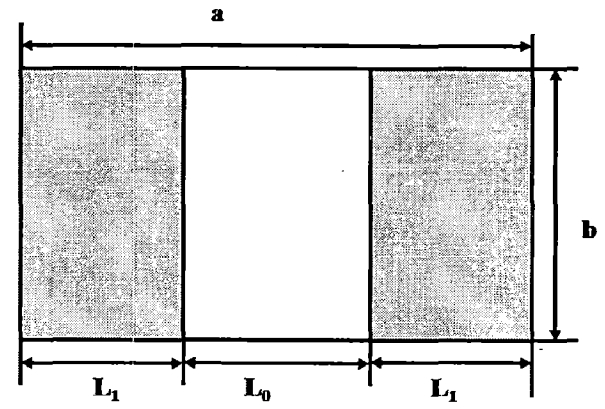

(a)

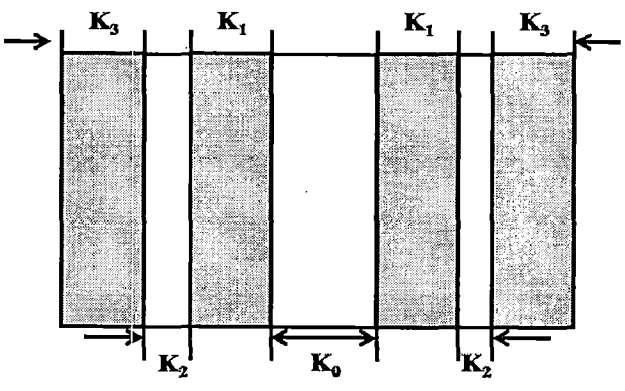

(b)

Fig. 2.14 Geometry of the cross face

(a) Cantor order-1 inductive irises

(b) Cantor order-2 inductive irises [21]

TABLE 2.2[21]

Dimensions of the inductive irises in the cross face

Interface area: a=22.86(mm) b= 10.16(mm)		-15.4dB	-20dB
Cantor order 1 Inductive irises	L_0	7.62	5.72
	L_1	7.62	8.57
Cantor order 2 Inductive irises	K_0	7.22	5.28
	K_1	2.41	1.76
	K_2	2.41	1.76
	K_3	3.00	5.27

2.3.2 Low reflection Power Divider:

Ben-Qing Gao et. al proposed two kinds of low reflection power dividers by inserting two kinds of fractal capacitive irises in the cross face of the H-plane T-junction. The two kinds of fractal irises are of the type of Cantor order-1 fractal and the Cantor order-2 fractal respectively, as shown in Fig. 2.15 and the dimensions of these irises is listed in Table 2.3

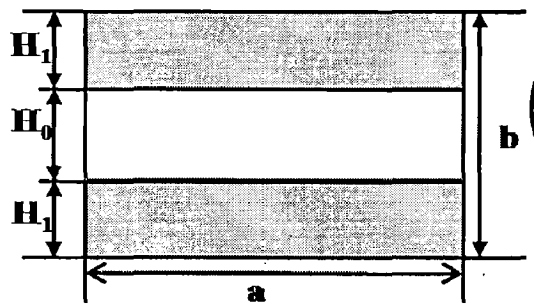

(a)

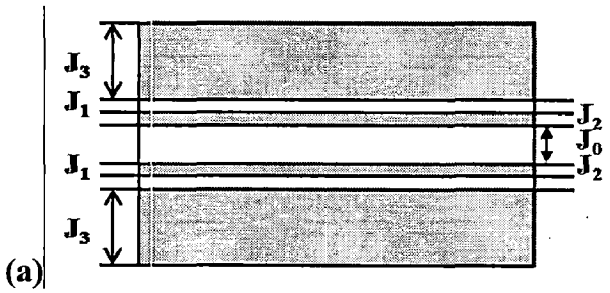

(b)

Fig. 2.15 Geometry of the cross face (a) Cantor 1 capacitive irises (b)Cantor 2 capacitive irises [21]

TABLE 2.3 [21]

Sizes of capacitive irises in the cross face

Interface area: a=22.86(mm) b= 10.16(mm)		mm
Cantor order 1 Inductive irises	H_0	3.39
	H_1	3.39
Cantor order 2 Inductive irises	J_0	2.34
	J_1	0.78
	J_2	0.78
	J_3	2.34

2.3.3 Numerical Analysis [21]

Ben-Qing Gao et al. have done the numerical analysis of the proposed designs using three plane mode-matching technique (TPMMT) and FDTD method, which presented a clearer picture of the necessity and effectiveness of using fractal geometry in a H plane waveguide T-junction. They first applied these two numerical analysis methods on conventional H-plane tee junction as shown in Fig. 2.16.

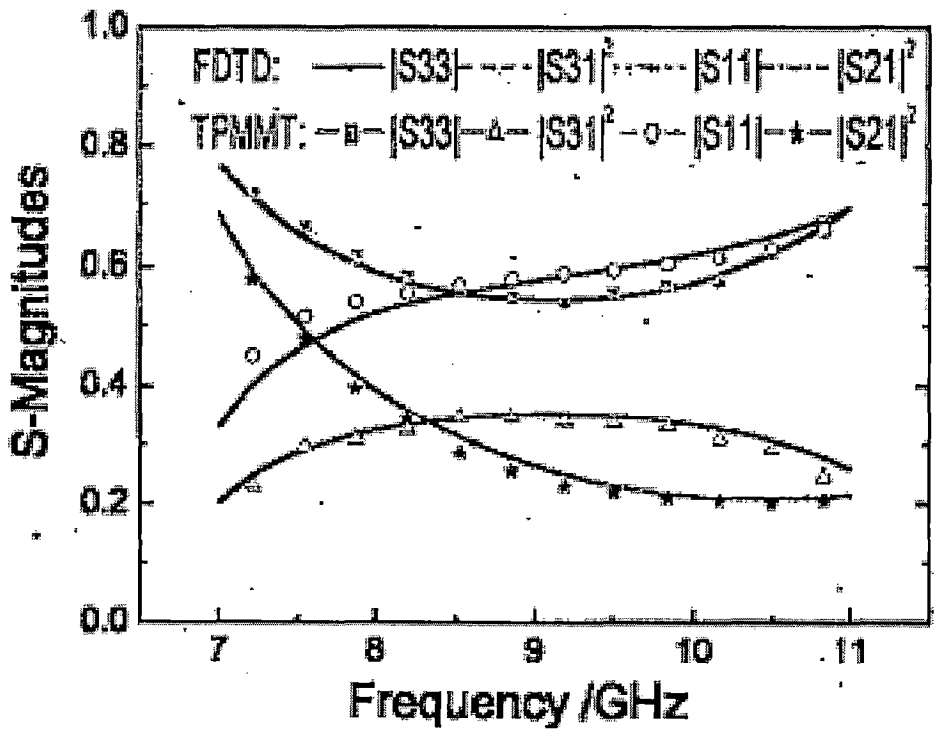

Fig. 2.16 Scattering coefficients of conventional H plane T-Junction [21]

According to the fig.2.16, results obtained on this basis were in good agreement. Therefore, they used FDTD method for the numerical simulation of the structures which were obtained by the introduction of fractal apertures, shown in Figs 2.14 and 2.15, in the H-arm. Figs. 2.17 and 2.18 shows the numerical results for the two types of branch crossing couplers, for which dimensions of fractal apertures were given in table 2.2. From these results it is evident that both of these couplers perform a very even coupling characteristic over a wide bandwidth i.e. 7.5-10 GHz and the coupling coefficient ($|S_{31}|$) of the Cantor order-1 fractal lies between 15 to 16 dB and 20 to 21 dB which is less than 1dB while that of Cantor order 2 fractal lies between 15.4 to 15.5dB and 20.3 to 20.4 dB (roughly) which is less than 0.1dB. Also the increase of fractal order brings an obvious decrease on the total area of the irises.

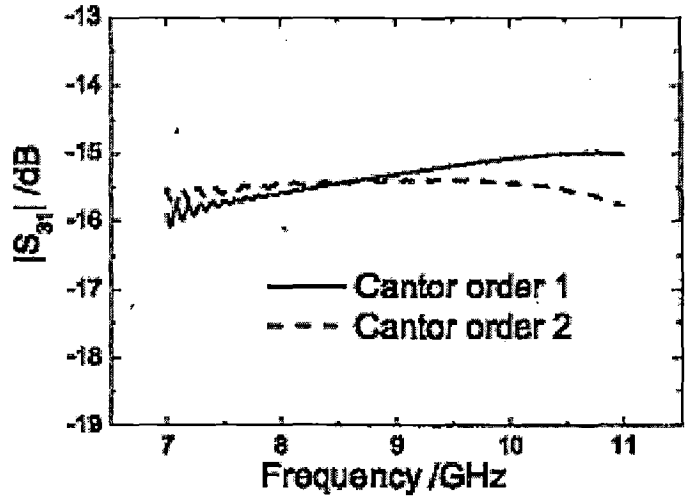

Fig. 2.17 -15.4dB coupling characteristics of the novel couplers [21]

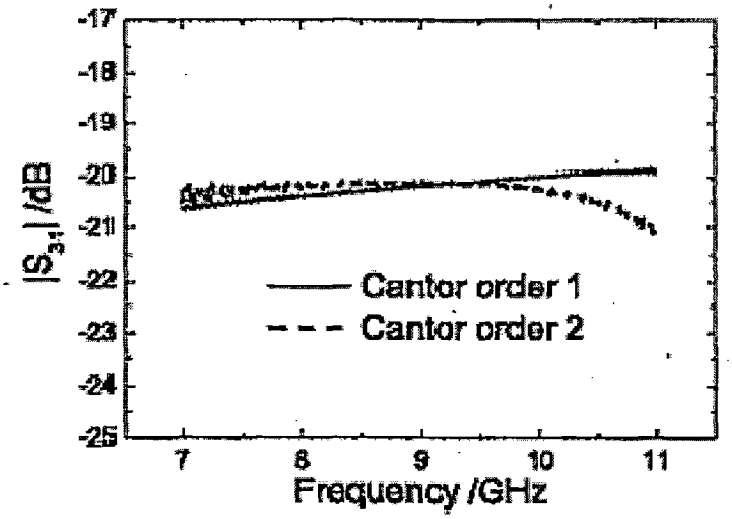

Fig. 2.18 -20dB coupling characteristics of the novel couplers [21]

In addition they also measured the reflection characteristics, i.e. $|S_{33}|$ (using FDTD) of the proposed low reflection power dividers, for which the dimension of fractal apertures introduced in the H-arm is given in table 2.3. Further they compared these characteristics with the conventional one. This comparison is given in Fig. 2.19.

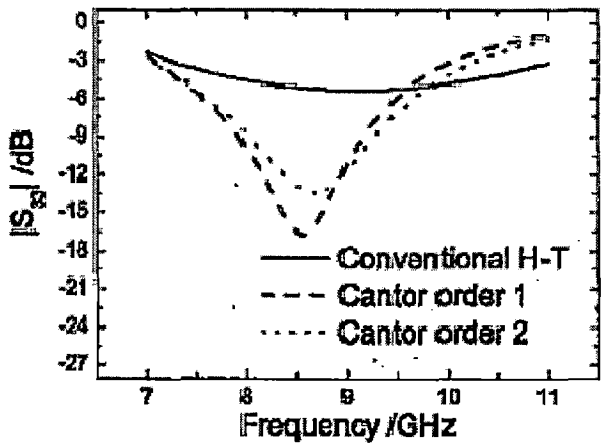

Figu. 2.19 Reflection characteristics of three kinds of H-plane T-junction [21]

From this comparison it is evident that reflection coefficient at port-3 ($|S_{33}|$) has decreased by the presence of fractal irises. Thus, it is evident that by using fractals we can design low cost waveguide power dividers.

2.4 METAMATERIALS

2.4.1 Introduction

Metamaterials are new artificial materials [28] with unusual electromagnetic properties that are not found in naturally occurring materials. All natural materials such as glass, diamond and other dielectrics have positive electrical permittivity, magnetic permeability and an index of refraction. Metamaterials are artificially fabricated (engineered) materials which are termed as negative index materials (NIM) or double negative (DNG) media or left handed materials (LHM) or backward wave (BW) media .All these material have negative value of electrical permittivity, magnetic permeability and an index of refraction. With these unusual material parameters, new kinds of miniaturized antennas and microwave components or devices can be created for the wireless communications and the defense industries.

2.4.2 Waveguide based metamaterial

Kshetrimayum [29] has proposed that periodic waveguide structures loaded with double strips printed on dielectric exhibit a double negative (DNG) passband where both electrical permittivity and magnetic permeability are negative. The printed periodic waveguide structure also shows negative index of refraction and backward wave propagation.

Fig. 2.20(a) illustrates 3-D geometry of a rectangular waveguide loaded with double strips printed on dielectric layer. There are two possible two-port network representations. One such two-port network representation using three set of impedances Y1, Y2 and Y3 is illustrated in Fig. 2.20(b)

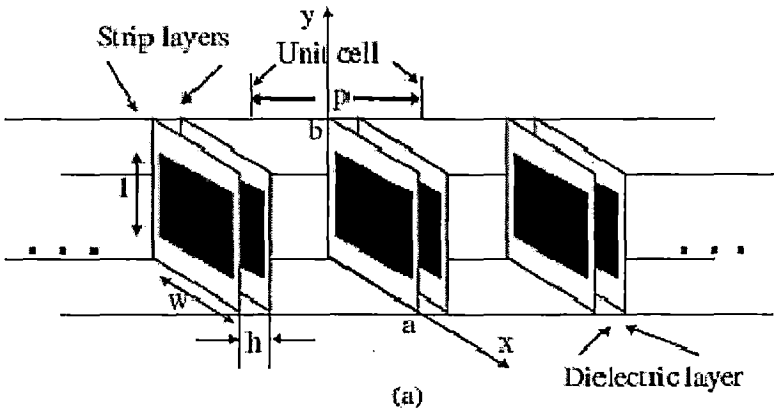

Fig. 2.20(a) Architecture for waveguide based DNG metamaterials [29]

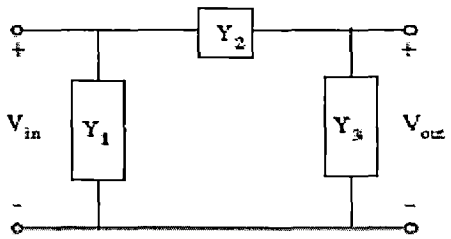

Fig. 2.20(b) Equivalent two-port network representation for a unit cell [29]

In this case if Y_1, Y_3 are inductive and Y_2 is capacitive, this structure behaves as a left handed transmission line network unlike the conventional transmission line in the DNG passband region.

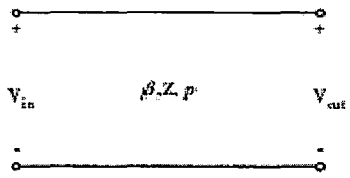

Fig 2.20(c) Two-port network representation of a lossless transmission line (waveguide) of a periodic unit cell

Another approach in two port network realization is the lossless transmission line of length p. Here two-port network representation of a lossless transmission line (waveguide) of length p for a unit cell of the periodic waveguide based structure is shown in Fig. 2.20(c)

In table 2.4 he considered three cases for different values of dimensions of the waveguide, inserts position and their separation and extracted the real permittivity, permeability and index of refraction.

TABLE 2.4 [29]

Dimensions of three cases under investigation of the newly proposed DNG metamaterials					
parameters	W	L	H	P	ε_r
Case I	8.00mm	6.00mm	1.00mm	3.00mm	3.78
Case II	8.00mm	6.00mm	2.00mm	3.00mm	3.78
Case III	8.00mm	6.00mm	1.00mm	3.00mm	7.00

These extracted parameters were plotted. These plots are given in Figs. 2.21, 2.22 and 2.23. From Fig.2.21 corresponding to case I, magnitude of real part of relative permittivity reached its most positive value, i.e., 400 at 10.87 GHz passed through zero at 10.88 GHz and then reached its most negative value, i.e., -1000 at 10.9 GHz. Similar pattern was for case II. However, for case III there was double resonance which could be due to increased electromagnetic interaction between the two printed strips on dielectric whose electrical permittivity was higher than other two previous cases and hence there two DNG passbands were observed.

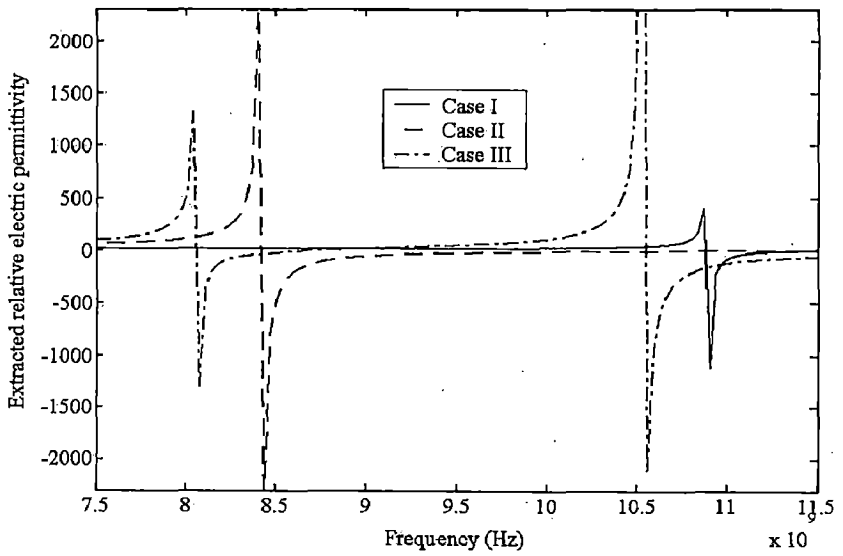

Fig. 2.21 Extracted relative electric permittivity [29]

From Fig.2.22 corresponding to case II magnitude of extracted relative permeability reached its most positive value, i.e., 30 at 8.4 GHz, passed through zero at 8.42GHz and then reached its most negative value, i.e., -30 at 8.45GHz. However for Case I a similar pattern was observed. For case III, again there was double resonance in plot of extracted relative magnetic permeability similar to the case of extracted electric permittivity.

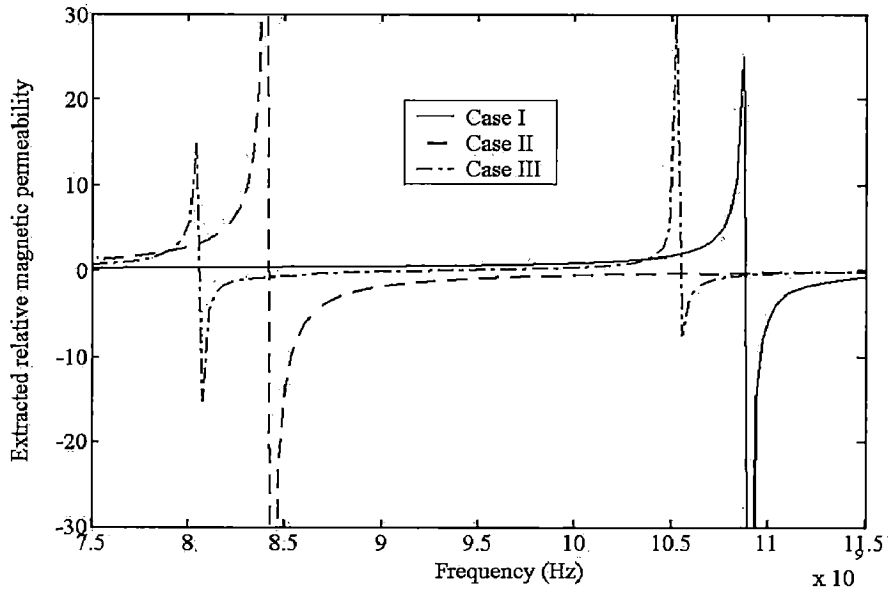

Fig. 2.22 Extracted relative magnetic permeability [29]

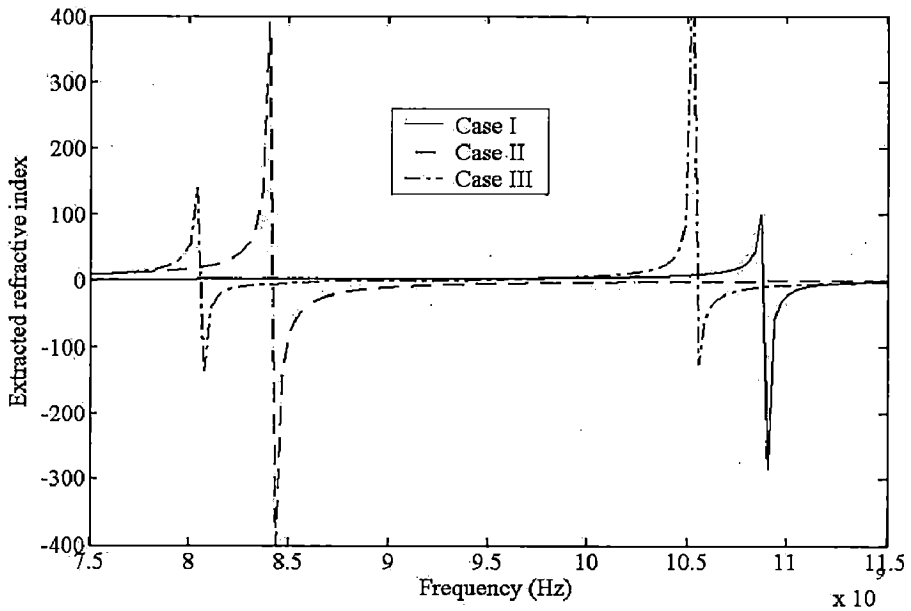

Fig.2.23 Extracted index of refraction [29]

From Fig.2.23 corresponding to case II real part of the amplitude of refractive index reaches its most positive value, i.e., 400 at 8.4GHz, passes through zero at 8.425GHz and then reaches its most negative value, i.e., -400 at 8.43GHz. Similar pattern was observed for case I. For case III, there was double resonance similar to the other cases.

Thus, it is observed that material and wave parameters of a periodic waveguide structure loaded with double printed strips on dielectric exhibit the properties of metamaterials viz., negative electric permittivity, negative magnetic permeability, negative index of refraction and backward wave propagation in the DNG passband region. Also we find that there is a *possibility of improving frequency response by using fractal patches* instead of simple metallic patches.

2.4.3 Application of Fractals in the Design of Metamaterial

Metamaterial can be classified into two groups which are negative permittivity and negative permeability materials. The first class was originally realized by strip wires [12] and the second class by split ring resonators (SRR) [8]. A third class, so-called "Left-handed Materials (LHM)", could be realized with the composition of these two classes. But due to design complexity of these two primary methods and a lot of research in this direction suggested an alternative using fractals.

M. Palandoken [23] et al. had investigated a fractal negative epsilon Metamaterial by using a second order fractal Hilbert curve with mirror symmetry as shown in Fig. 2.24.

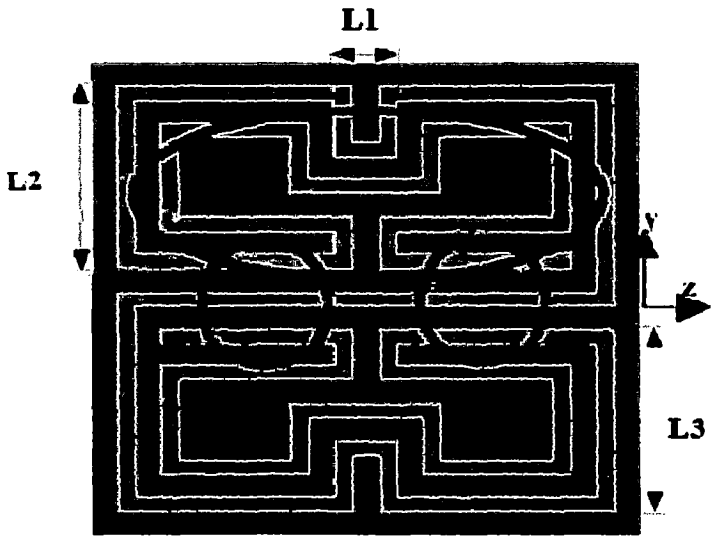

Fig. 2.24 Geometry of negative epsilon Metamaterial [21]

The advantage of using this fractal based design is that due to the absence of slotted SRRs in the ground plane, left handed material (LHM) microwave components with reduced back radiation can be designed on the same substrate layer with magnetic metamaterials.

F. Miyamaru [13] et al. had investigated the electromagnetic response of H-fractal structures, consisting of self similar metallic lines or slits in metallic films deposited on silicon substrate. They generated the H fractal structure shown in Fig. 2.25 and investigated that resonant

frequency can be reduced (or red shifted, i.e., wavelength was increased) by increasing either the fractal level or sample size.

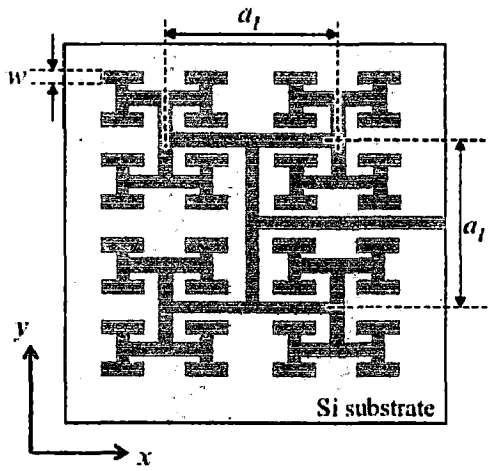

Fig. 2.25 Schematic picture of an enlarged part of the fractal metamaterial structure[13]

Thus, it is evident that using fractals in the design of metamaterial we can obtain a design that will work on red shifted frequencies without increasing sample size that can be costlier for certain designs.

CHAPTER – 3

Design of Waveguide Filter

In this chapter, the design methodology, simulation and experimental results of a fractal waveguide band-pass filter are presented.

3.1 Design Methodology of Fractal Waveguide Band Pass Filter

In this dissertation a waveguide filter is designed which has two pass-bands in 7-16GHz frequency range. For this we introduce two closely coupled fractal resonant apertures inside a waveguide at certain lengths [30]. This type of placement of two fractal apertures causes a filtering behaviour in which filtered bands have center frequencies as the earlier resonant frequencies. However, width of these pass bands can be controlled by choosing the separation of the apertures appropriately. Since we have to get two frequency bands therefore, we will select a fractal aperture which will be having two resonant frequencies in this band. In this design therefore, we have used a 2nd iterated modified Devil's staircase fractal as shown in Fig. 3.1. Generation procedure for devil's staircase fractal can be referred from sec. 2.1.3 and later it can be modified. Resonant behaviour of modified devil's staircase fractal is investigated in [31]. In [31] a 3rd iterated modified devil's staircase fractal was presented which was having three resonant frequencies between the 7-16GHz frequency band. Therefore, in contrast we have used a 2nd iterated devil's staircase fractal which will be having two resonant frequencies in 7-16 GHz frequency band since, iterations are scaled down to two instead of three.

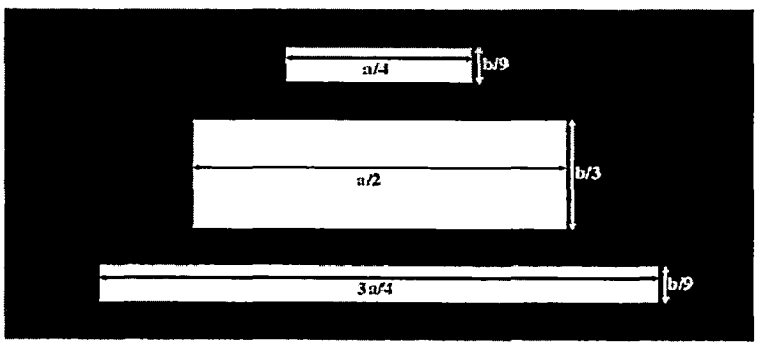

Fig. 3.1 A 2nd Iterated Modified Devil's Staircase Fractal

In this design we have used WR90 waveguide sections for which a = 22.86 mm and b = 10.16mm. If waveguide dimensions are a and b (as usual) then, central aperture is a/2 in length and b/3 in width, upper aperture is a/4 in length and b/9 in width and lower aperture is 3a/4 in length and b/9 in width. These dimensions are standard ones for modified devil's staircase [31]. However, we can play with these dimensions to get desired passbands, for this suppose if we want the centre frequencies of passbands (or resonant frequencies of fractal aperture) to be separated by a factor 's' (say) then, either we have to modify the dimensions of these apertures or we have to use another fractal so that resulting fractal structure has the scale factor as 's'[18].

Now, we insert two such fractal apertures inside a waveguide one at a distance l_1 and other at a distance l_2 from this. In addition waveguide extends to a length l_1 more. The transmission line equivalent is shown in Fig. 3.2 where the fractal apertures are replaced by equivalent shunt susceptances if located l_2 distance apart.

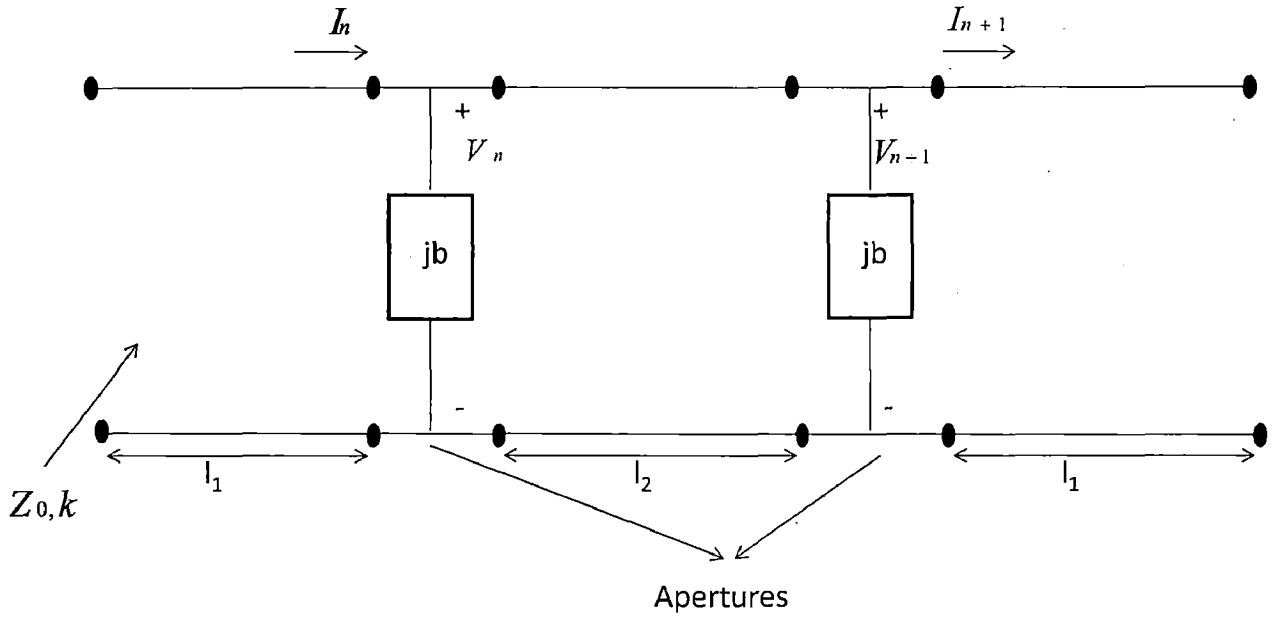

Fig. 3.2 Equivalent 2-Port Network Presentation

In normalized form we can obtain the ABCD matrix for the given two port network by cascading the ABCD matrix of a transmission line section of length l_1, a shunt susceptance, a transmission line section of length l_2, a shunt susceptance and a transmission line section of length l_1 [32]. In this way we can write ABCD matrix for the complete structure as.

$$\begin{bmatrix} A & B \\ C & D \end{bmatrix} = \begin{bmatrix} \cos\theta_1 & j\sin\theta_1 \\ j\sin\theta_1 & \cos\theta_1 \end{bmatrix} * \begin{bmatrix} 1 & 0 \\ jb & 1 \end{bmatrix} * \begin{bmatrix} \cos\theta_2 & j\sin\theta_2 \\ j\sin\theta_2 & \cos\theta_2 \end{bmatrix}$$

$$* \begin{bmatrix} 1 & 0 \\ jb & 1 \end{bmatrix} * \begin{bmatrix} \cos\theta_1 & j\sin\theta_1 \\ j\sin\theta_1 & \cos\theta_1 \end{bmatrix} \quad (3.1)$$

Where θ_i ($\forall\ i = 1, 2$) are the electrical lengths of the line sections defined as $\theta_i = kl_i$, where k is the propagation constant and l is the physical length of the line. From the ABCD matrix S parameters for this network can be obtained from equations (3.2) and (3.3) [32]:

$$|S_{11}| = |S_{22}| = \frac{A + \frac{B}{Z_0} - \frac{C}{Z_0} - D}{A + \frac{B}{Z_0} + \frac{C}{Z_0} + D} \quad (3.2)$$

$$|S_{12}| = |S_{21}| = \frac{2}{A + \frac{B}{Z_0} + \frac{C}{Z_0} + D} \quad (3.3)$$

3.2 Design Procedure and Simulation Results

First we simulate this aperture using HFSS to obtain the shunt susceptance 'b' [Appendix B] of the fractal aperture at different frequencies in the frequency range of 7 to 16 GHz. Once we are in possession of this data we calculate the ABCD parameters using MATLAB code [Appendix A], [33] and hence S parameters (S_{11} and S_{21}) for our design at these frequencies. Later, parametric analysis for the lengths l_2 is performed using MATLAB to obtain the optimized result in order to get the desired widths of pass-bands. Here, use of MATLAB is advantageous in the sense that it saves a lot of simulation time when we repeatedly change the length l_2 and that is why we have not done the whole simulation on HFSS. In contrast, changing l_1 and l_3 does not affect the plots of these scattering parameters ($|S_{11}|$ and $|S_{21}|$) since, separation of aperture is responsible for the width of pass-bands [26,30]. On this basis, for different values of l_2 (aperture separation) plots of scattering parameters ($|S_{11}|$ and $|S_{21}|$) as a function of frequency are given in Figs. 3.3 and 3.4. Here, we can clearly see our two pass-bands. Under the fabrication limitations, out of these plots, we have chosen the one with

respect to l_2 (aperture separation) = 6mm, l_1 may have any value. In this design we have taken l_1 = 35mm.

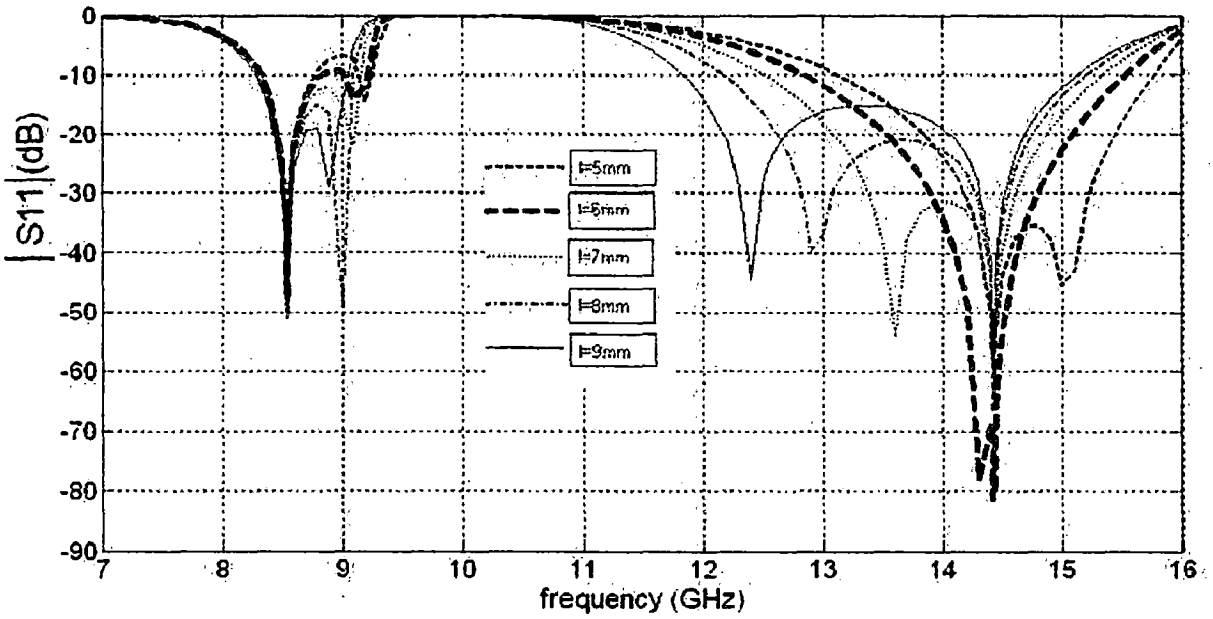

Fig. 3.3 Plot of $|S_{11}|$ for waveguide filter

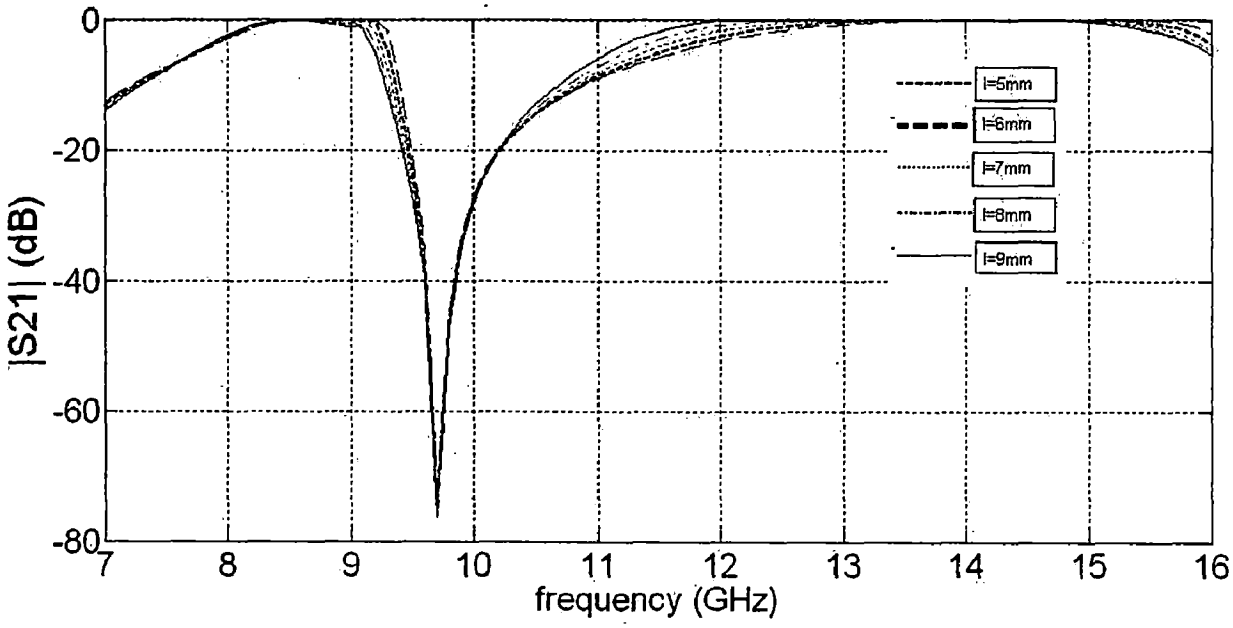

Fig. 3.4 Plot of $|S_{21}|$ for Waveguide Filter

For these values, if this waveguide filter is operated between 7 to 16 GHz. It will pass two bands from 8.4 to 9.2 GHz and 13 to 15.5 GHz, as shown in Figs. 3.5 and 3.6.

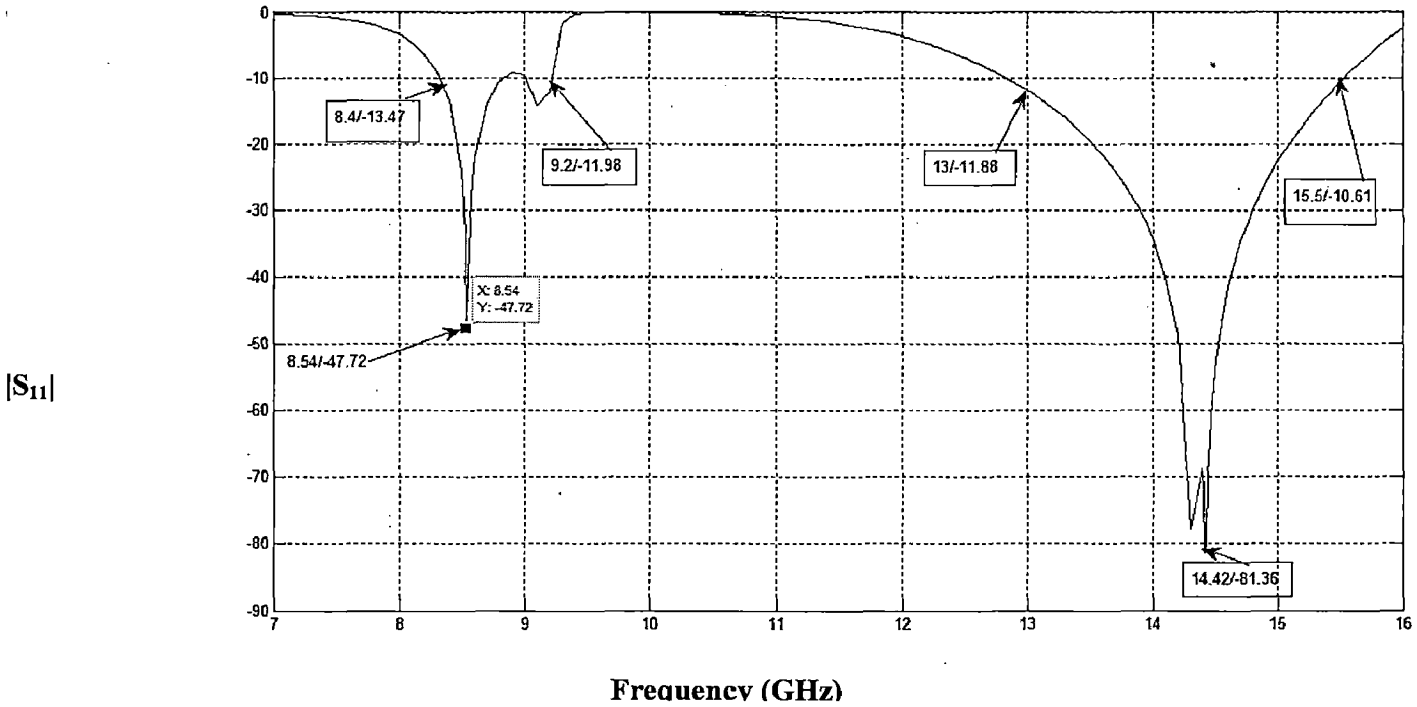

Fig. 3.5 Plot of $|S_{11}|$ for Waveguide Filter

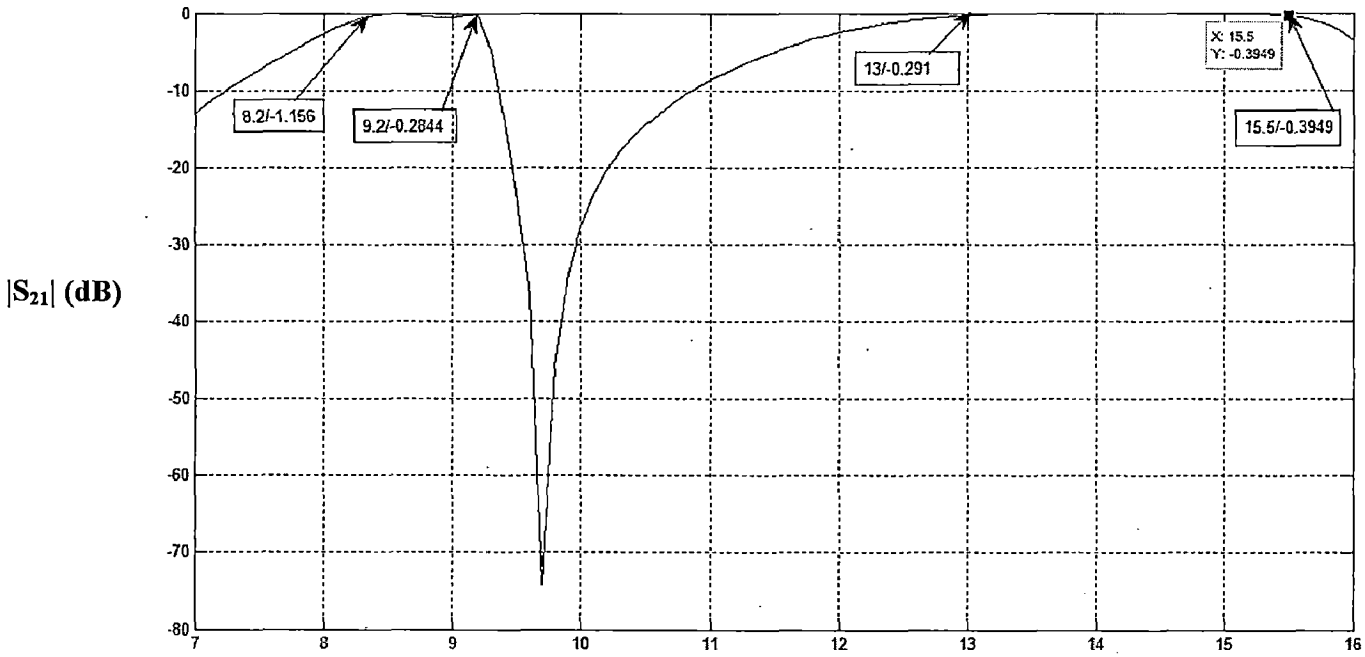

Fig. 3.6 Plot of $|S_{21}|$ for Waveguide Filter

3.3 Flow Chart for Designing Waveguide Filter

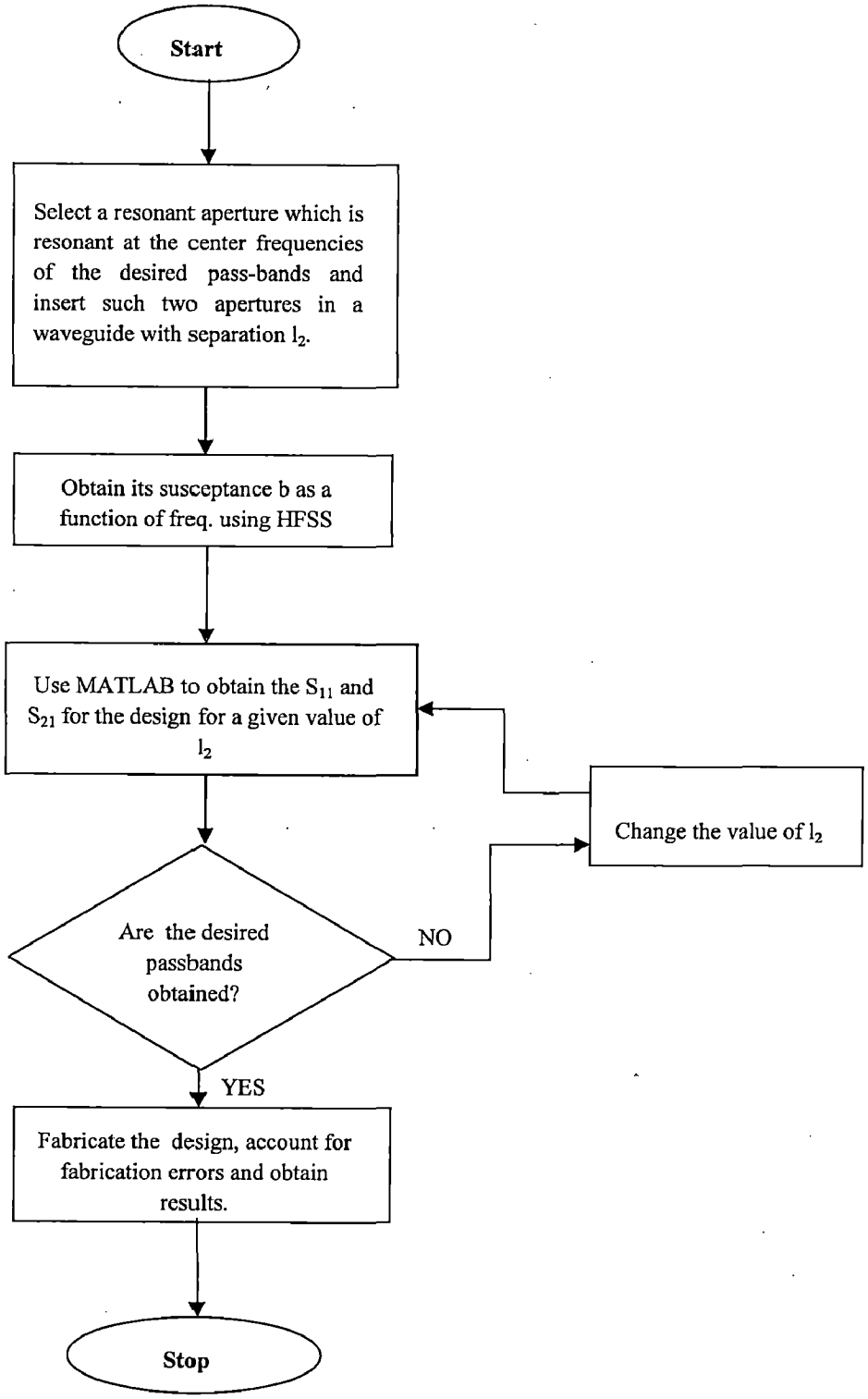

3.4 CST Simulation of Waveguide Filter

Besides above approach we have used CST to simulate our design directly and cross checked the validity of our above approach to design the waveguide filter. For this, we place two

apertures closely coupled as shown in Fig. 3.7 and simulate the resulting structure using Transient Field Solver of CST. We get S_{11} and S_{21} as shown in Figs. 3.8 and 3.9 respectively.

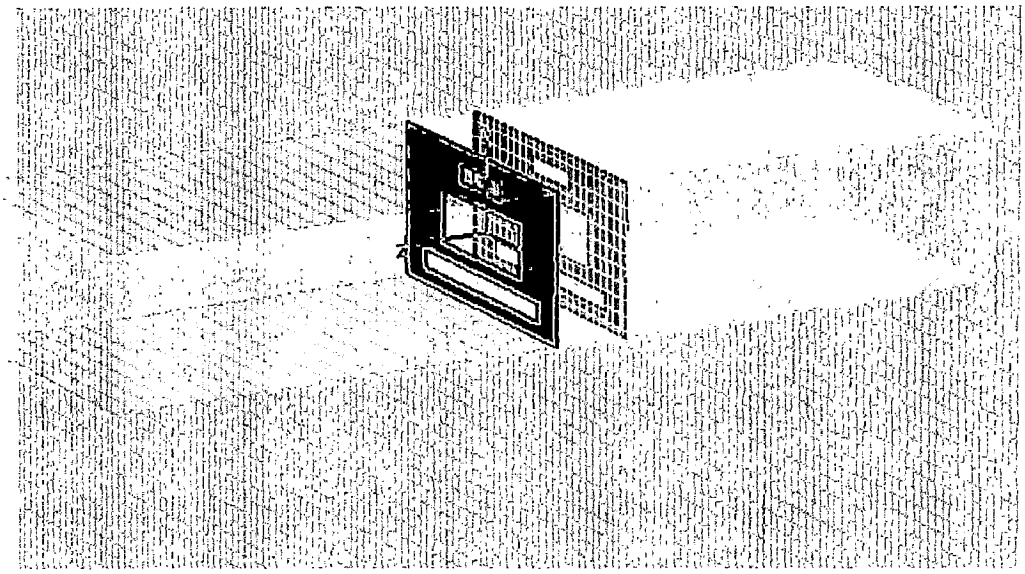

Fig. 3.7 CST Simulated Model of Waveguide Filter

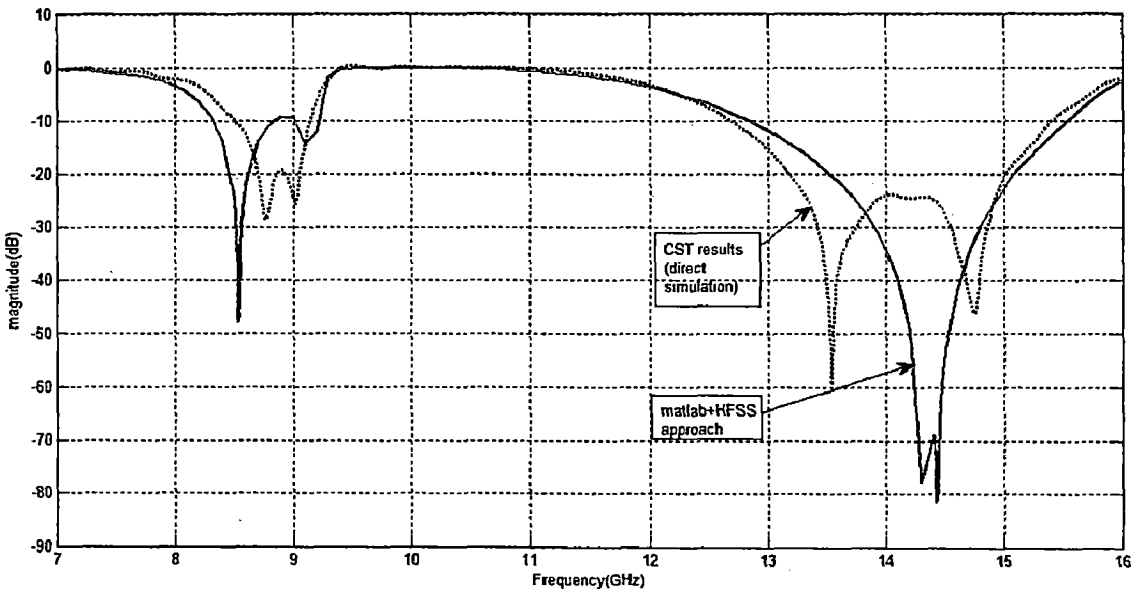

Fig. 3.8 Plot of $|S_{11}|$ Vs Frequency

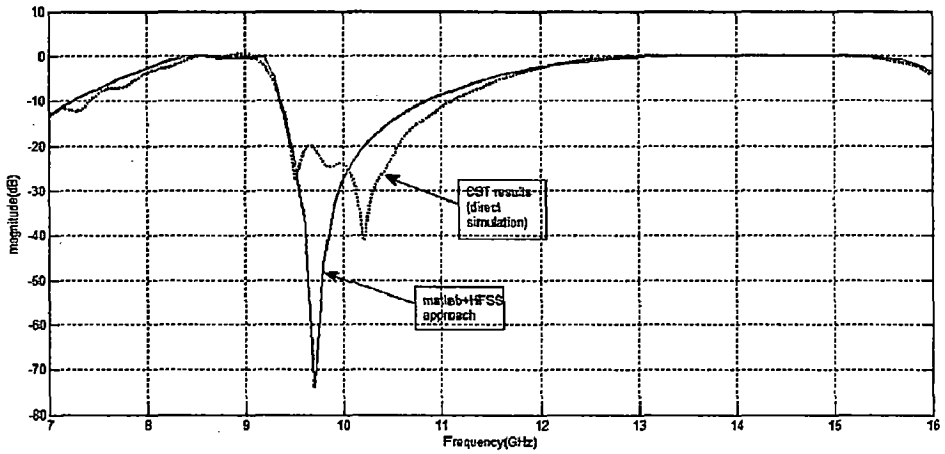

Fig. 3.9 Plot of $|S_{21}|$ Vs Frequency

The proximity of the results in above two approaches leads to the validation of our two port network approach for designing the waveguide filter. However, there is some difference in the two results which is due to the fact that the 2-port network approach does not take into account effectively the presence of higher order waveguide modes, which may affect the susceptance of the two apertures due to their close proximity. However, this approach offers an advantage in terms of saving simulation time, since several time consuming simulations will be required if the electromagnetic simulator is used to arrive at the optimized result.

3.5 Experimental Results

The photograph of complete fabricated structure of waveguide filter is shown in Fig. 3.10.

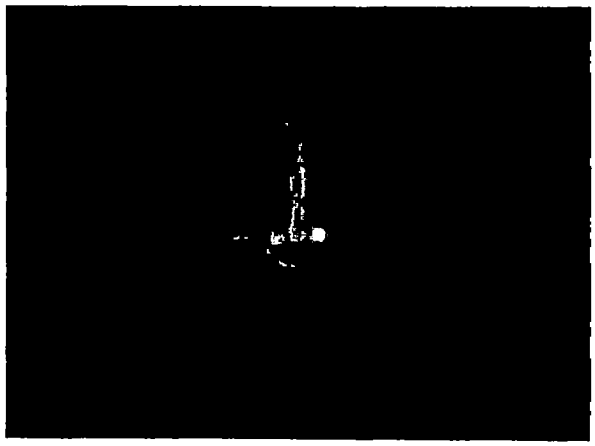

Fig. 3.10 Photograph of Fabricated Waveguide Filter

Frequency response of fabricated waveguide filter has been experimentally measured on vector network analyzer (VNA). Measurement setup for this experiment is shown in Fig. 3.11.

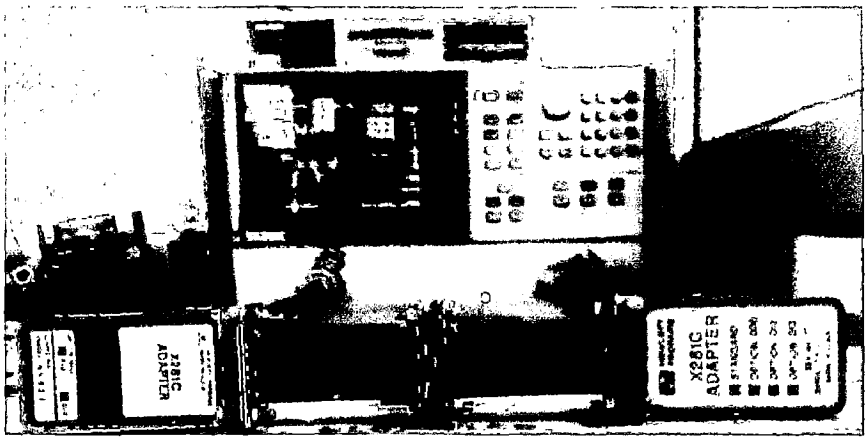

Fig. 3.11 Measurement Setup for Waveguide Filter

In this observation, we observe S_{11} and S_{21} only on the screen of the VNA because $S_{11}=S_{22}$ (by symmetry) and $S_{21}=S_{12}$ (by reciprocity).The plots of these scattering parameters S11 and S_{21} are given in Figs. 3.12 and 3.13 respectively.

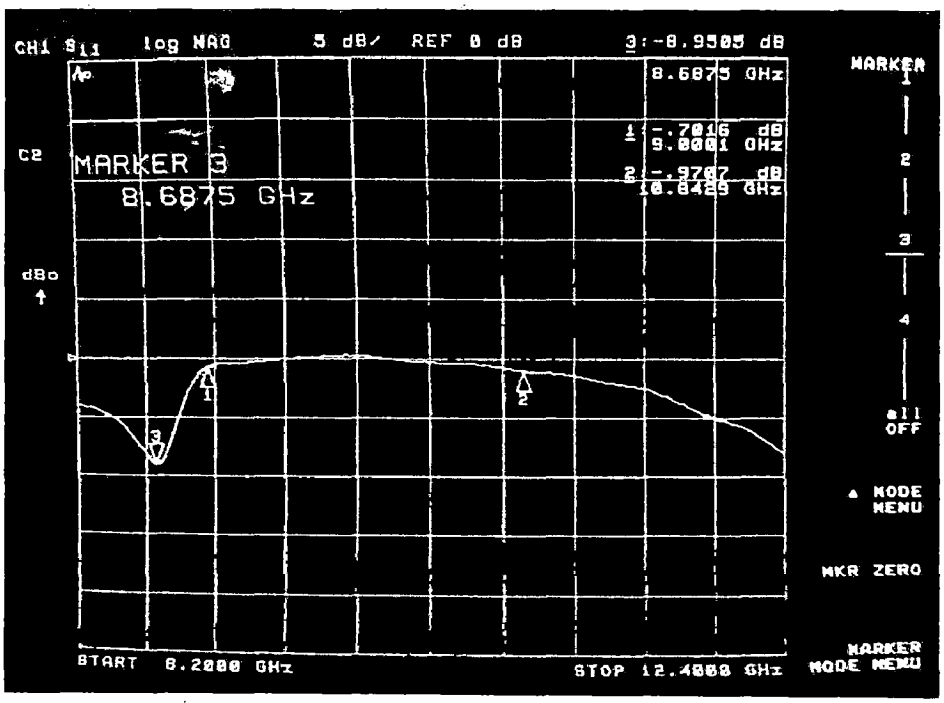

Fig. 3.12 Plot of $|S_{11}|$ Vs Frequency

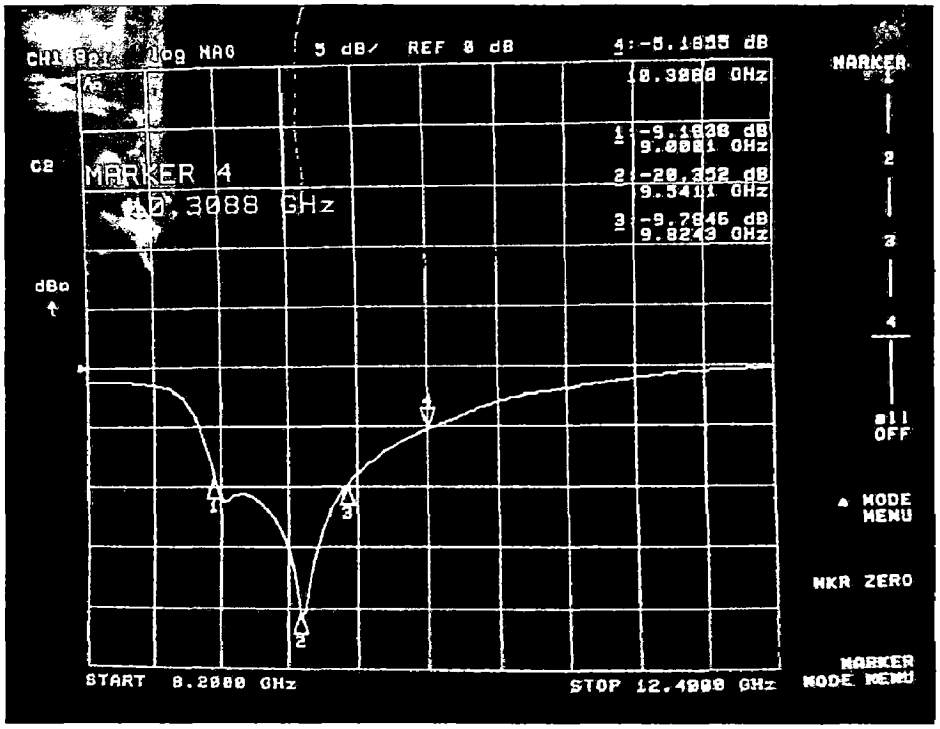

Fig. 3.13 Plot of $|S_{21}|$ Vs Frequency

The above shown scattering parameters were measured over the frequency band 8.2-12.4 GHz (X- band) but our filter is designed to have two pass band bands between 7 -16 GHz. So in order to measure frequency response over the whole frequency range for which the filter has been fabricated, we have used microwave power source and microwave power meter to measure the frequency response of the filter. Measurement setup for this is shown in Fig. 3.14.

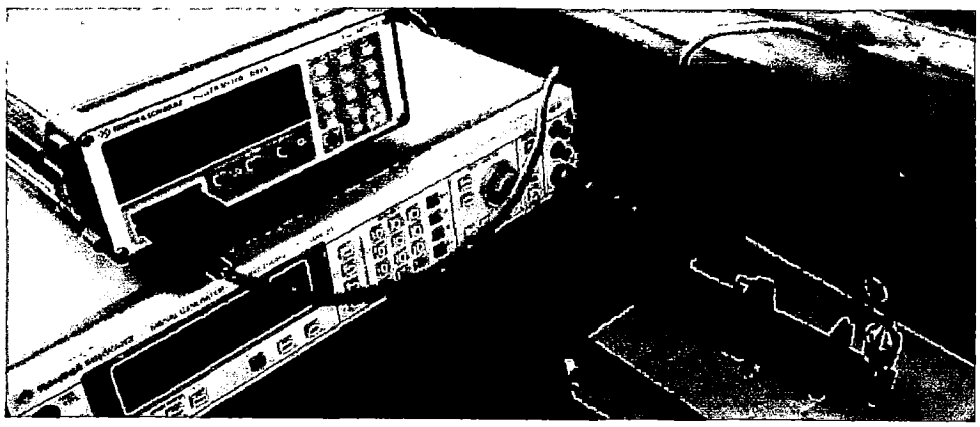

Fig. 3.14 Measurement Setup for Waveguide Filter

For a two-port network with input power P_{in} and output power P_{out}, by the definition of insertion loss we have [32]:

$$\frac{P_{out}}{P_{in}} = |S_{21}|^2$$

or

$$10 \log P_{out} - 10 \log P_{in} = 20 \log|S_{21}|$$

and if P_{in}=1mW (0dBm) then

$$10 \log P_{out} = 20 \log|S_{21}|$$

Thus, we can say that plot of power output power (dB) will be same as that of plot of magnitude of scattering parameter $|S_{21}|$ (dB). Therefore, we have calculated the power output at 0dBm power input to predict the nature of plot ($|S_{21}|$). This plot is given in Fig. 3.15.

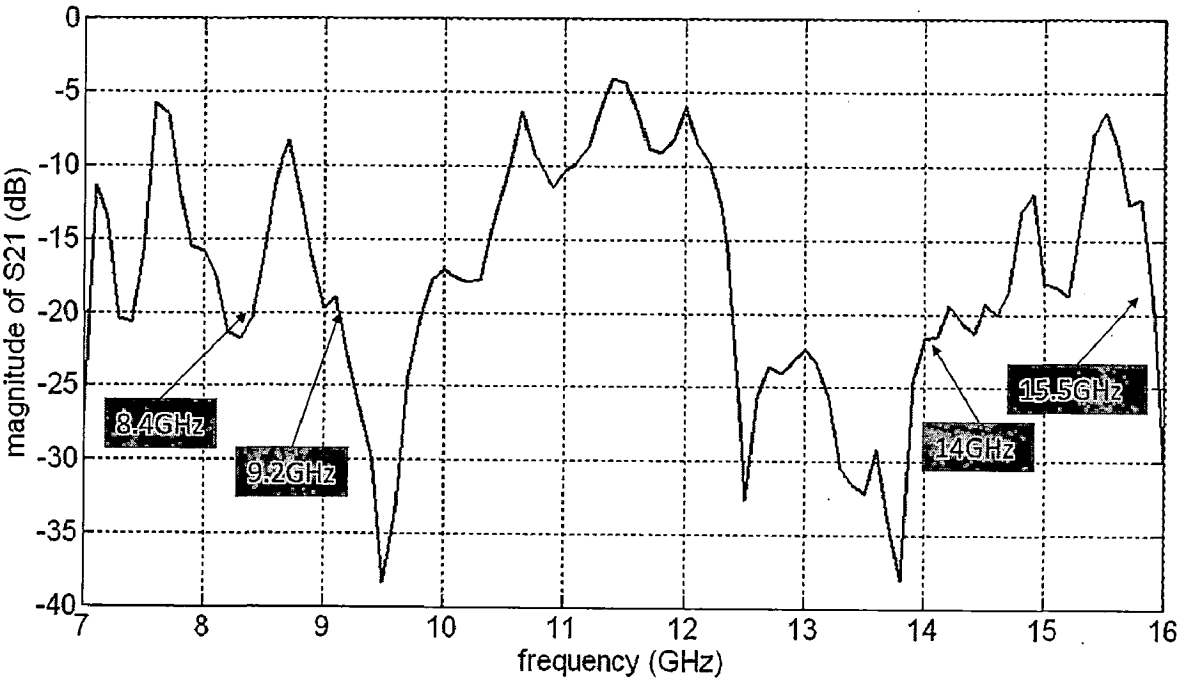

Fig. 3.15 Plot of $|S_{21}|$ Vs Frequency

Thus, if we compare the results between 8.2 to 12.4 GHz measured using VNA and power meter we see that nature of plots is same. However, 3 to 4 dB difference is there, which is due to the losses in the coaxial to waveguide adapter, that is used to couple the power source to the waveguide filter, and then waveguide filter to the power meter. Further, these adapters may have their own frequency response in this frequency range which is also responsible for the discrepancies in the results. In addition, these figures show that waveguide filter has two pass-bands between 8.4 to 9.2 GHz and 14 to 15.5 GHz (ref. Fig. 3.15). Therefore, on the basis of second measurement, we can predict that the designed waveguide filter has two pass bands between 7-16 GHz.

CHAPTER – 4

DESIGN OF WAVEGUIDE POWER DIVIDER

In this chapter we present the design methodology for the design of a waveguide power divider. Simulation results along with experimental results for the designed waveguide power divider are also presented.

4.1 Design Methodology of Waveguide Power Divider

Waveguide power divider has been designed using an H plane waveguide Tee junction. Normally H-plane Tee junction plays the role of a tight coupler. Consider the H plane tee shown in Fig. 4.1.

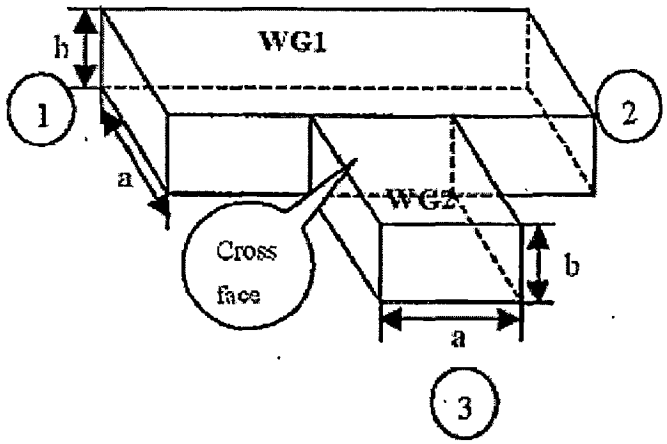

Fig. 4.1 Conventional H Plane Tee junction [19]

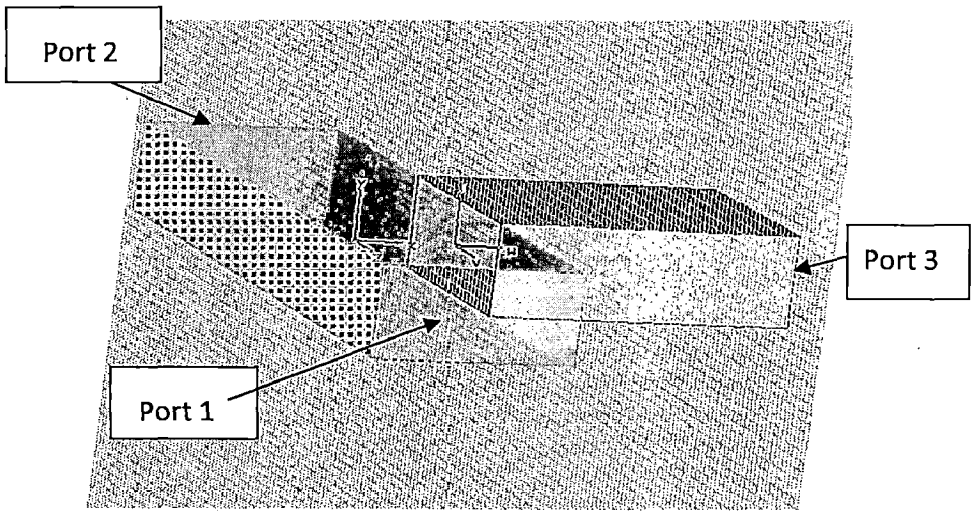

Fig. 4.2 CST Simulated Model of H Plane Tee junction

In this junction, if power incident on port-1 is P_1 and power out at port-2 and port-3 is P_2 and P_3 respectively then we can say that [32]:

$$\frac{P_2}{P_1} = |S_{21}|^2 \tag{4.1}$$

$$\frac{P_3}{P_1} = |S_{31}|^2 \tag{4.2}$$

From this relationship we can say that power out at port-2 depends on $|S_{11}|$ and $|S_{21}|$ and power out at port-3 depends on $|S_{11}|$ and $|S_{31}|$. Further, in addition to see the actual power coupled to the ports, we have performed the full-3 port analysis of this junction on CST Microwave Studio. Results obtained are shown in figs. 4.3, 4.4, 4.5 and 4.6.

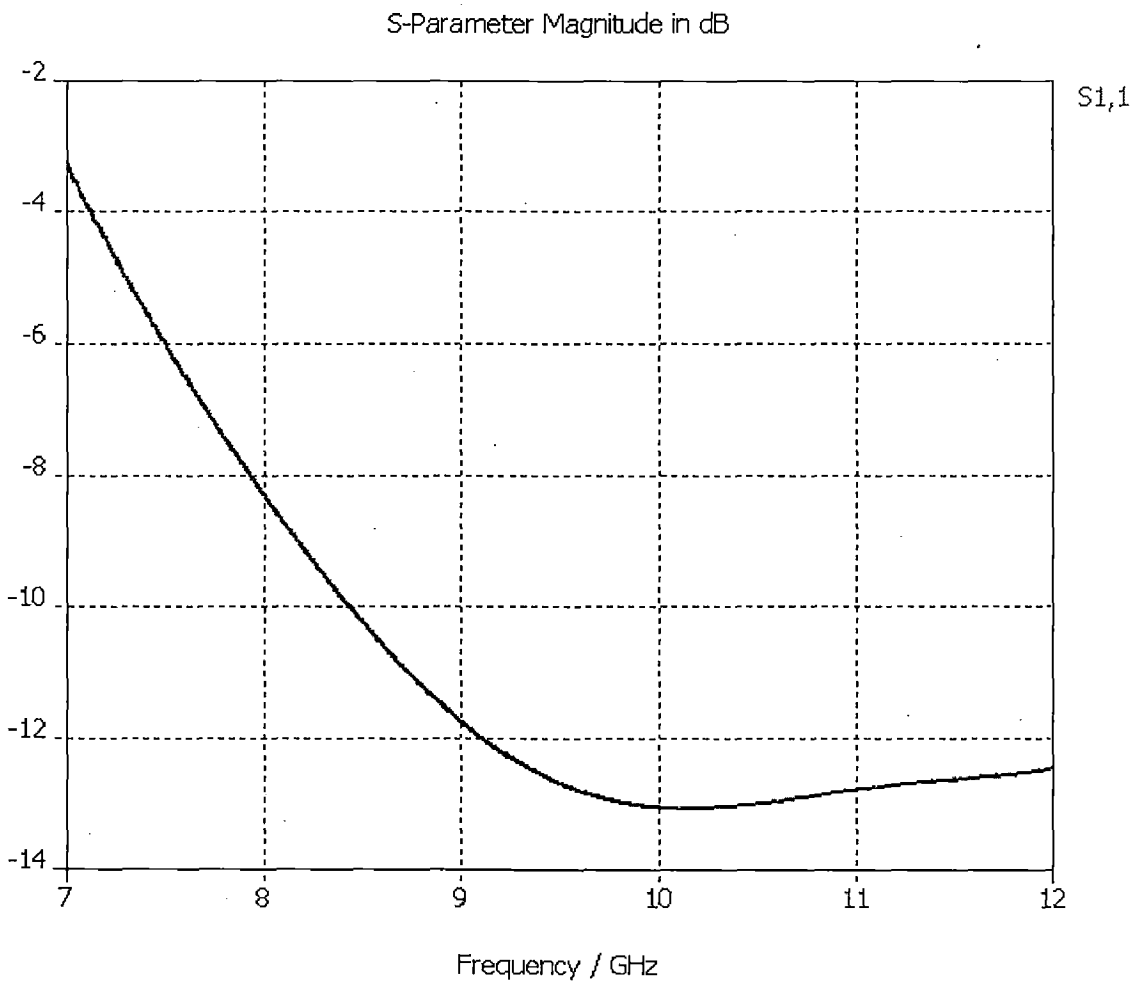

Fig. 4.3 CST Simulated $|S_{11}|$ for Conventional H-plane Tee junction

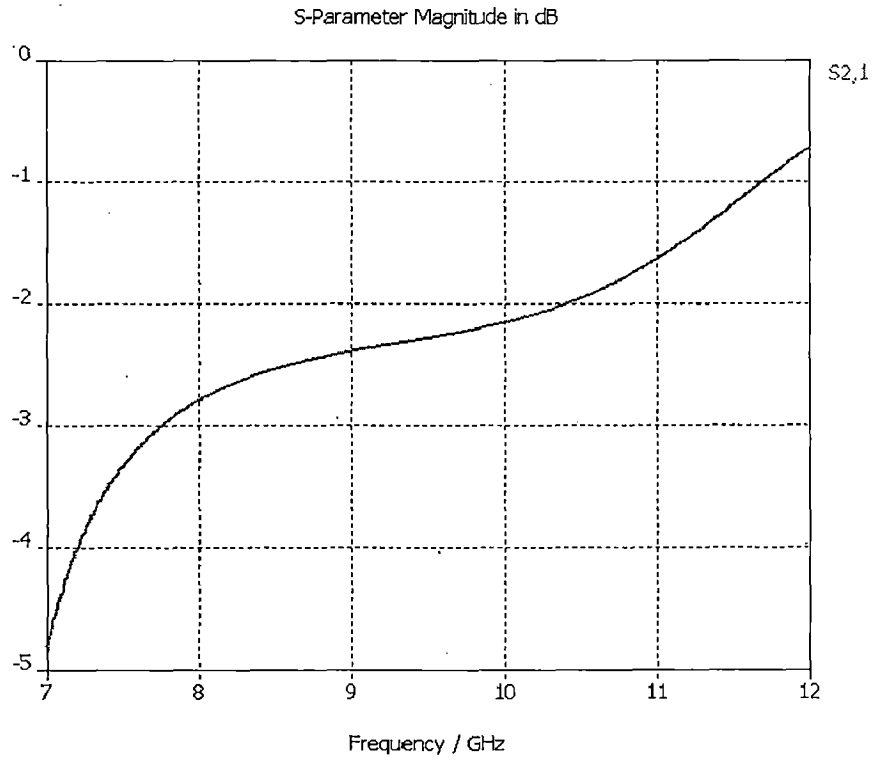

Fig. 4.4 CST Simulated $|S_{21}|$ for Conventional H-plane Tee junction

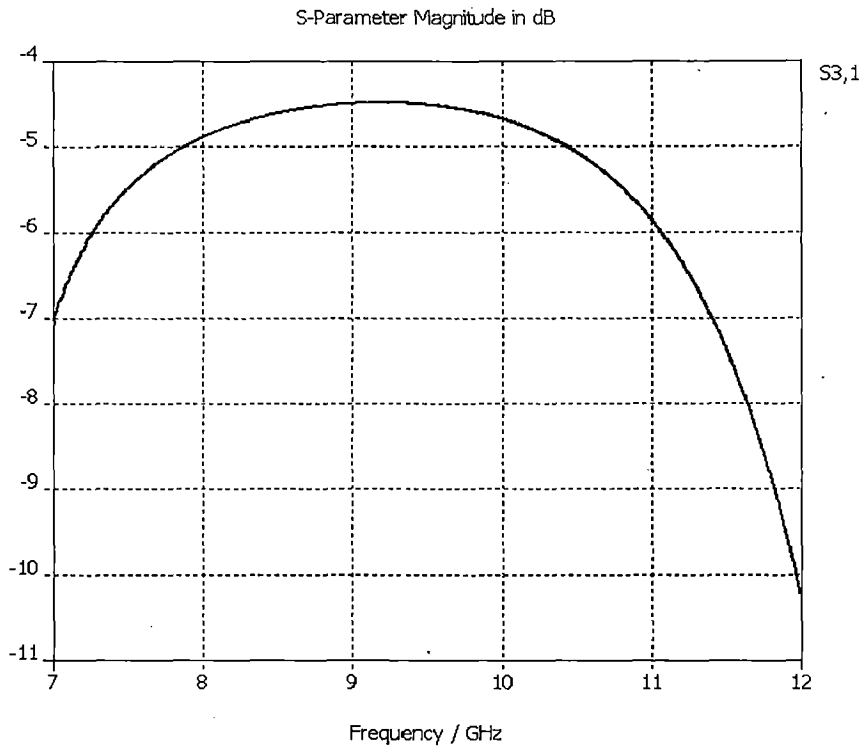

Fig. 4.5 CST Simulated $|S_{31}|$ for Conventional H-plane tee junction

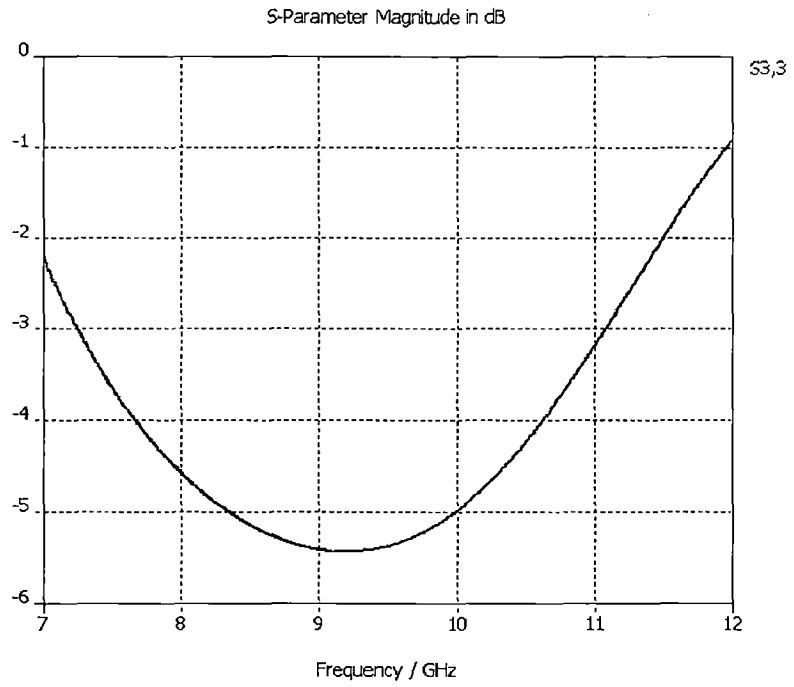

Fig. 4.6 CST Simulated $|S_{33}|$ for Conventional H-plane Tee junction

From these results, if we take an arbitrary frequency point 8.5 GHz (say) then corresponding to this frequency we have $|S_{11}| = -10$ dB (0.3162), $|S_{21}| = -2.5$ dB (0.7499) and $|S_{31}| = -4.7$ dB (0.5821). Therefore, at this frequency $P_2/P_1 = (0.7499)^2 = 0.5625$ (approx) and $P_3/P_1 = (0.5821)^2 = 0.3388$ (approx) (ref. eqs. 4.1 and 4.2) and rest power $|S_{11}|^2P_1 = 0.09$ is reflected back on port-1. Now, if somehow we can control the power going into the cross face (H-arm) to obtain desired coupling ratio, then we can use this junction as a waveguide power divider. As a matter of fact if we introduce an aperture in the cross face (H-arm) then for the resulting structure, it is evident that the power going (coupled) into the H-arm will be reduced and the properties of the aperture will control the amount of power coupled. Therefore, in this way we can use this H-plane tee junction as waveguide power divider. In addition, due to the resonant behaviour of apertures this coupling mechanism will have a particular frequency range for which coupling will be enhanced. So for obtaining a multiband behaviour we have used fractals.

4.2 Design Procedure and Simulation Results

Since fractal apertures exhibit multiband transmission property, it is evident that it is possible to design a multiband w/g power divider by placing a fractal diaphragm in the H-arm. In this

design, therefore, we have taken fractal diaphragms and inserted them in the H-arm of H-plane tee junction and optimization is done on CST Microwave Studio, for the desired power in the respective arms. In this work, we optimize the design for power to be divided in 10:1 ratio i.e. 1/10 of input power goes to port-3 and remaining 9/10 to port-2. For this we have to make a compromise between the values of $|S_{11}|$, $|S_{21}|$ and $|S_{31}|$ in order to obtain the desired value of power in respective arms. Therefore, first we have inserted 2nd iterated plus shape fractal aperture in the cross face (H-arm) of H-plane tee junction [31]. However, any fractal geometry, which is resonant in the desired frequency band of operation, can be used instead of this, but due to ease of fabrication, we have chosen this one. To obtain both the bands in desired frequency range we have changed the scale factor of the fractal geometry from 0.7 to 0.5 [31]. Scale factor modified fractal geometry is shown in fig. 4.7.

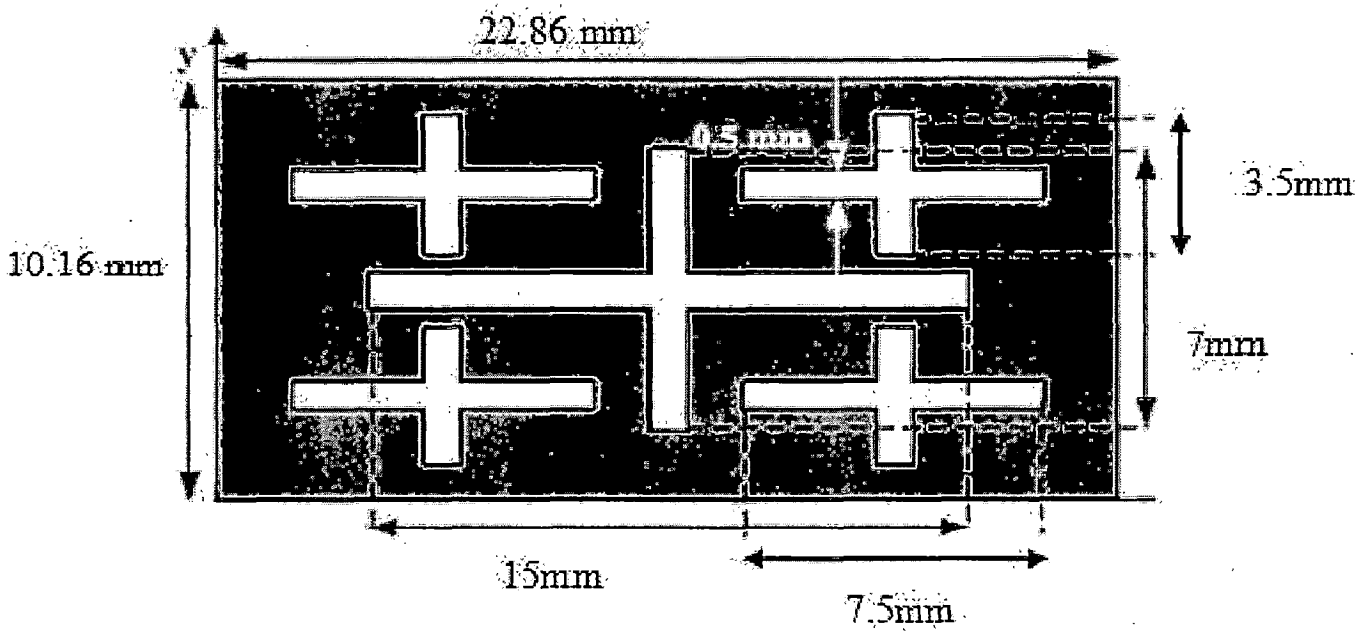

Fig. 4.7 Dimensions of 2nd Iterated Plus Shaped Fractal Aperture

Firstly, we have inserted a single aperture in the H-arm of H-plane tee junction at a fixed distance d from the junction and by repeated simulations we find that there does not exist any value of this distance d for which we obtain desired results. However, by these repeated simulations we observe that frequency response of this structure does not change much as we move away from the junction and after a distance of 6mm from the junction results are almost independent of d. Simulated model corresponding to the aperture location in the H-arm at 6mm is shown in fig. 4.8 and extracted full 3-port scattering parameters are shown in fig. 4.9.

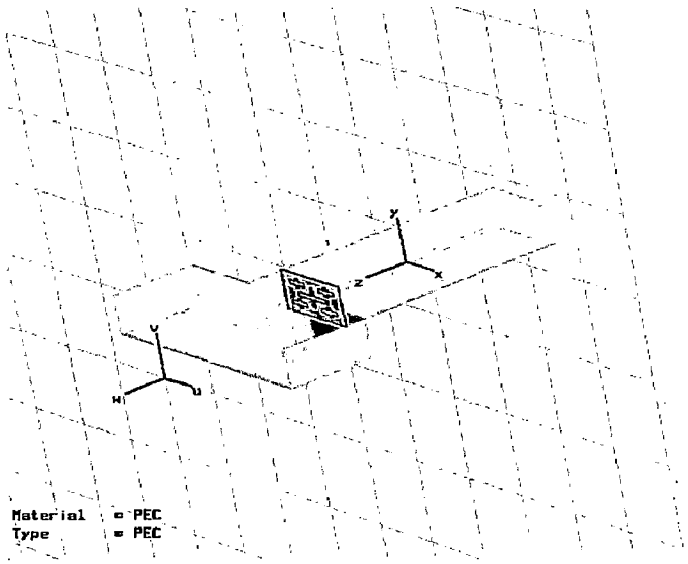

Fig. 4.8 CST Simulated Model of Power Divider

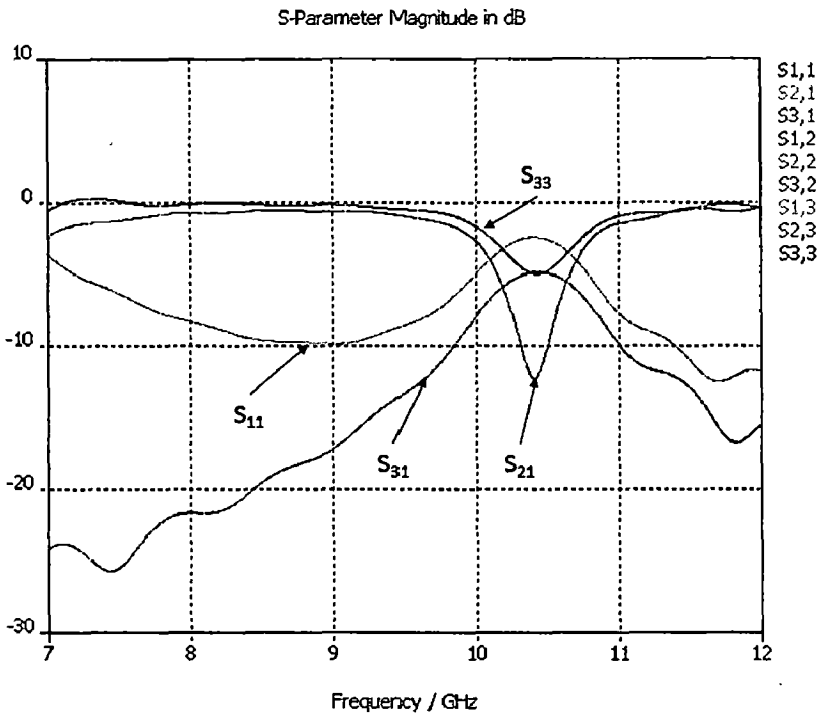

Fig. 4.9 CST Simulated Scattering Parameters of Power Divider

Since, single aperture does not give desired results so we further modify this design by inserting two apertures in the H-arm and optimize their relative positions using CST Microwave Studio. Optimized parameters are given in table 4.1

TABLE 4.1 Design Specifications of Power Divider

Length of main guide(mm)	70
Length of H arm(mm)	58
Distance of first aperture from junction in port-3(mm)	18
Distance of second aperture from junction in port-3(mm)	38

CST simulated model of this power divider is shown in Fig. 4.10 and simulated results of scattering parameters S_{11}, S_{21}, S_{31} and S_{33} are shown in Figs. 4.11, 4.12, 4.13 and 4.14 respectively.

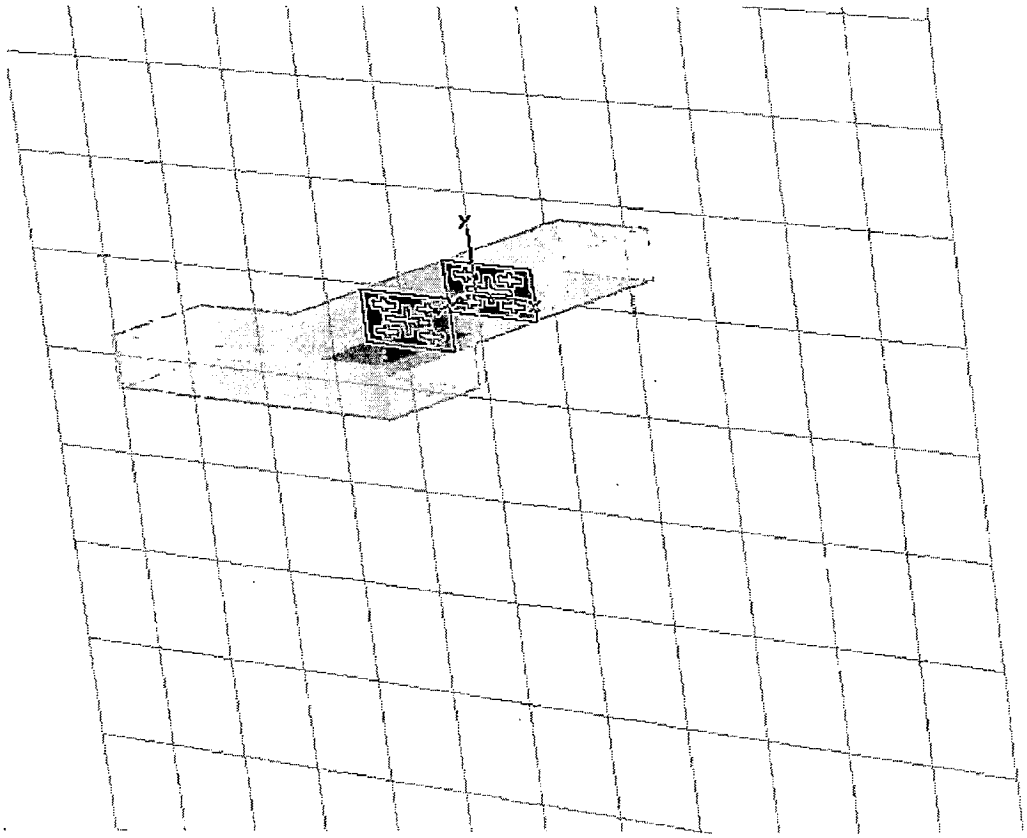

Fig. 4.10 CST Simulated Model of Power Divider

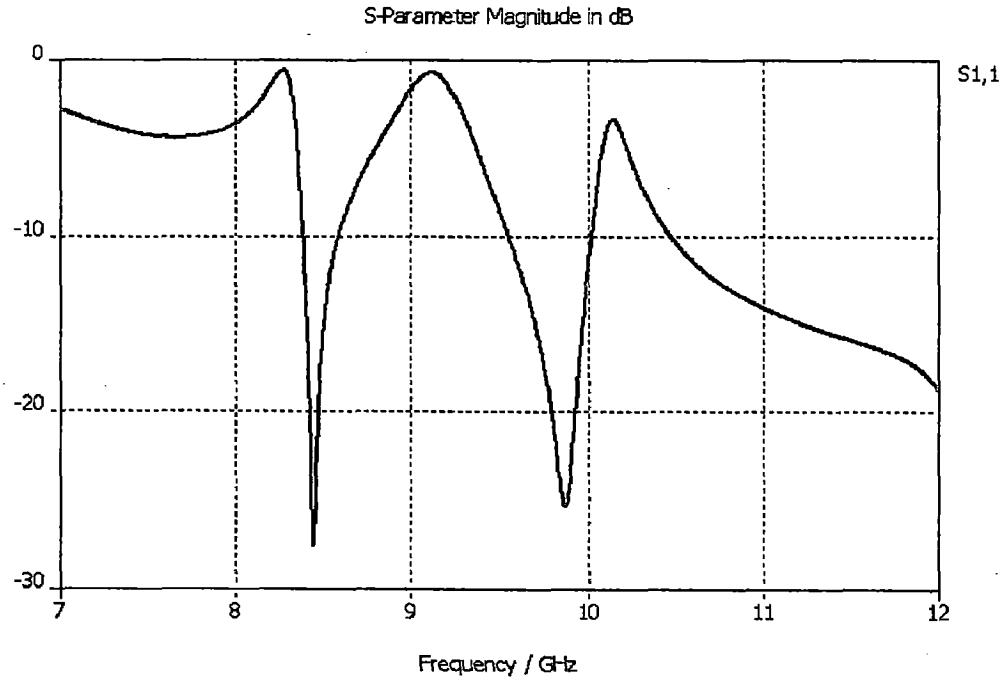

Fig. 4.11 $|S_{11}|$ Vs Frequency

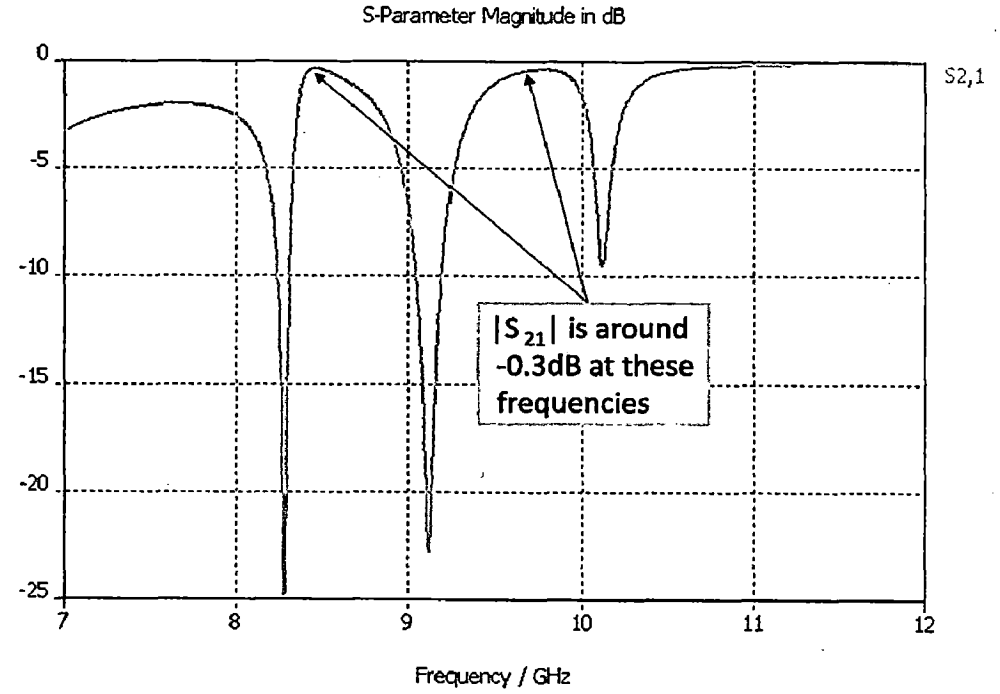

Fig. 4.12 $|S_{21}|$Vs Frequency

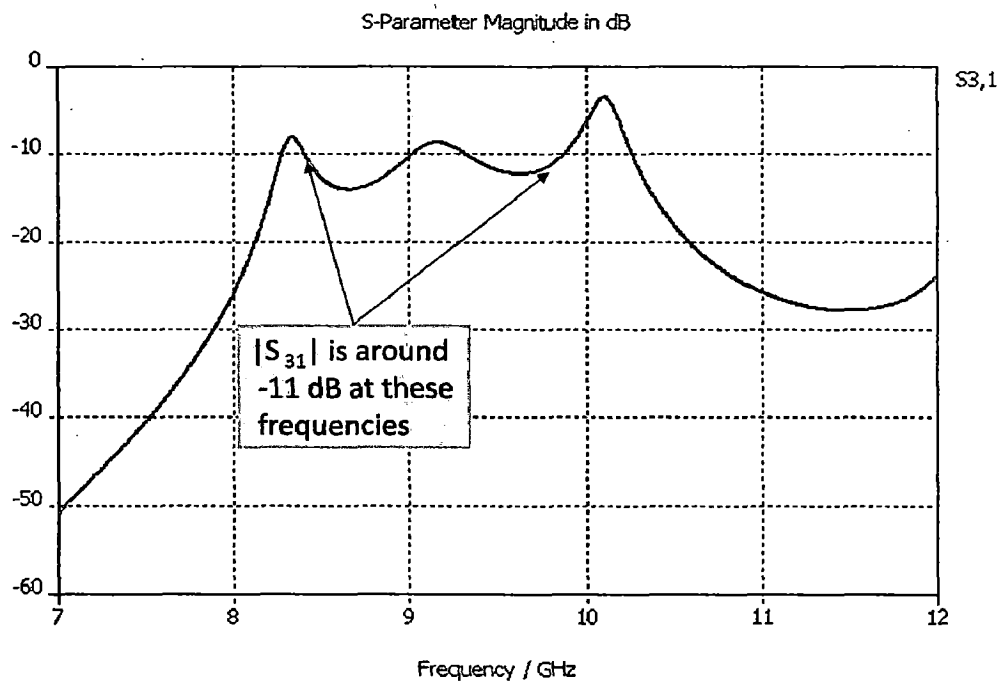

Fig. 4.13 $|S_{31}|$Vs Frequency

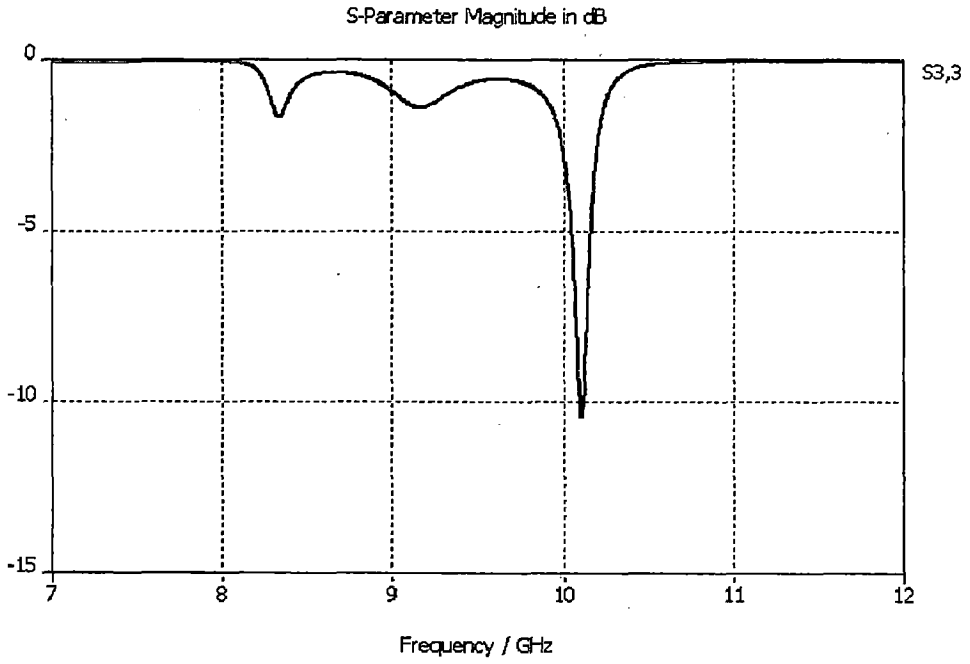

Fig. 4.14 $|S_{33}|$Vs Frequency

These simulated scattering parameters shows that by using 2nd iterated fractal we have obtained two frequencies (8.5 GHz, 9.9 GHz), for which this H plane power divider has the desired behaviour, since here P_2/P_1= 0.9 (-0.3dB) and P_3/P_1= 0.095 (-11dB). (ref. eqs. 4.1 and 4.2, and figs. 4.12 and 4.13) and therefore, it can be used as a waveguide power divider which has two frequencies for which power is being divided in 10:1 ratio.

4.3 Experimental Results

The power divider proposed in the previous section was fabricated and its frequency response was measured on Vector Network Analyzer (VNA). Measurement setup is shown in figs. 4.15 (a) and (b).

For this first we connect matched load at the end of H-arm of the power divider and measure two port parameters S_{11} and S_{12} since S_{22} will be same as S_{11} and S_{21} will be same as S_{12} by symmetry and reciprocity (ref. Figs. 4.2 or 4.1). Plots of measured S_{11} and S_{12} are given in figs. 4.16 and 4.17 using measurement setup shown in fig. 4.15 (a).

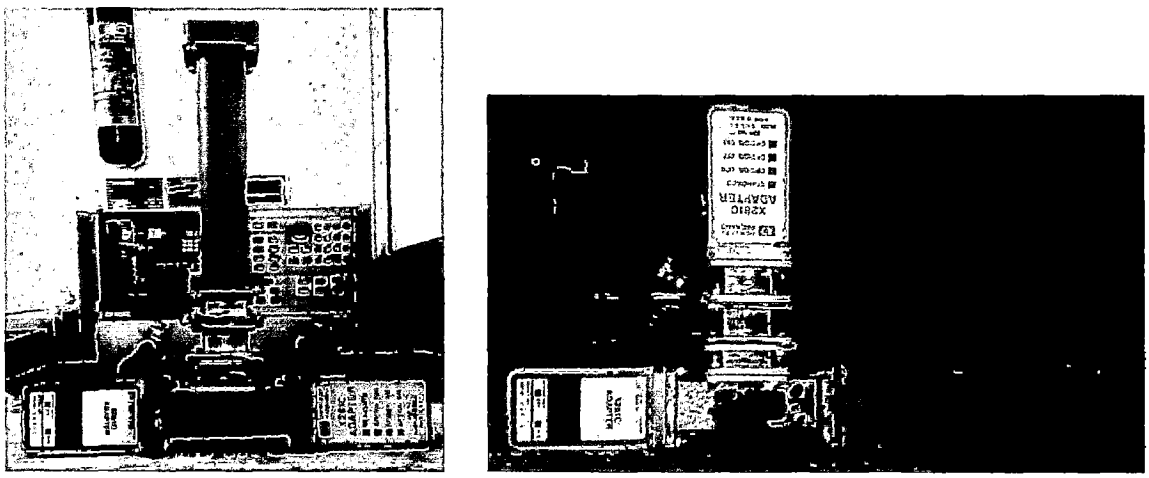

(a) (b)

Fig. 4.15 Measurement Set up for Measuring Frequency Response of Power Divider: (a) Matched Load at H–arm and (b) Matched Load at Through-arm.

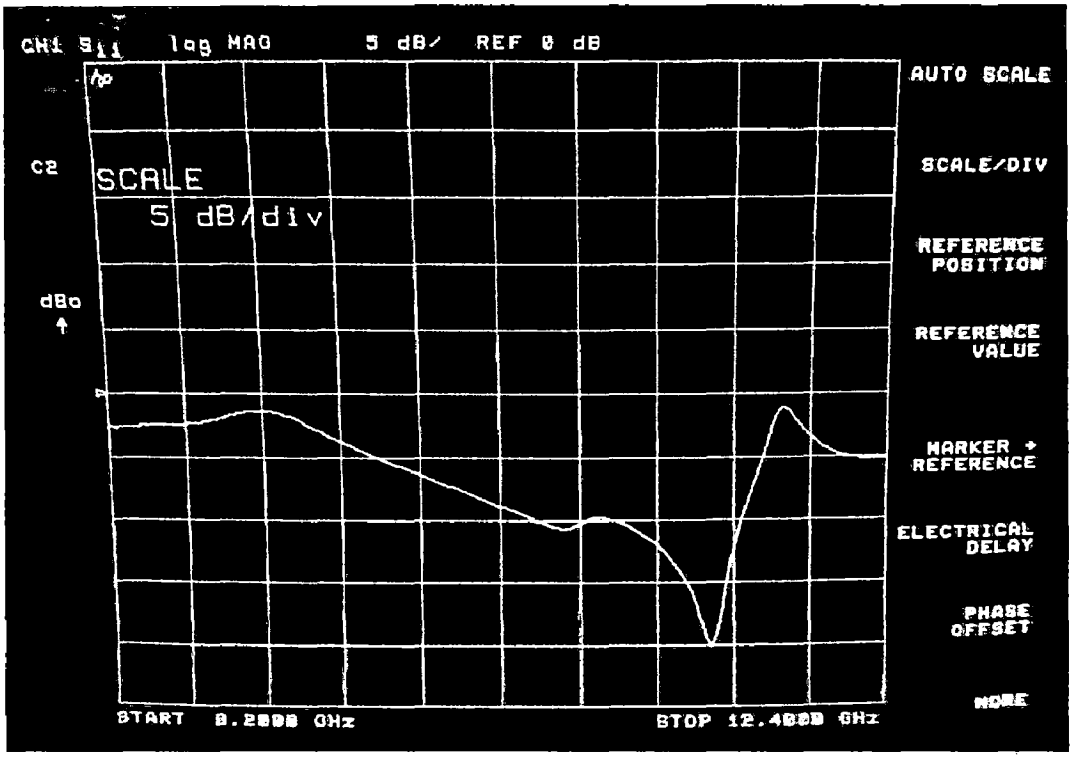

Fig. 4.16 Plot of $|S_{11}|$ Vs Frequency

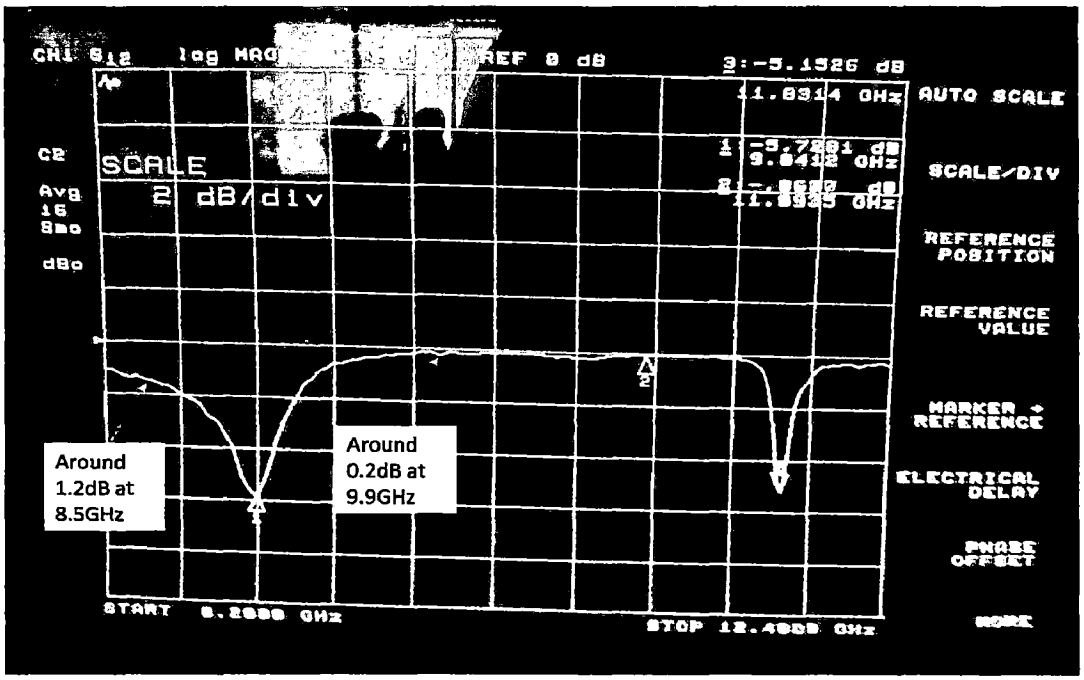

Fig. 4.17 Plot of $|S_{21}|$ Vs Frequency

Further, using measurement setup shown in fig. 4.15 (b) the measured S_{21}, S_{11}, and S_{22} are shown in figs. 4.18, 4.19 and 4.20, respectively. These three plots are actually S_{31}, S_{22} and S_{33} according to the nomenclature used in fig. 4.2.

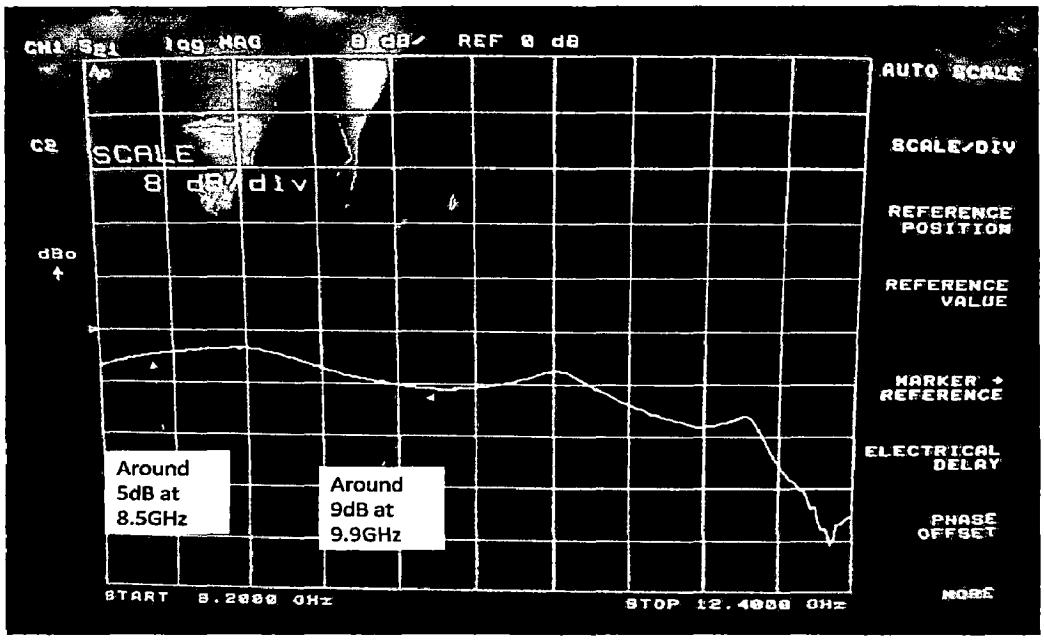

Fig. 4.18 Plot of $|S_{31}|$ Vs Frequency

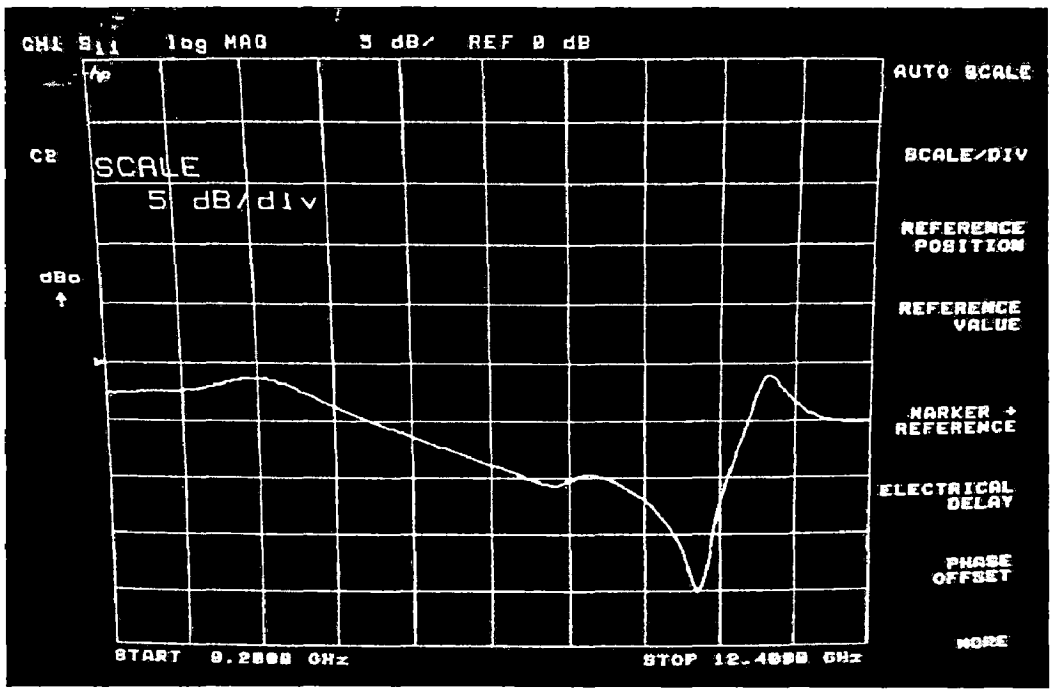

Fig. 4.19 Plot of $|S_{22}|$ Vs Frequency

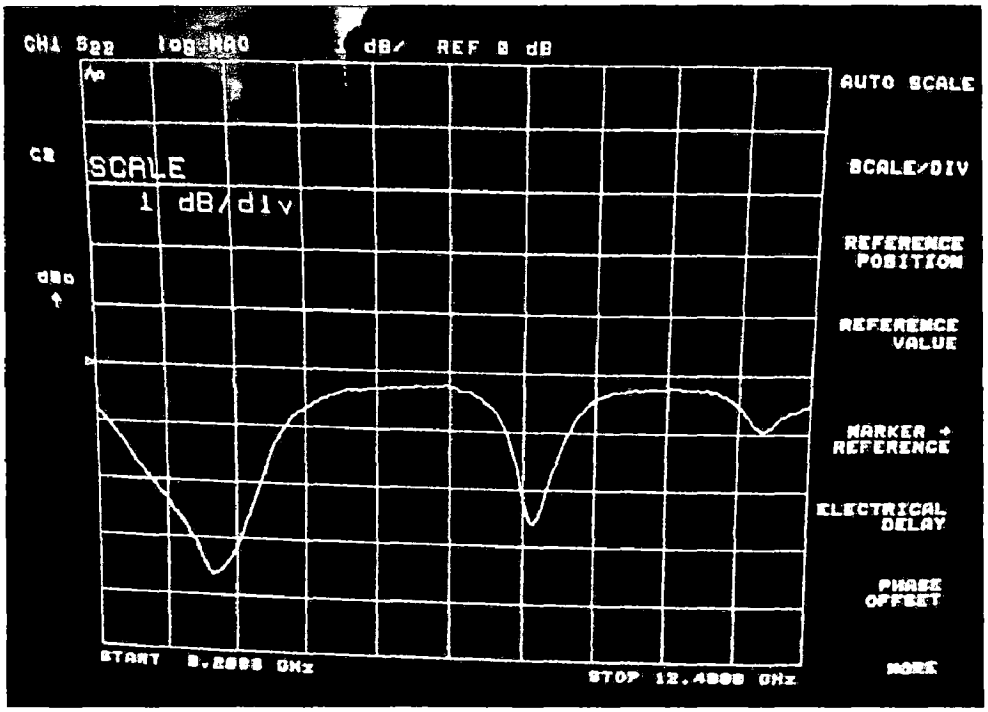

Fig. 4.20 Plot of $|S_{33}|$ Vs Frequency

Thus, figs. 4.16 to 4.20 show the plots of magnitudes (in dB) of S_{11}, S_{21} or S_{12}, S_{31} or S_{32} or S_{13} or S_{23}, S_{22} and S_{33} respectively according to nomenclature used in fig. 4.2. In addition, with the help of the eqs. (4.1) and (4.2) and figs. 4.17 and 4.18, we have obtained the power ratios for the two frequencies estimated on the basis of simulation. Overall comparison of the simulated and measured results is given in table 4.2.

TABLE 4.2

S.No.	Simulated Parameters					Measured Parameters				
	Frequency (GHz)	$\|S_{21}\|$ (dB)	$\|S_{31}\|$ (dB)	P_2/P_1	P_3/P_1	Frequency (GHz)	$\|S_{21}\|$ (dB)	$\|S_{31}\|$ (dB)	P_2/P_1	P_3/P_1
1.	8.5	0.363	11	0.915	0.09	8.5	1.2	5	0.75	0.316
2.	9.9	0.383	10.8	0.913	0.1	9.9	0.2	8	0.93	0.152

Mismatch in the simulated and measured results corresponds to the fabrication errors because even a 0.1 mm shift in the position of fractal diaphragm can cause a considerable

change in the results. Also, since we have used two fractal diaphragms, the error can be enhanced by an error in separation between the diaphragms. In addition one more possible source of error is that, in the fabrication of plus apertures. Since the aperture is having very small thickness (0.5mm), we have used the cellulose-based adhesive tape to support the base of apertures in the fractal diaphragm, which also maintains the apertures in same plane. However, the properties of this tape also affect the fractal characteristics. In other words a more sophisticated fabrication process is needed in order to match the simulated and measured results.

The simulation and experimental results confirm that it is possible to design a multiband waveguide power divider where coupling and frequency bands can be controlled by using the appropriate design of fractal diaphragms and their respective separation in H-arm. Further, the control of power division ratio is possible by placing suitable apertures in the H-arm.

CHAPTER – 5

DESIGN OF WAVEGUIDE BASED METAMATERIAL

In this chapter the design of a waveguide based metamaterial is presented. Simulation results along with experimental results for waveguide based metamaterial are presented and discussed.

5.1 Design Methodology for Waveguide Based Metamaterial

As we know the architectures or geometries that are known to us for the design of double negative (DNG) metamaterial are fairly complex in nature. So in this work an architecture is proposed for the design of DNG metamaterial in shielded waveguide environment. In this proposed design fractals are used for obtaining multiple passbands characteristics where electric permittivity, magnetic permeability and hence refractive index are negative. Since by the definition of electric permittivity and magnetic permeability we have [32],

$$\varepsilon = \varepsilon_0(\varepsilon_r' - j\varepsilon_r'') \tag{5.1}$$

$$\mu = \mu_0(\mu_r' - j\mu_r'') \tag{5.2}$$

Where ε_r' and μ_r' are real parts of relative electric permittivity and magnetic permeability, respectively. In other words, in these DNG passbands ε_r' and μ_r' are negative.

For designing waveguide based metamaterial, we have taken different fractal metal patches which are printed on a dielectric substrate on both sides (of it) and analysed the propagation characteristics of the resulting structure in order to see that, how many DNG passbands, this fractal based structure possesses. Three such fractal structures, separated by a parametric distance (p), which controls the magnitudes of effective medium parameters electric permittivity (ε_r') and magnetic permeability(μ_r') (ref. equations (5.3) and (5.4)), are inserted in an X- band waveguide. The resulting structure is simulated using CST Microwave Studio and scattering parameters are extracted. Further, these S parameters are converted into transmission parameters (A, B, C and D) by using equations (5.5) to (5.8) and with the help of MATLAB (Appendix C), and equivalent effective medium parameters electric permittivity (ε_r') and magnetic permeability(μ_r') are calculated using equations (5.3) and (5.4), [29].

$$\varepsilon_r' = \frac{C}{j\omega\epsilon_o pA} \tag{5.3}$$

$$\mu_r' = \frac{B}{j\omega\mu_o pA} \tag{5.4}$$

$$A = \frac{(1+S_{11})(1-S_{22})+S_{12}S_{21}}{2S_{21}} \tag{5.5}$$

$$B = Z_0 \frac{(1+S_{11})(1+S_{22})-S_{12}S_{21}}{2S_{21}} \tag{5.6}$$

$$C = \frac{(1-S_{11})(1-S_{22})-S_{12}S_{21}}{2Z_0S_{21}} \tag{5.7}$$

$$D = \frac{(1-S_{11})(1+S_{22})+S_{12}S_{21}}{2S_{21}} \tag{5.8}$$

5.2 Simulation Results

First, H-fractal metal patches have been considered and the resulting structure has been simulated on CST Microwave Studio. For H-fractal, length of 'H' is 14 mm (length is assumed to be measured along broader side of the waveguide) and a scale factor of 0.5 is taken for other iterations. Here 2nd iterated H-fractal is used. The simulated model of this H-fractal based metamaterial is given in fig. 5.1

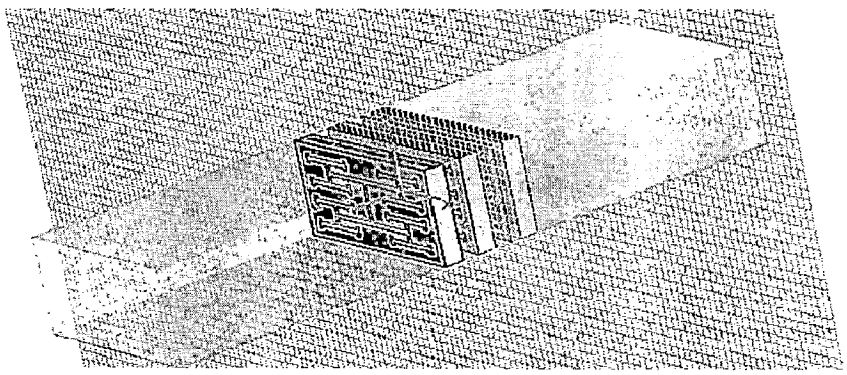

Fig. 5.1 CST Simulated Model of H-fractal Based Metamaterial

S-parameters of the structure are extracted from simulation and using equations (5.5) to (5.8), these are converted into A, B, C and D parameters [Appendix-C]. In addition using equation (5.3) and (5.4) equivalent effective medium parameters, electric permittivity (ε_r') and magnetic permeability(μ_r') are calculated and plotted to see the DNG behaviour. These plots are given in Figs. 5.2 and 5.3.

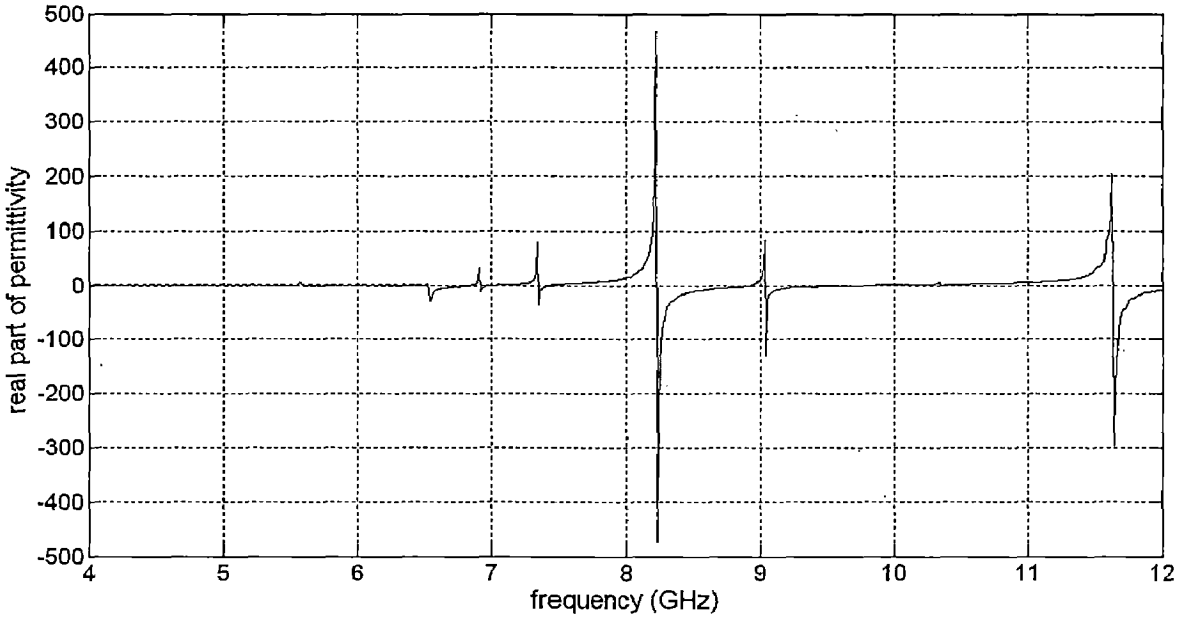

Fig. 5.2 Real Part of permittivity (ε_r') Vs Frequency

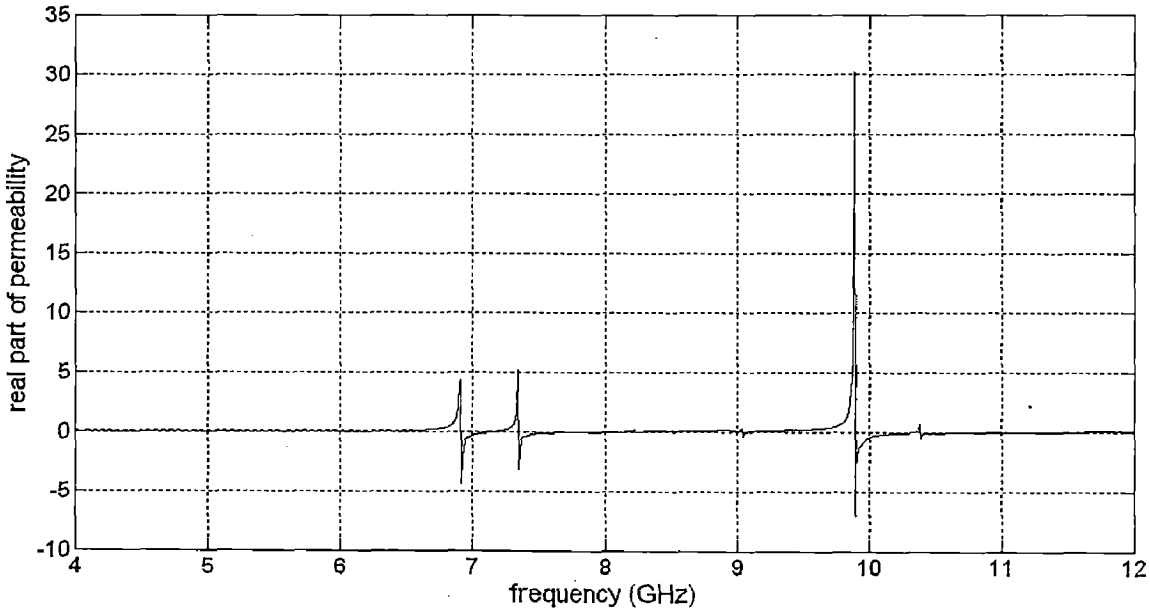

Fig. 5.3 Real Part of permeability (μ_r') Vs Frequency

From the Figs. 5.2 and 5.3, we see that real part of relative permittivity (ε_r') is negative at six frequencies whereas real part of relative permeability (μ_r') is negative at five frequencies. In other words, we get five DNG passbands at 6.95 GHz, 7.3 GHz, 9.05 GHz, 9.9 GHz and 10.45 GHz, respectively.

In a similar manner, we have considered 2nd iterated plus shaped fractal patches instead of H-fractal. Dimensions of this fractal are shown in Fig. 4.4. CST simulated model of this structure is shown in fig.5.4 and following the procedure mentioned for H-fractal, ε_r' and μ_r' were extracted for this structure. These are shown in Figs. 5.5 and 5.6.

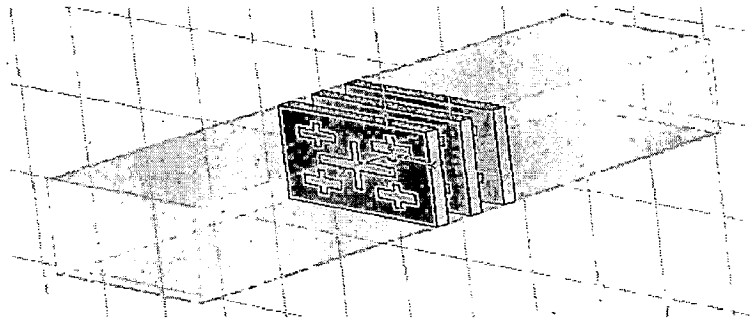

Fig. 5.4 CST Simulated Model of Plus fractal Based Metamaterial

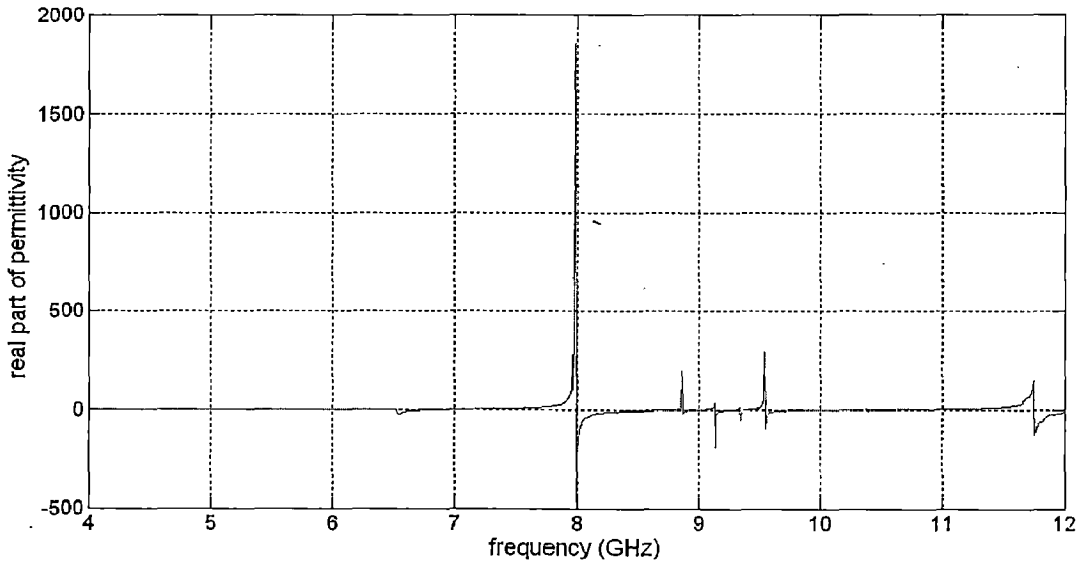

Fig. 5.5 Real Part of permittivity (ε_r') Vs Frequency

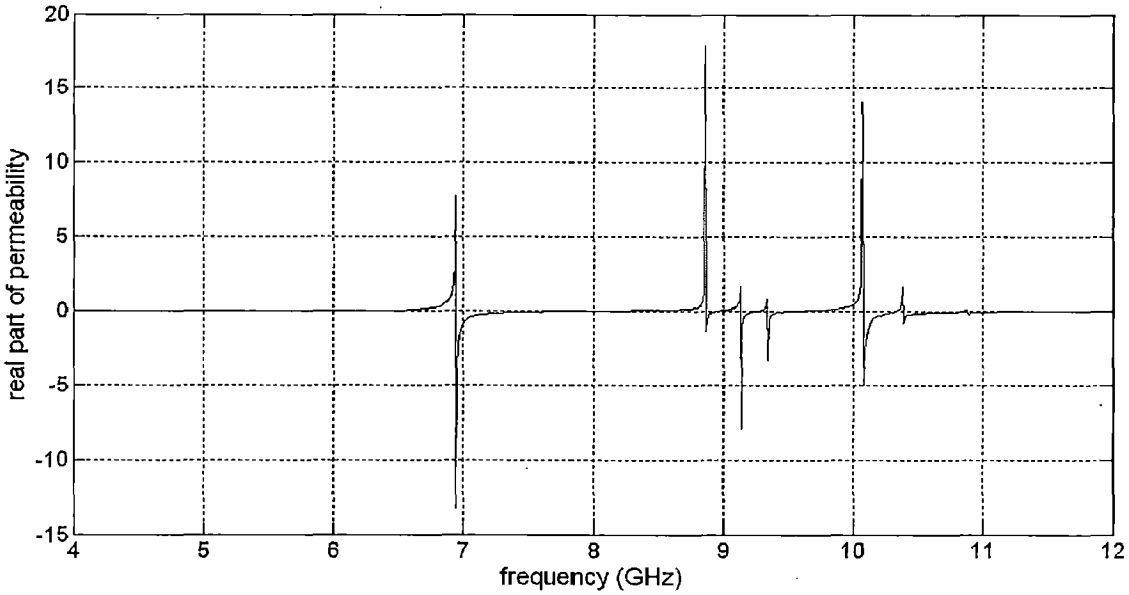

Fig. 5.6 Real Part of permeability (μ_r') Vs Frequency

It is evident from the Figs. 5.5 and 5.6 that ε_r' is negative at seven frequencies and μ_r' is also negative at seven frequencies. However, out of these seven frequencies, ε_r' and μ_r' are simultaneously negative at only four frequencies. These are 8.95 GHz, 9.05 GHz, 9.25 GHz and 10.3 GHz. Thus, only four DNG passbands are obtained.

We have also used 3rd iterated devil's staircase fractal [31] in place of plus fractal. Dimensions of 3rd iterated devil's staircase fractal is shown in Fig. 5.7 and the CST simulated model is shown in Fig. 5.8, where p is the length of a unit cell.

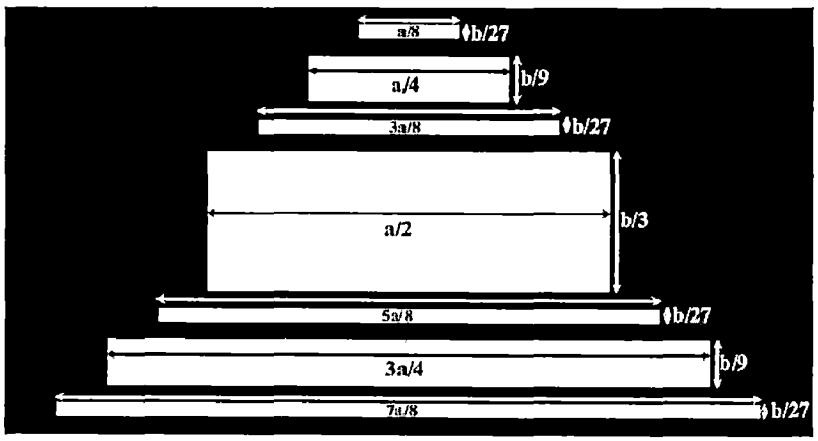

Fig. 5.7 A 3rd Iterated Modified Devil Staircase fractal

(a = 22.86 mm, b = 10.16 mm)

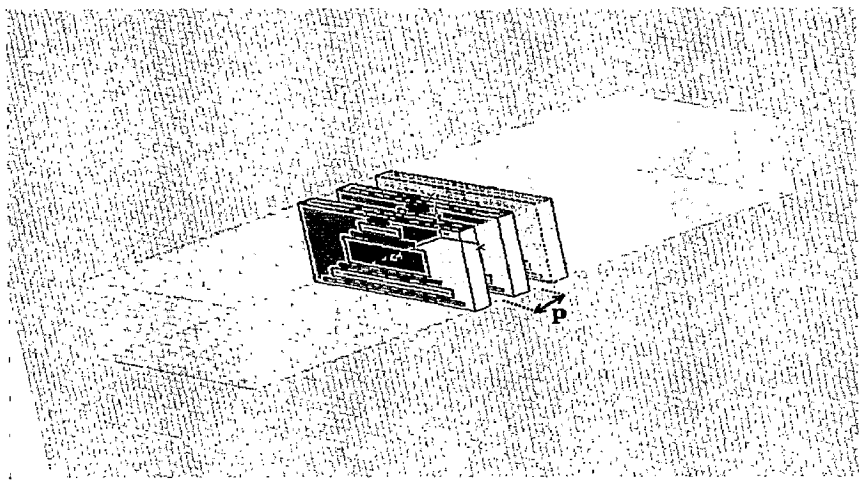

Fig. 5.8 Simulated Model of Design Proposed

In this model, we have taken p = 4.529mm since substrate available in the laboratory has a thickness of 1.529mm and waveguide flanges to maintain the separation between the fractal structures, has a thickness of 3mm. However, value of this parameter affects the magnitude of extracted parameters only. Therefore, we don't need to optimize our design to come at a specific value of this parameter p. This structure, when simulated using CST Microwave Studio, gives the scattering parameters S_{11}, S_{12}, S_{21} and S_{22} as shown in Figs. 5.9 to 5.12.

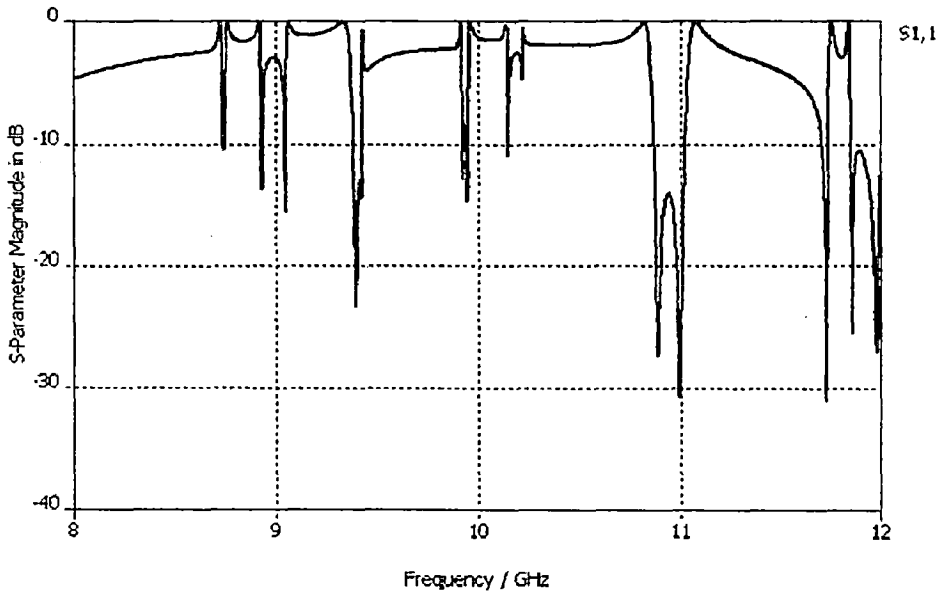

Fig. 5.9 $|S_{11}|$ Vs Frequency for Proposed Design

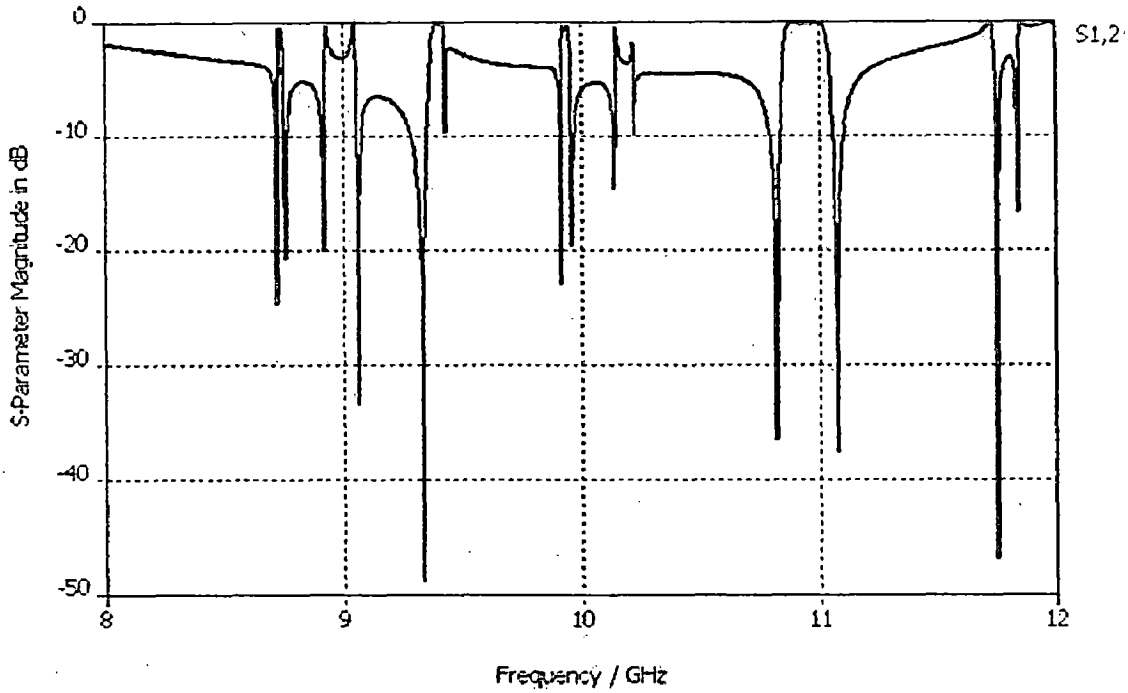

Fig. 5.10 $|S_{12}|$ Vs Frequency for Proposed Design

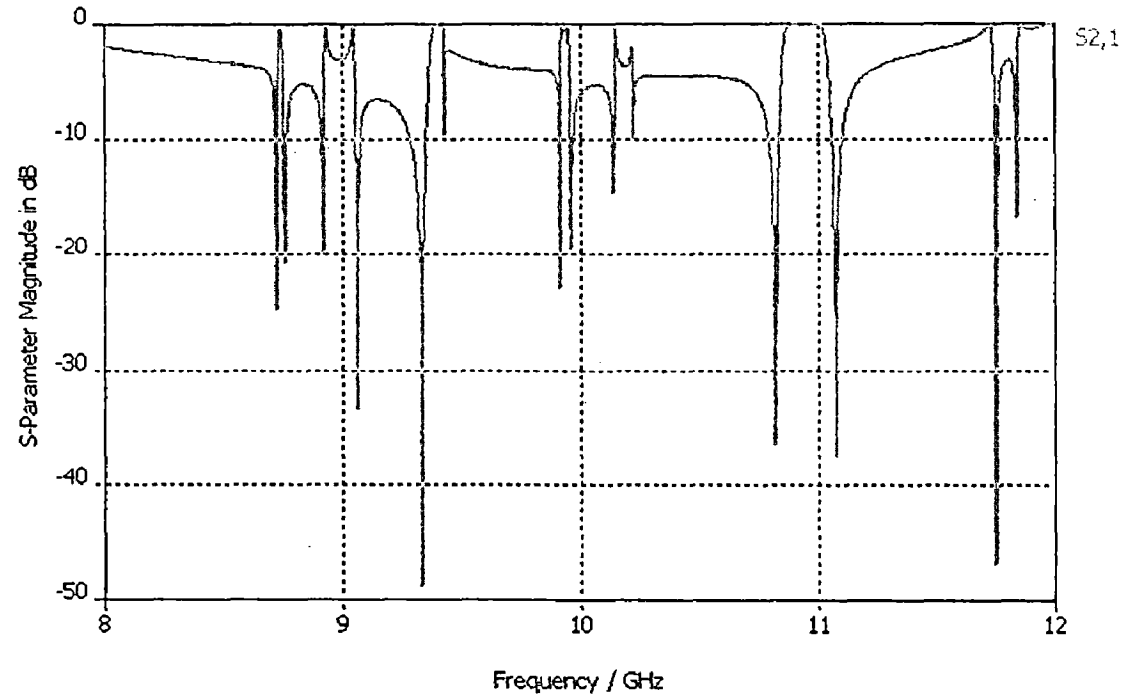

Fig. 5.11 $|S_{21}|$ Vs Frequency for Proposed Design

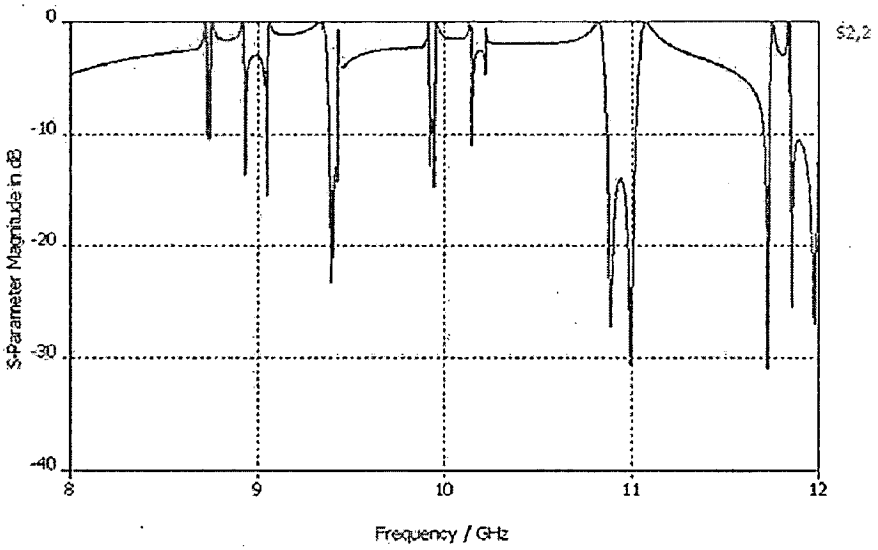

Fig. 5.12 $|S_{22}|$ Vs Frequency for Proposed Design

These results exhibits the reciprocal and symmetric nature of the designed structure which means $S_{12} = S_{21}$ (by reciprocity) and $S_{11} = S_{22}$ (by symmetry).

Again in the similar manner the values of ε_r' and μ_r' are extracted. These are shown in Figs.5.13 and 5.14, respectively.

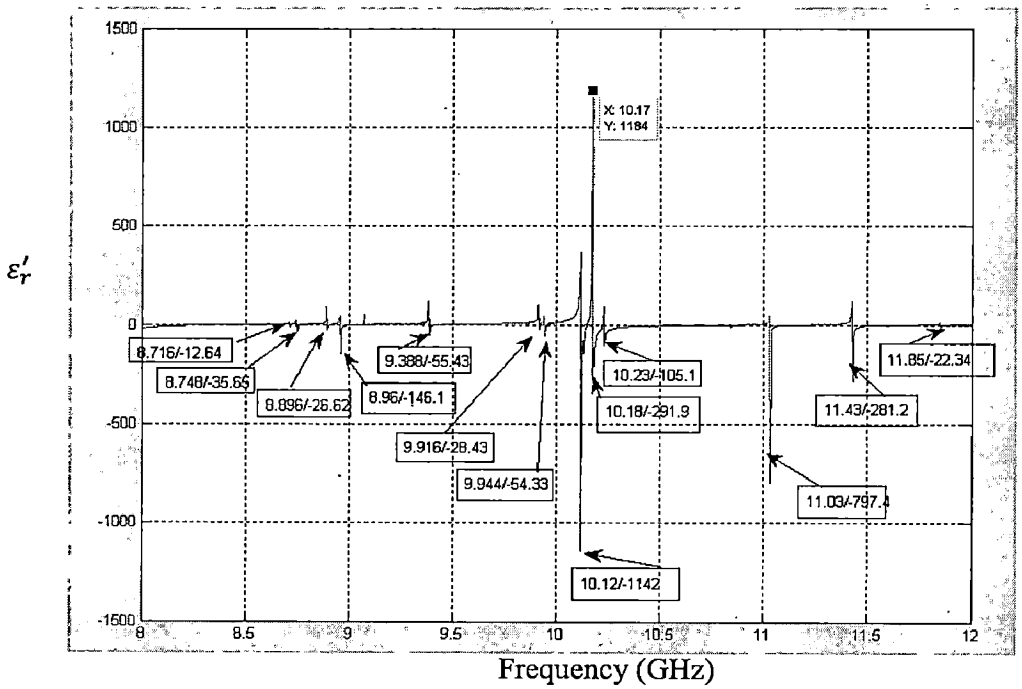

Fig. 5.13 ε_r' Vs Frequency

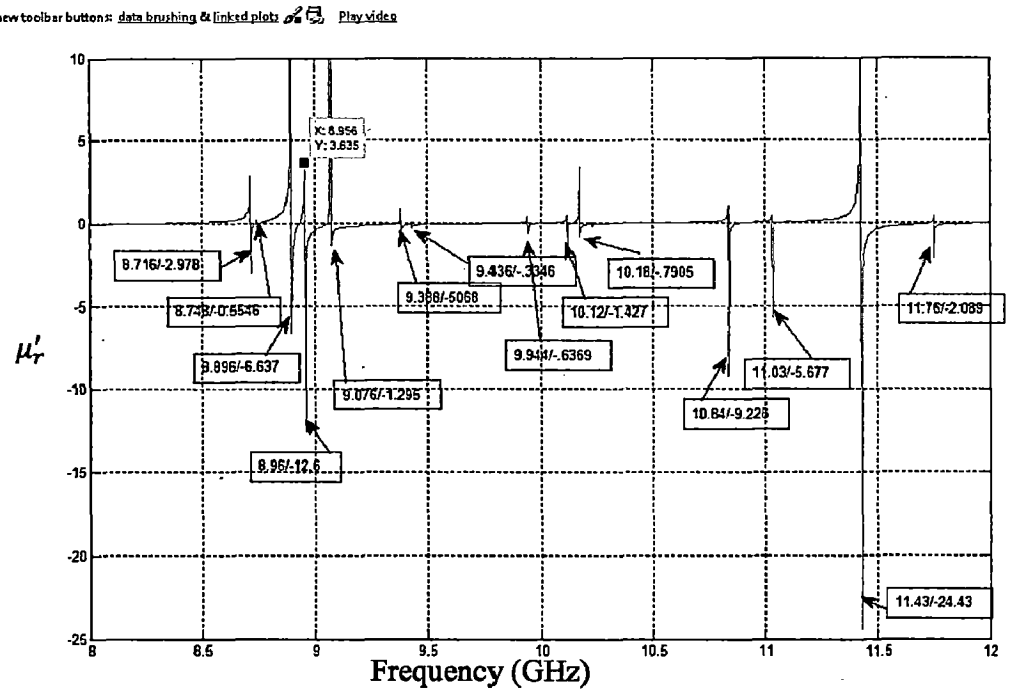

Fig. 5.14 μ_r' Vs Frequency

It can be seen from these Figs. that ε_r' and μ_r' are simultaneously negative at around 13 frequencies. Hence DNG behaviour is shown by this structure at these frequencies.

5.3 Experimental Results

For experimental investigations, the devil's staircase structure shown in Fig. 5.15 was fabricated and three such diaphragms were placed in a rectangular X-band waveguide.

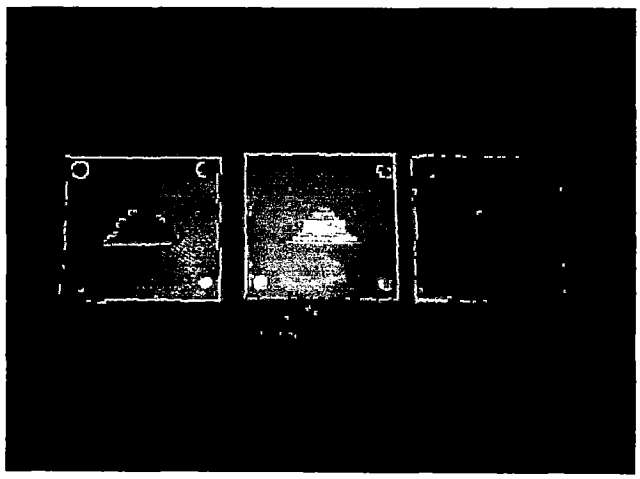

Fig. 5.15 Photograph of Fabricated Components

In addition complete fabricated structure of waveguide based metamaterial is shown in Fig. 5.16

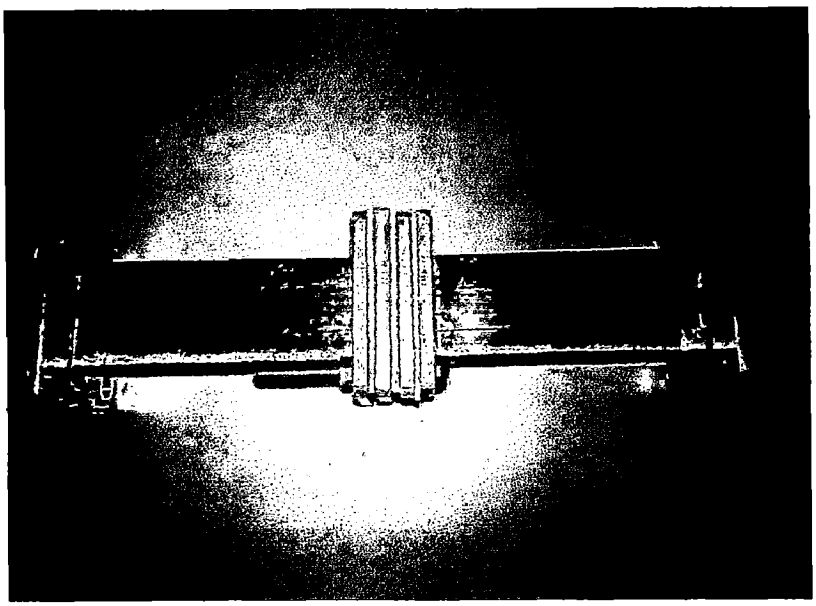

Fig. 5.16 Fabricated Waveguide Based Metamaterial

Frequency response of fabricated design has been measured using Vector Network Analyzer (VNA). Fig. 5.17 shows the measurement setup.

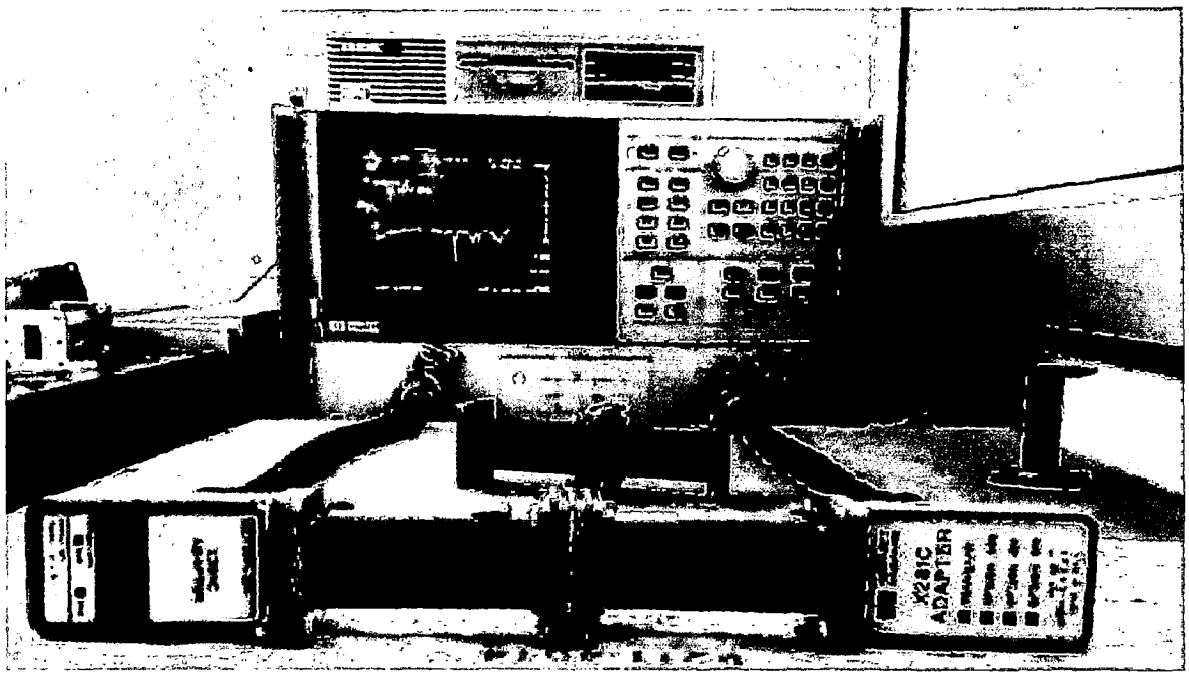

Fig. 5.17 Measurement Setup for Waveguide Based Metamaterial

The measured frequency response is shown in Figs. 5.18 and 5.19

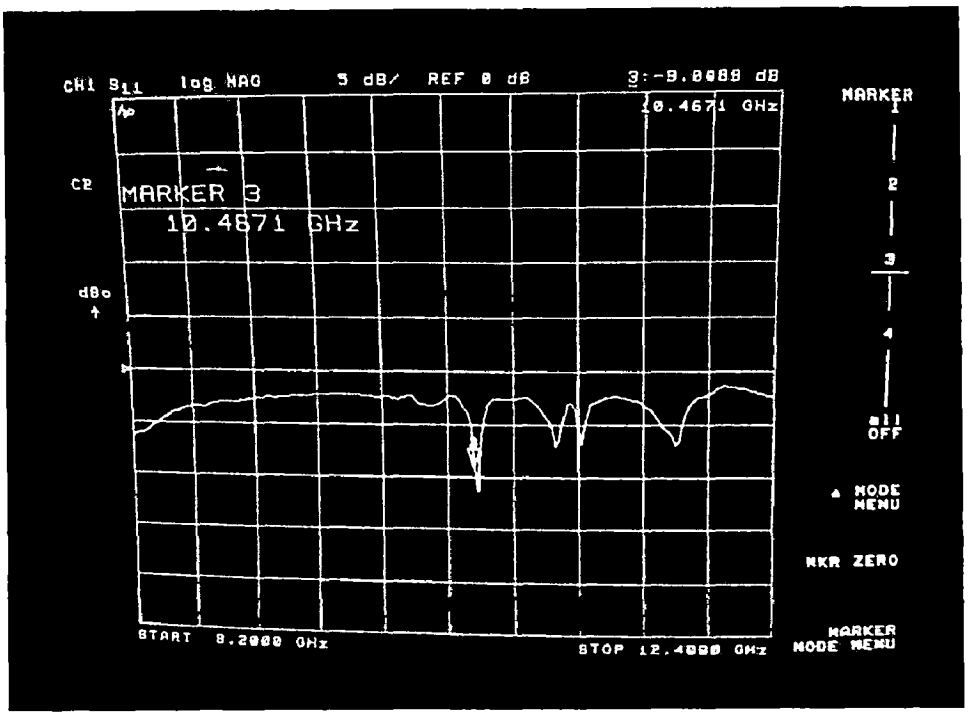

Fig. 5.18 $|S_{11}|$ Vs frequency plot observed on VNA

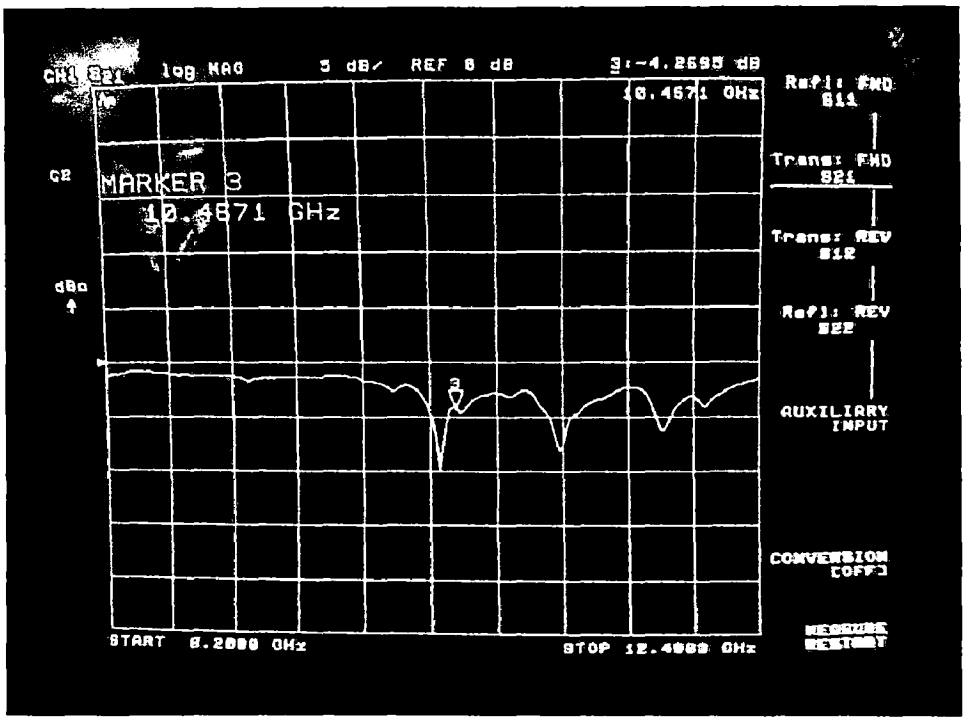

Fig. 5.19 $|S_{21}|$ Vs frequency plot observed on VNA

The effective medium parameters ε_r' and μ_r' were extracted from the measured dat and are plotted in the Figs. 5.22 and 5.23.

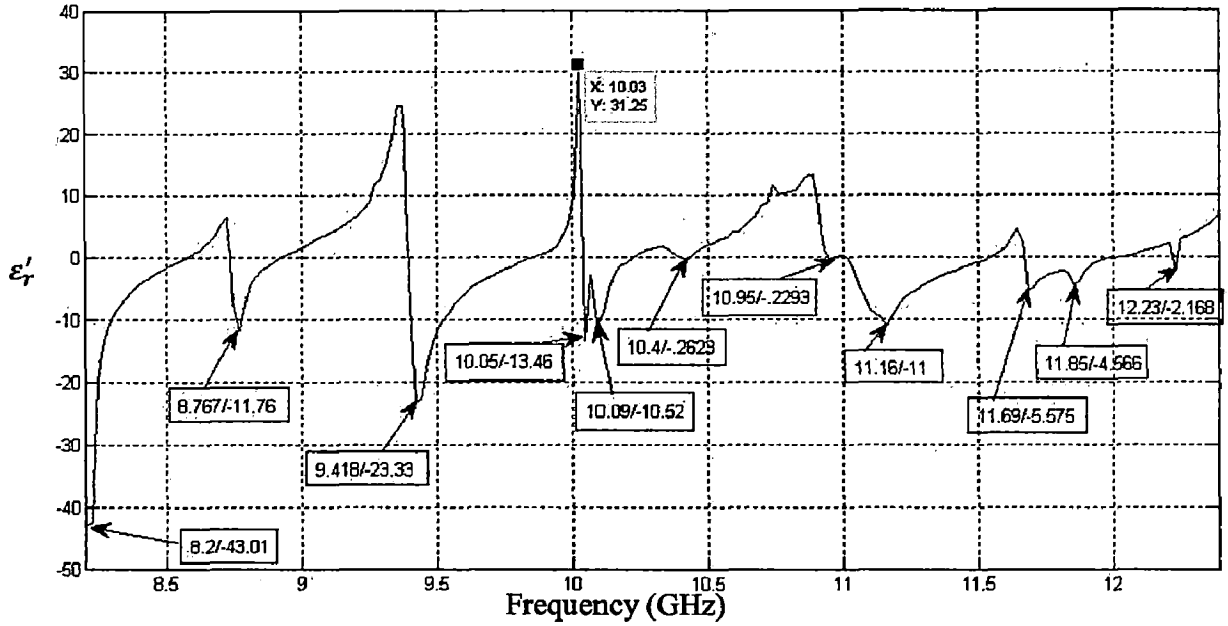

Fig. 5.22 Real part of effective Permittivity (ε_r') Vs Frequency

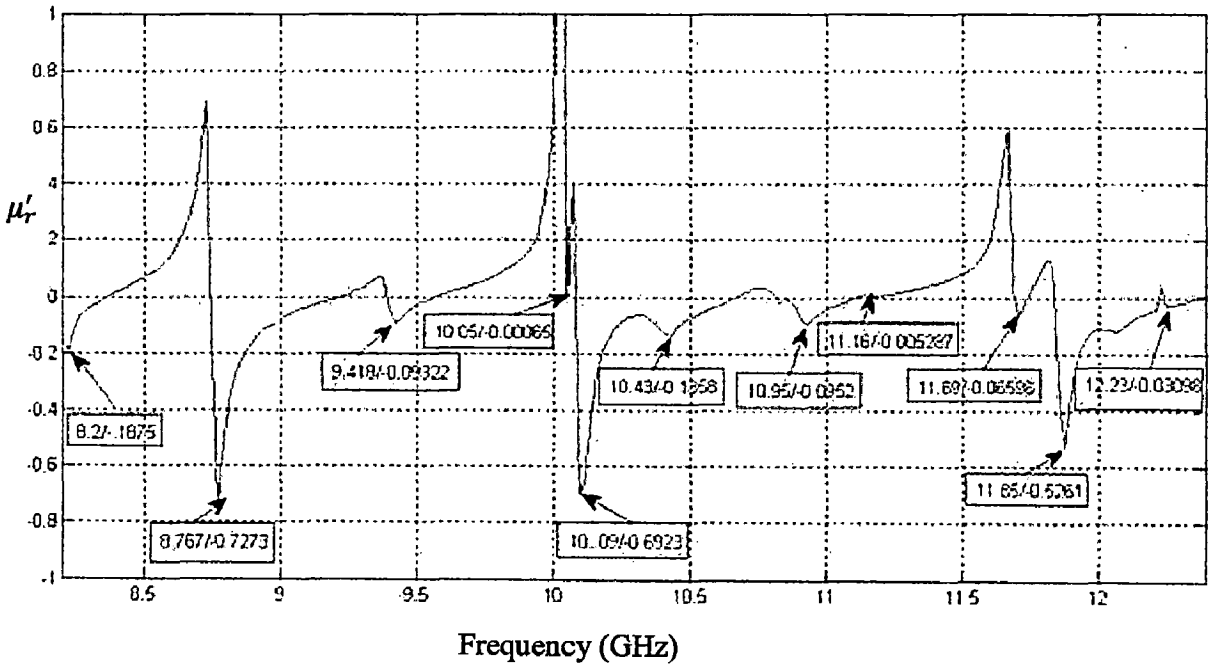

Fig. 5.23 Real part of effective permeability (μ_r') Vs Frequency

Comparison of simulated and experimental result is given in table 5.1

TABLE 5.1

S.No.	Simulated Parameters			Measured Parameters		
	Frequency (GHz)	ε_r'	μ_r'	Frequency (GHz)	ε_r'	μ_r'
1	8.716	-12.64	-2.978	8.2	-43.01	-0.1875
2	8.748	-35.65	-0.554	8.767	-11.76	-0.7273
3	8.896	-26.62	-6.637	9.418	-23.33	-0.0930
4	8.960	-146.1	-12.60	10.05	-13.46	-0.00065
5	9.388	-55.43	-0.507	10.09	-10.52	-0.6923
6	9.916	-28.43	-0.334	10.43	-0.2629	-0.1358
7	9.944	-54.43	-0.637	10.95	-0.2293	-0.0952
8	10.12	-1142	-1.427	11.16	-11	-0.0053
9	10.18	-291.9	-0.791	11.69	-5.575	-0.0659
10	10.23	-105.1	-0.132	11.85	-4.566	-0.5261
11	11.03	-797.1	-5.677	—	—	—
12	11.43	-28.12	-24.43	—	—	—
13	11.85	-22.34	-2.089	—	—	—

From this table, we observe that experimental measurement validate our design in the sense that we obtain same frequencies or very nearly the same frequency as predicted on the basis of simulation result. However magnitudes of these quantities differ which is due to the

fact there is always some unavoidable measurement or fabrication error that can be due to slight misalignment of fractal structures and this is largely reflected on the magnitude of these values because in the formulae for magnitude we have ratio of two measured values (ref equations (5.3) and (5.4)). Therefore, it is evident that using fractals we can get multiband metamaterial structures.

CHAPTER-6

CONCLUDING REMARKS AND FUTURE SCOPE

6.1 Concluding Remarks

In this dissertation, we have investigated possible applications of fractal apertures in waveguides to realize multiband filters and power dividers and for realization of DNG waveguide medium. Following waveguide structures have been investigated through simulation and experimental measurements:

- Waveguide filter which has two passbands between 7 to 16 GHz frequency band.
- Waveguide power divider, which is basically an H-plane Tee junction consisting of two fractal apertures in its H-arm. These two apertures and their respective position in H-arm controls the amount of power coupled to the H-arm.
- Waveguide based metamaterial

All these structures employ fractals to have multiband behaviour. For waveguide filter two simulation schemes are presented of which one employs the use of HFSS and MATLAB and second is direct simulation using CST. The comparison of the results from these two approaches validates our approach. Further, we have measured its frequency response using VNA which is limited to X-band (8.2-12.4 GHz). In order to obtain data for 7-16 GHz frequency range, we have used microwave power source and power meter for predicting the complete frequency response of the designed waveguide filter. The measured and simulated results are in good agreement.

Waveguide power divider designed in this work is a novel design which highlights the use of fractals to have multiband nature. This structure has been simulated using CST and simulation results were verified by the measurement on VNA.

Metamterial structure designed in a shielded waveguide environment presented in this work is also a novel proposed design. Application of fractals in this design provides multiple DNG passbands over X-band. Simulation results, which include calculating S-parameters and converting them into ABCD-parameters followed by medium parameters extraction were verified by measuring frequency response of the structure on VNA. Frequencies at which

structure shows DNG behaviour, match in the simulated and measured results except in magnitude, which arises because of fabrication inaccuracies.

6.2 Future Scope

The work presented in this dissertation is limited in scope because of time constraints. More rigorous investigation is required for arising at systematic design procedures. Some possible future directions are:

- Investigations on different type of fractals to arrive at the structure that will be most suitable for filter design. This should include the development of a systematic design procedure for the control of pass-bands and out of band rejection ratio.
- Suitable methods need to be developed for the design of fractal waveguide power dividers with emphasis on the control of pass-bands and coupling ratio.
- Design of power dividers with unequal power division should be investigated.
- Waveguide based metamaterials require a more comprehensive investigation where it is important to investigate the methods for precise control of DNG frequencies.

REFERENCES

[1] G L Matthaei, *Microwave Filters Impedance Matching Networks and Coupling Structures*, McGraw-Hill, 1964.

[2] I. C. Hunter, *Theory and design of microwave filters, IEE Electromagnetic Wave Series,*

[3] Wilburl L. Pritchard, Henri G. Suyderhoud and Robert A. Nelson, *Satellite Communication Systems Engineering,* Prentice Hall, Englewood Cliffs, New Jersey, 1993.

[4] D. Oloumi, A. Kordzadeh, and A. A. Lotfi Neyestanak, "Size Reduction and Bandwidth Enhancement of a Waveguide Bandpass Filter Using Fractal-Shaped Irises," *IEEE Antennas And Wireless Propagation Letters*, vol. 8, pp. 1214-1217, 2009.

[5] D.V. Sivukhin, "The energy of electromagnetic waves in dispersive media," *Opt.Spektrosk,* vol. 3, pp. 308-312 1957.

[6] V. G. Veselago, "The electrodynamics of substances with simultaneously negative values of ε and μ," *Soviet Physics Uspekhi,* vol. 10, pp. 509-514, 1968.

[7] J. B. Pendry, A. J. Holden, W. J. Stewart, and I. Youngs, "Extremely Low Frequency Plasmons in Metallic Mesostructures," *Physical Review Letters,* vol. 76, pp. 4773, 1996.

[8] J. B. Pendry, A. J. Holden, D. J. Robbins, and W. J. Stewart, "Low frequency plasmons in thin-wire structures," *Journal of Physics: Condensed Matter,* vol. 10, pp. 4785-4809, 1998.

[9] Ricardo Marques, Ferran Martin, Mario Sorolla, *Metamaterial with Negative Parameters: Theory Design and Microwave Applications,* John Wiley & Sons 2008.

[10] K. J. Russell, "Microwave power combining techniques," *IEEE Trans. Microwave Theory Tech.,* vol. 27, pp. 472478, May 1970.

[11] A. Sanada, K. Fukui, and S. Nogi, "A waveguide type power divider / combiner of double-ladder multiple-port structure," *IEEE Trans. Microw. Theory Tech.*, vol. 42, no. 7, pp. 1154–1161, Jul. 1994.

[12] R. Smith, W. 1. Padilla, D. C. Vier, S. C. Nemat-Nasser and S.Schultz, "Composite Medium with Simultaneously Negative Permeability and Permittivity," *Physical Review Letters*, vol. 84, 4184, 2000.

[13] F. Miyamaru, Y. Saito, M. W. Takeda, B. Hou, L. Liu, W. Wen, and P. Sheng, "Terahertz electric response of fractal metamaterial structures," *Physical Review B 77,* 2008.

[14] Benoit B. Mandelbrot, *The Fractal Geometry of Nature*, New York, W.H. Freeman and Company, 1977.

[15] Anthony Barcellos, "The Fractal Geometry of Mandelbrot," *The College Mathematics Journal*, vol. 15, No. 2, pp. 98-114, 1984.

[16] Duglas H. Werner and Suman Ganguly, "An overview of fractal antenna engineering," *IEEE Antennas and Propagation magazine*, vol. 45, no.1, pp-38-57, 2003.

[17] Fractal Geometry, Advanced Topics in Mathematics, March 2010 [online]. Available: http://mail.colonial.net/~abeckwith/006B0D39-70E903AC-006B0D39.

[18] Heinz-Otto Peitgen, Hartmut Jürgens, Dietmar Saupe, "Chaos and Fractals: New Frontiers of Science ," Second Edition, Springer-Verlag New York, Inc.,2004.

[19] Fekadu Mihret Geremew, "Investigations on wideband and multiband fractal slot antenna designs" Master's Thesis, Indian Institute of Technology Roorkee, 2009.

[20] Sachendra Nath Sinha and Manish Jain, "A Self-Affine Fractal Multiband Antenna", IEEE antennas and wireless propagation letters, Vol. 6, 2007.

[21] Bozhi Li, Ben-Qing Gao, "H-Plane Rectangular Waveguide T-Junction with Fractal Irises," *4th International Conference on Microwave and Millimeter Wave Technology Proceedings,* 2004.

[22] Mejdoubi A. Brosseau, C., "Reflectance and absorbance of all-dielectric metamaterial composites with fractal boundaries: A numerical investigation," *Journal of Applied Physics*, vol. 105, issue 2, Jan 2009.

[23] M. Palandoken and H. Henke, "Fractal Negative-Epsilon Metamaterial," *IEEE AP-S International Symposium,* 2005.

[24] R. Vahldieck and W. J. R. Hoefer, "Finline and metal insert filters with improved passband separation and increased stopband attenuation," *IEEE Trans. Microw. Theory Tech.*, vol. MTT-33, no. 12, pp. 1333–1339, Dec. 1985.

[25] A. J. Robinson, R. D. Seager, and J. C. Vardaxoglou, "Waveguide with resonant array inserts," *Electron. Lett.*, vol. 28, no. 23, Nov. 1992.

[26] M. Ohira, H. Deguchi, M. Tsuji, and H. Shigesawa, "Novel waveguide filters with multiple attenuation poles using frequency selective surfaces," *IEEE MTT-S Int. Microwave Symp.*, June 2005.

[27] N. Marcuvitz, *Waveguide Handbook,* New York: McGraw-Hill, pp. 378-379, 1951.

[28] R. S. Kshetrimayum, "A Brief Intro to Metamaterials," *IEEE Potentials*, vol. 23, issue 5, pp. 44-46, Dec. 2004-Jan. 2005.

[29] Rakhesh Singh Kshetrimayum, "Novel Architecture for Waveguide Based Metamaterials," *17th International Zurich Symposium on Electromagnetic Compatibility,* 2006.

[30] R. D. Seager, J. C.Vardaxoglou, and D. S. Lockyer, "Close coupled resonant aperture inserts for waveguide filtering applications," *IEEE Microw. Compon. Lett.*, vol. 11, no. 3, pp. 112–114, Mar. 2001.

[31] Basudeb Ghosh, Sachendra N. Sinha, and M. V. Kartikeyan, "Radiation From Rectangular Waveguide-Fed Fractal Apertures," *IEEE Transactions on Antennas and Propagation, vol. 58, no. 6,pp. 2088-2093, June 2010*

[32] David M. Pozar, *Microwave Engineering*, John Wiley and Sons, 1998.

[33] Stephen J. Chapman, *MATLAB Programming for Engineers*, Thomson Learning, 2004.

APPENDIX-A

MATLAB Code for Calculation of S- Parameters from Susceptance Data

```
%-----------------------------------------------------------------
clc;
clear all
l1 = input('enter the value of l1 = ');
l2 = input('enter the value of l2 = ');
%l3 = input('enter the value of l3 = ');
%% Read data from the susceptance data file
[fid, message] = fopen('Devil2.txt', 'r');%open the file and return a pointer to the file
data = fscanf(fid, '%f',[5 inf]);%read data in the form of 5xinf matrix form from the file
fclose(fid);%closes the file
b = (data(4,:));%store the forth row of the data in b
f = (data(1,:));%store the first row of the data in f
n = size(b,2);%find the size of data
for(k=1:n)
   t(k) = (3.14/15)*f(k);%find beta directly using GHz values in the data note that unit is 1/cm
   beta(k)=sqrt(t(k)^2-(pi/2.286)^2);
   A1 = [cos((beta(k)*l1)/2) i*(sin((beta(k)*l1)/2));i*(sin((beta(k)*l1)/2))  cos((beta(k)*l1)/2)];
   A2 = [cos((beta(k)*l2)/2) i*(sin((beta(k)*l2)/2));i*(sin((beta(k)*l2)/2))  cos((beta(k)*l2)/2)];
   %A3 = [cos((beta(k)*l3)/2) i*(sin((beta(k)*l3)/2));i*(sin((beta(k)*l3)/2))  cos((beta(k)*l3)/2)];
   B = [1 0;b(k)*i 1];
   Y = A1*B*A2*B;
   p(k) = sqrt(1-(15/(2.286*f(k)))^2);
   Z(k) = 377/p(k);
   S(k) =(Y(1,1) +Y(1,2)- Y(2,1) - Y(2,2))/(Y(1,1) +Y(1,2)+ Y(2,1) + Y(2,2));
S1(k) = 2/(Y(1,1) +Y(1,2)+ Y(2,1) + Y(2,2));
end
magniS = abs(S);
magniS1 = abs(S1);
ans = [data(1,:)' magniS' magniS1']
plot(data(1,:),20*log10(magniS));
hold on
plot(data(1,:),20*log10(magniS1));
grid on
```

APPENDIX-B

Susceptance Data for 2nd Iterated Modified Devil's Staircase Fractal

Frequency	S_{11}(db)	S_{11}(angle)	Susceptance	|S11|	
	7.00	-1.5251	147.032	-3.0834	0.8390
	7.10	-1.9262	143.237	-2.6770	0.8011
	7.20	-2.3551	139.687	-2.3572	0.7625
	7.30	-2.8177	136.301	-2.0929	0.7230
	7.40	-3.3213	133.020	-1.8663	0.6822
	7.50	-3.8752	129.800	-1.6663	0.6401
	7.60	-4.4921	126.600	-1.4853	0.5962
	7.70	-5.1892	123.385	-1.3179	0.5502
	7.80	-5.9904	120.118	-1.1601	0.5017
	7.90	-6.9307	116.763	-1.0086	0.4503
	8.00	-8.0635	113.282	-0.8605	0.3952
	8.10	-9.4759	109.631	-0.7133	0.3359
	8.20	-11.3229	105.761	-0.5643	0.2716
	8.30	-13.9239	101.619	-0.4110	0.2013
	8.40	-18.1233	97.141	-0.2502	0.1241
	8.5000	-28.1626	+92.274	-0.0782	+0.0391
	8.5100	-30.4290	+91.770	-0.0602	+0.0301
	8.5200	-33.5402	+91.270	-0.0421	+0.0210
	8.5300	-38.4990	+90.795	-0.0238	+0.0119
	8.5400	-51.5489	+90.662	-0.0053	+0.0026
	8.5500	-43.4974	-90.585	+0.0134	+0.0067
	8.5600	-35.8594	-91.007	+0.0322	+0.0161
	8.5700	-31.8281	-91.521	+0.0513	+0.0256
	8.5800	-29.0626	-92.057	+0.0705	+0.0352
	8.5900	-26.9504	-92.605	+0.0899	+0.0449
	8.6000	-25.2379	-93.161	+0.1096	+0.0547
	8.70	-16.0419	-99.083	0.3195	0.1577
	8.80	-11.3838	-105.649	0.5601	0.2697
	8.90	-8.2044	-112.886	0.8442	0.3888
	9.00	-5.8190	-120.782	1.1913	0.5117
	9.10	-3.9772	-129.245	1.6337	0.6326
	9.20	-2.5663	-138.091	2.2283	0.7442
	9.30	-1.5225	-147.058	3.0866	0.8392
	9.40	-0.7953	-155.855	4.4615	0.9125
	9.50	-0.3338	-164.218	7.0765	0.9623
	9.60	-0.0857	-171.966	14.1698	0.9902
	9.70	-0.0013	-179.006	115.2780	0.9998
	9.80	-0.0376	174.675	-21.4573	0.9957
	9.90	-0.1599	169.038	-10.3259	0.9818

10.00	-0.3424	164.018	-6.9832	0.9613
10.10	-0.5660	159.540	-5.3605	0.9369
10.20	-0.8176	155.528	-4.3943	0.9102
10.30	-1.0880	151.918	-3.7484	0.8823
10.40	-1.3710	148.648	-3.2827	0.8540
10.50	-1.6626	145.670	-2.9285	0.8258
10.60	-1.9601	142.940	-2.6482	0.7980
10.70	-2.2617	140.422	-2.4195	0.7708
10.80	-2.5666	138.088	-2.2281	0.7442
10.90	-2.8743	135.913	-2.0647	0.7183
11.00	-3.1847	133.874	-1.9228	0.6931
11.10	-3.4977	131.954	-1.7979	0.6685
11.20	-3.8139	130.139	-1.6864	0.6446
11.30	-4.1334	128.416	-1.5860	0.6213
11.40	-4.4570	126.773	-1.4946	0.5986
11.50	-4.7852	125.201	-1.4108	0.5764
11.60	-5.1188	123.692	-1.3334	0.5547
11.70	-5.4586	122.239	-1.2613	0.5334
11.80	-5.8053	120.836	-1.1939	0.5125
11.90	-6.1601	119.477	-1.1304	0.4920
12.00	-6.5240	118.157	-1.0704	0.4718
12.10	-6.8982	116.871	-1.0133	0.4519
12.20	-7.2841	115.617	-0.9589	0.4323
12.30	-7.6831	114.390	-0.9067	0.4129
12.40	-8.0971	113.187	-0.8566	0.3937
12.50	-8.5279	112.005	-0.8081	0.3746
12.60	-8.9778	110.841	-0.7612	0.3557
12.70	-9.4495	109.693	-0.7157	0.3369
12.80	-9.9461	108.558	-0.6713	0.3182
12.90	-10.4713	107.434	-0.6279	0.2995
13.00	-11.0294	106.318	-0.5854	0.2809
13.10	-11.6258	105.208	-0.5435	0.2622
13.20	-12.2673	104.103	-0.5023	0.2436
13.30	-12.9621	103.000	-0.4615	0.2249
13.40	-13.7211	101.897	-0.4211	0.2060
13.50	-14.5581	100.791	-0.3810	0.1871
13.60	-15.4922	99.681	-0.3409	0.1680
13.70	-16.5496	98.565	-0.3009	0.1488
13.80	-17.7685	97.439	-0.2608	0.1293
13.90	-19.2070	96.302	-0.2205	0.1096
14.00	-20.9609	95.151	-0.1798	0.0895
14.10	-23.2038	93.985	-0.1386	0.0692
14.20	-26.3054	92.801	-0.0969	0.0484
14.30	-31.3168	91.607	-0.0544	0.0272
14.4000	-45.2635	+90.560	-0.0109	+0.0055
14.4100	-49.7541	+90.601	-0.0065	+0.0033
14.4200	-59.6169	+91.352	-0.0021	+0.0010
14.4300	-58.6403	-91.221	+0.0023	+0.0012

14.4400	-49.3978	-90.592	+0.0068	+0.0034
14.4500	-45.0125	-90.562	+0.0112	+0.0056
14.4600	-42.1054	-90.622	+0.0157	+0.0078
14.4700	-39.9258	-90.712	+0.0202	+0.0101
14.4800	-38.1805	-90.816	+0.0247	+0.0123
14.4900	-36.7241	-90.928	+0.0292	+0.0146
14.5000	-35.4738	-91.045	+0.0337	+0.0168
14.60	-28.0058	-92.314	0.0796	0.0398
14.70	-23.9487	-93.660	0.1272	0.0635
14.80	-21.1109	-95.064	0.1767	0.0880
14.90	-18.9018	-96.528	0.2284	0.1135
15.00	-17.0739	-98.061	0.2829	0.1401
15.10	-15.4991	-99.674	0.3406	0.1679
15.20	-14.1018	-101.380	0.4023	0.1972
15.30	-12.8333	-103.197	0.4688	0.2282
15.40	-11.6592	-105.149	0.5413	0.2612
15.50	-10.5540	-107.263	0.6214	0.2967
15.60	-9.4964	-109.583	0.7114	0.3351
15.70	-8.4675	-112.167	0.8147	0.3772
15.80	-7.4471	-115.108	0.9371	0.4243
15.90	-6.4089	-118.566	1.0888	0.4781
16.00	-5.3070	-122.877	1.2927	0.5428

APPENDIX C

MATLAB Code for converting S parameters into ABCD parameters for metamaterial

```
clc;
clear all;
S11 =importdata('S11.txt');
S21 =importdata('S21.txt');
S12=importdata('S12.txt');
S22=importdata('S22.txt');
argS11 =importdata('argS11.txt');
argS21 =importdata('argS21.txt');
argS12 =importdata('argS12.txt');
argS22 =importdata('argS21.txt');
f1=1;
f2=1001;
f = S11(f1:f2,1);

SS1=[S11(f1:f2,1) S11(f1:f2,2) S21(f1:f2,2) S12(f1:f2,2) S22(f1:f2,2)];
SS2=[S11(f1:f2,1) argS11(f1:f2,2) argS21(f1:f2,2) argS21(f1:f2,2)
argS21(f1:f2,2) ];
S1=SS1(f1:f2,2);
S2=SS1(f1:f2,3);
aS1=SS1(f1:f2,4);
aS2=SS1(f1:f2,5);
S3=SS2(f1:f2,2);
S4=SS2(f1:f2,3);
aS3=SS2(f1:f2,4);
aS4=SS2(f1:f2,5);
s1=10.^(S1/20);
s2=10.^(S2/20);
% s3= S3*180/pi;
% s4= S4*180/pi;
ss3=S3*pi/180;
ss4=S4*pi/180;
s11 = s1.*exp(j*ss3);
s21 = s2.*exp(j*ss4);
s12=s21;
s22=s11;
A =((1+s11).*(1-s22)+s12.*s21)./(2.*s21);
B = ((1+s11).*(1+s22)-s12.*s21).*50./(2.*s21);
C=((1-s11).*(1-s22)-s12.*s21)./(2.*50.*s21);
D = ((1-s11).*(1+s22)+s12.*s21)./(2.*s21);
ep= C./(j.*2.*3.14.*f.*(8.8*10^(-3)).*(.004529).*A);
mu= B./(j.*2.*3.14.*f.*(4*314).*(.004529).*A);
ep1=real(ep);
ep2=imag(ep);
plot(f,ep1);grid on;hold on;
plot(f,ep2);grid on;hold on;
mu1=real(mu);
mu2=imag(mu);
plot(f,mu1);grid on;hold on;
plot(f,mu2);grid on;hold on;
```